RESEARCH REPORT

Institute of Transportation Studies | UNIVERSITY OF CALIFORNIA

Measuring Changes in Air Quality from Reduced Travel in Response to COVID-19

Michael Kleeman, Ph.D., Professor, Department of Civil and Environmental Engineering, University of California, Davis
Shenglun Wu, Graduate Student, Department of Civil and Environmental Engineering, University of California, Davis

December 2023

ITS UCDAVIS Institute of Transportation Studies

Report No.: UC-ITS-2021-07 | DOI: 10.7922/G26W98FP

Technical Report Documentation Page

1. Report No. UC-ITS-2021-07	**2. Government Accession No.** N/A	**3. Recipient's Catalog No.** N/A
4. Title and Subtitle Measuring Changes in Air Quality from Reduced Travel in Response to COVID-19		**5. Report Date** December 2023 **6. Performing Organization Code** ITS-Davis
7. Author(s) Michael J. Kleeman, PhD, https://orcid.org/0000-0002-0347-7512 Shenglun Wu, https://orcid.org/0000-0002-2156-7968		**8. Performing Organization Report No.** UCD-ITS-RR-24-07
9. Performing Organization Name and Address Institute of Transportation Studies, Davis 1605 Tilia Street Davis, CA 95616		**10. Work Unit No.** N/A **11. Contract or Grant No.** UC-ITS-2021-07
12. Sponsoring Agency Name and Address The University of California Institute of Transportation Studies www.ucits.org		**13. Type of Report and Period Covered** Final Report (April 2020 – September 2023) **14. Sponsoring Agency Code** UC ITS
15. Supplementary Notes DOI:10.7922/G26W98FP		

16. Abstract

Lack of a strong reduction in ambient ozone (O_3) concentrations during reduced traffic periods associated with COVID-19 calls into question the conventional wisdom that mobile sources dominate air pollution in California. Fossil-fueled motor vehicles emit oxides of nitrogen (NO_x) and volatile organic compounds (VOCs) that are precursors to O_3 formation, but the chemical reaction system that forms O_3 is complex. The ratio of NO_x/VOCs determines if the O_3 formation regime is NO_x-limited (reducing NO_x reduces O_3) or NO_x-rich (reducing NO_x increases O_3). This project developed new methods to directly measure O_3 chemistry in the atmosphere and applied them over long-term campaigns in multiple California cities to quantify traffic contributions to O_3 formation. A seasonal-cycle was observed of NO_x-rich O_3 chemistry during cooler months trending toward NO_x-limited chemistry in warmer months. Superimposed on this seasonal cycle was a spatial pattern of NO_x-rich chemistry in dense urban cores and NO_x-limited chemistry in areas downwind of urban cores. Chemistry-based models with source tagging were also developed to better understand these trends. Seasonal changes to biogenic VOC and gasoline evaporative VOC emissions likely explain the seasonal changes in O_3 formation chemistry. Reduced traffic emissions in March 2020 did not reduce O_3 concentrations because the chemistry was heavily NO_x-rich during the spring season. Extended model predictions suggest that similar traffic reductions could have reduced ambient O_3 concentrations in small and intermediate cities if they would have occurred in summer months. Traffic reductions alone would not be sufficient to reduce O_3 concentrations in the urban cores of larger cities. Reduced emissions from transportation sources can improve air quality in California, but transportation sources no longer exclusively dominate O_3 formation. Future emissions controls should be coordinated across multiple sectors (including transportation) to achieve their objectives.

17. Key Words Air quality, nitrogen oxides, ozone, vehicle emissions, traffic volume		**18. Distribution Statement** No restrictions.	
19. Security Classification (of this report) Unclassified	**20. Security Classification (of this page)** Unclassified	**21. No. of Pages** 87	**22. Price** N/A

Form Dot F 1700.7 (8-72) Reproduction of completed page authorized

About the UC Institute of Transportation Studies

The University of California Institute of Transportation Studies (UC ITS) is a network of faculty, research and administrative staff, and students dedicated to advancing the state of the art in transportation engineering, planning, and policy for the people of California. Established by the Legislature in 1947, ITS has branches at UC Berkeley, UC Davis, UC Irvine, and UCLA.

Acknowledgments

This study was made possible with funding received by the University of California Institute of Transportation Studies from the State of California through the Road Repair and Accountability Act of 2017 (Senate Bill 1). The authors would like to thank the State of California for its support of university-based research, and especially for the funding received for this project.

The chamber measurements made in the current analysis were partially supported by the California Air Resources Board under Project #RD19012. The ambient VOC measurements used in the current analysis were made under support from the Coordinating Research Council Project #A-121 and A-121-2. The authors thank the members of the Technical Advisory Committee for their feedback and guidance during the project.

The authors thank Dr. Thomas Young, Dr. Peter Green, Chris Alaimo, and Luann Wong at UC Davis for their help with VOC measurements during the RECAP-CA field campaign.

The authors thank Albert Dietrich at the South Coast Air Quality Management District for help with site preparation and access during sample collection in Redlands as part of the RECAP-CA field study. The authors thank the research team hosting the RECAP-CA field study at the California Institute of Technology, including Paul Wennberg, John Seinfeld, Benhamin Schulze, and Ryan Ward. We also thank the research team from NOAA who made measurements during RECAP-CA, including Matthew Coggon, Jessica Gilman, Michael Robinson, Patrick Veres, and Andy Neuman. Finally, we thank the research team at the California Air Resources Board who made measurements during RECAP-CA, including Toshihiro Kuwayama and Shang Liu.

Disclaimer

Measuring Changes in Air Quality from Reduced Travel in Response to COVID-19

Michael Kleeman, Ph.D., Professor, Department of Civil and Environmental Engineering, University of California, Davis
Shenglun Wu, Graduate Student, Department of Civil and Environmental Engineering, University of California, Davis

December 2023

ITS UCDAVIS Institute of Transportation Studies

Report No.: UC-ITS-2021-07 | DOI: 10.7922/G26W98FP

Table of Contents

Table of Contents

List of Tables

List of Figures

List of Acronyms and Abbreviations

AQMD	Air Quality Management District
BTEX	benzene/ toluene / ethylbenzene / xylene
BVOC	biogenic volatile organic compound
CIT	California Institute of Technology
CTM	chemical transport model
FEP	fluorinated ethylene propylene
IVOC	Intermediate volatility compounds
MDA8	maximum daily 8-hour average
NAAQS	National Ambient Air Quality Standards
NOAA	National Oceanic and Atmospheric Administration
NOx	nitrogen oxides
O_3	ozone
OFP	O_3 formation potential
PAMS	Photochemical Assessment Monitoring Stations
ppbv	parts per billion by volume
PTR-MS	proton transfer reaction mass spectrometer
PTR-ToF-MS	proton transfer reaction time-of-flight mass spectrometer
RECAP-CA	Re-Evaluating the Chemistry of Air Pollutants in California
SOA	secondary organic aerosol
SoCAB	South Coast Air Basin
SVOC	semi-volatile organic compound
SWLS	Satisfaction with Life Scale
T1	Time 1, refers to the first survey in Oakland and Bakersfield, conducted before the pilot program participant joined the program
T2	Time 2, refers to the second survey in Oakland and Bakerfield, conducted toward the end of the pilot in each city
TERP	[the lumped species to represent all monoterpenes in SAPRC11]
VCP	volatile chemical product
VOC	volatile organic compound

Executive Summary

Executive Summary

The purpose of this study was to improve our understanding of present-day ozone (O_3) formation in California cities and the contribution that transportation sources make to elevated O_3 concentrations. Lack of a strong reduction in ambient O_3 concentrations during reduced traffic periods associated with COVID-19 calls into question the conventional wisdom that mobile sources dominate air pollution in California. Fossil-fueled motor vehicles emit oxides of nitrogen (NO_x) and volatile organic compounds (VOCs) that are both precursors to O_3 formation, but the chemical reaction system that forms O_3 is complex. The ratio of NO_x/VOCs determines if the O_3 formation regime is NO_x-limited (reducing NO_x reduces O_3) or NO_x-rich (reducing NO_x increases O_3).

In this project, two transportable smog chamber systems were created to directly measure the response of O_3 to perturbations in precursor NO_x and VOC concentrations under ambient conditions. Each system was built around three identical "smog chambers" (1 m^3 each) illuminated with UV lights. Chambers were transported in a trailer to the measurement site and filled with ambient air between 10am-12pm on each measurement day. One chamber was perturbed by adding ~8 ppb of NO_x, a second chamber was perturbed by adding ~8 ppb of a VOC representing urban atmospheres, and the third chamber was used as a base case comparison point.

Long-term measurements (shown in Figure ES1) were carried out in Pasadena and Redlands, California, during the summer of 2021 in coordination with a coordinated field campaign called Re-Evaluate the Chemistry of Air Pollution in California (RECAP-CA). The median observed O_3 sensitivity in Pasadena was stable in the NO_x-rich regime, but showed a seasonal trend in Redlands, where median O_3 formation was NO_x-rich in July and October and transitioned towards the NO_x-limited regime in August and September. This seasonal pattern is consistent with the expected trends in both biogenic VOC emissions and evaporative emissions semi-volatile organic compounds (SVOCs) such as gasoline and industrial solvents. Pasadena and Redlands had O_3-nonattainment days under both NO_x-limited and VOC-limited conditions.

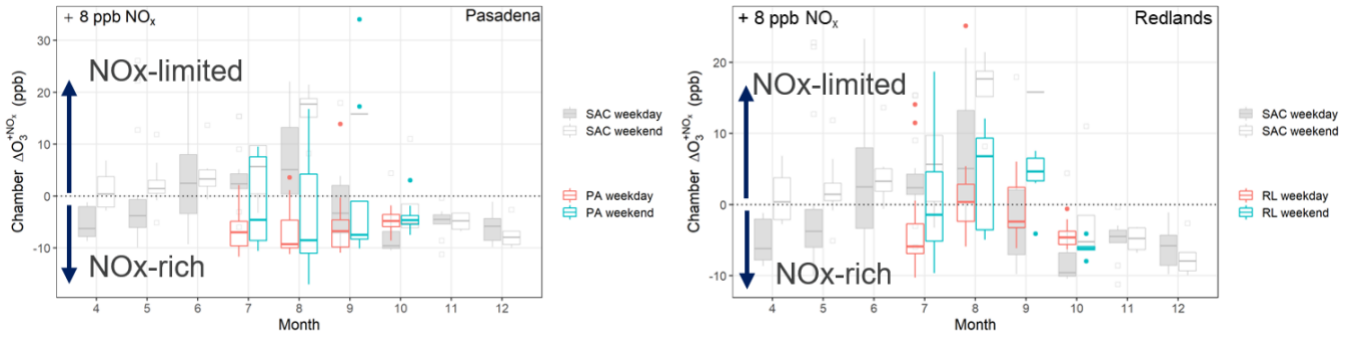

Figure ES 1. Time series of daily O_3 sensitivity results ($\Delta O_3^{+NO_x}$) on weekdays and weekends from chamber measurements in Pasadena and Redlands, CA, from July to October 2021. The background box and whisker plots (in grey) are the time series of O_3 sensitivity results from chamber measurements in Sacramento, CA, in 2020.

Locations next to higher population density favored NO_x-rich conditions. Chamber measurements suggest that Pasadena was in the NO_x-rich chemical regime on 90% of the measurement days during the study period, while Redlands was NO_x-rich on 70% of the measurement days. The highest measured O_3 concentrations occurred more frequently on days that were NO_x-limited, but the variability in the O_3 chemical regime also increased on high O_3 days.

A photochemical chamber model based on the SAPRC11 chemical mechanism was created to better understand the measured O_3 trends. O_3 isopleths (shown in Figure ES2) created with the chamber model predict that ~40% NO_x control would be required to transition the chemical regime from NO_x-rich to NO_x-limited conditions on ~95% of the days with the highest O_3 concentrations in the late summer and early fall. Substantially larger NO_x reductions would be needed in the spring due to the seasonal shift in the atmospheric chemical regime. The ~30% reduction in NO_x concentrations associated with reduced travel during the shutdown period in the spring of 2020 (*1*) did not cross this threshold.

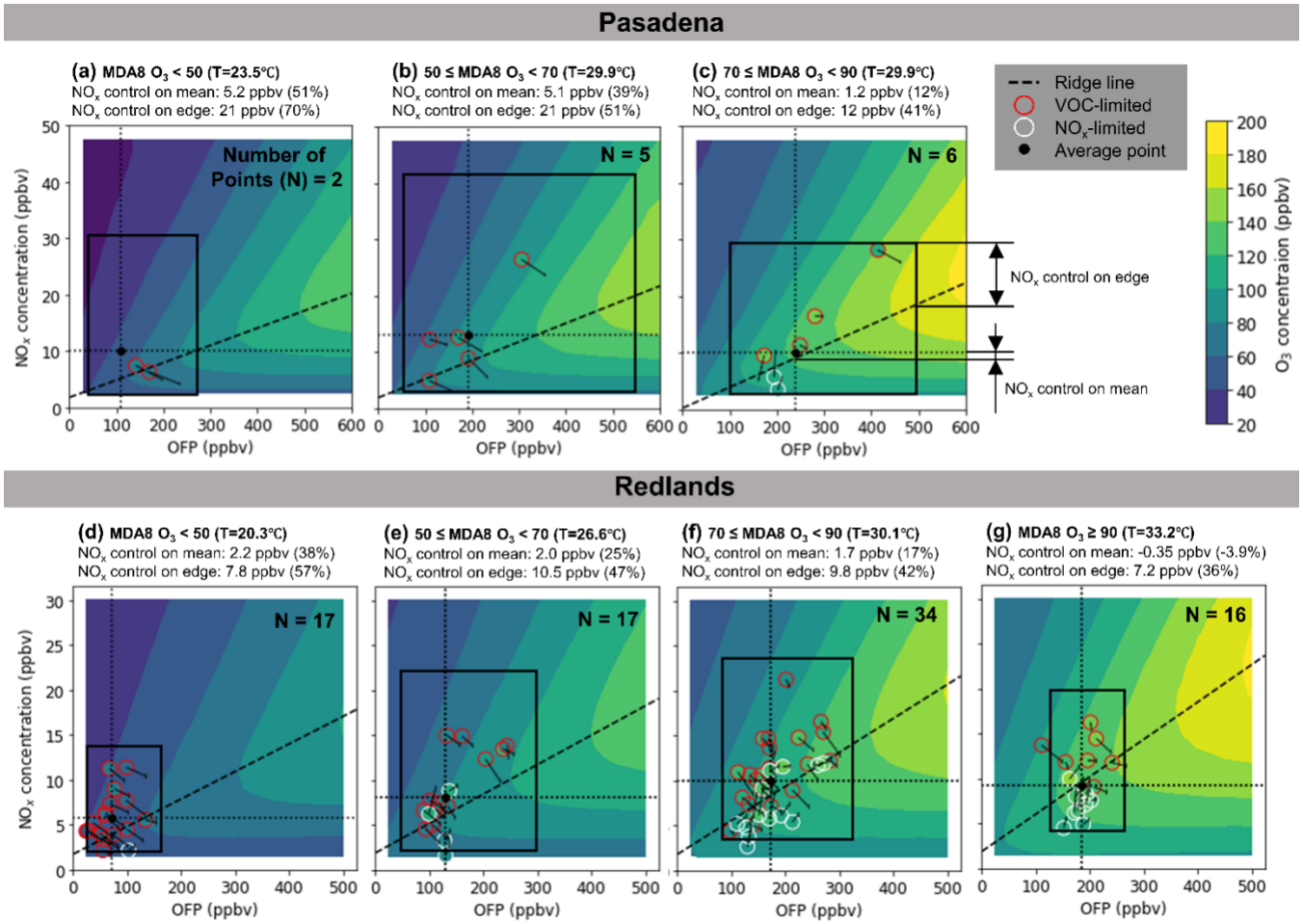

Figure ES 2. O_3 isopleth at Redlands, over four maximum daily 8-hour average (MDA8) O_3 concentration ranges experienced during the study. The intersection of light dotted lines represents the average measured NO_x and VOC levels. The box around the average represents the standard deviation of the measured values. The heavy dashed line represents the ridgeline of isopleth. Open circles represent chamber measurements for comparison to model predictions.

Results from the present study suggest that a balanced strategy of NO_x and VOC controls would be most beneficial to reduce O_3 concentrations in the near term. Biogenic sources are the single-largest contributor to O_3 formation in Pasadena and Redlands, but use of fossil fuels and Volatile Chemical Products (VCPs) also contribute to O_3 formation under current conditions. Potential future emissions control strategies could focus on encouraging the adoption of low carbon alternative fuels that emit less NO_x and accelerating the replacement of fossil-fueled mobile sources with electric vehicles (which reduces both NO_x and VOC) while simultaneously reducing volatile chemical product (VCP) emissions. This combined strategy across multiple sectors satisfies the requirement of simultaneous NO_x and VOC emissions controls to address both the near- and long-term needs for O_3 control.

Contents

1. Introduction

Tropospheric ozone (O_3) is a criteria pollutant that harms human health and the environment due to its strong oxidative properties. Limits for O_3 concentrations designed to protect public health are specified by the National Ambient Air Quality Standards (NAAQS) and the California State Air Quality Standards. These target values are periodically revised based on the most recent and best available epidemiological evidence. Despite extensive reductions in ambient O_3 concentrations over the past four decades in California, the state continues to violate the evolving health-based standards that have also decreased over that period. As a result, California continues to research strategies to better understand O_3 sources and formation mechanisms to reduce concentrations.

Oxides of nitrogen (NO_x) and volatile organic compounds (VOCs) are the precursor species in the O_3 formation cycle. NO_x and VOC concentrations can vary substantially depending on emissions from local sources such as motor vehicles, power plants, and the regional biosphere. O_3 pollution episodes typically occur during warm summer periods when the ultraviolet (UV) intensity (in Watts per square meter - W/m^2) is near its annual maximum. Population exposure to O_3 varies significantly based on location, time of day and year, and meteorological patterns. Reactive chemical transport models (CTMs) that simulate all these factors are often used to design O_3 mitigation strategies. In a typical design application, CTMs are first applied to a historical O_3 episode to ensure that they correctly reproduce the observed concentrations across the region of interest. Once satisfactory base-case model performance is attained, the emissions inputs to the models are reduced and the corresponding reduction in O_3 is simulated. There is often little or no ability to evaluate the accuracy of CTMs when calculating O_3 reductions in response to prospective emissions changes. Measured ratios of various photochemical indicator species can provide some confidence about the limiting precursors for O_3 formation but not the actual magnitude or the amount of O_3 reduction per unit of precursor reduction.

Long-term trends in NO_x and VOC concentrations have been studied in Los Angeles for more than 60 years with the goal to better understand how they influence O_3 concentrations. Measurements in Southern California confirm that ambient VOC concentrations decreased at an average rate of 7.5% per yr, while ambient NO_x concentrations decreased at an average rate of 2.6% per yr between the years 1980 to 2010 (*2*, *3*). Measurements in 2010 during the CalNex field campaign suggested that motor vehicles were still the dominant source of VOCs in the Los Angeles atmosphere (*3*, *4*). More recent VOC measurements during the pandemic period of 2020 showed that ambient VOC concentrations did not respond strongly to significant reductions in traffic volume (*5*), suggesting that non-transportation sources may play an increasingly significant role in the residual VOC emissions inventory.

Volatile chemical products (VCPs) have been suggested as a major source of O_3 formation (*6*). Intermediate volatility compounds (IVOCs) are often discussed in the context of secondary organic aerosol (SOA) formation (*7*) but are generally not considered to be dominant contributors to O_3 formation. The current study attempts

to interpret the time trends of VOC concentrations, O_3 sensitivity measurements, and model source apportionment calculations to help identify present-day dominant sources of O_3 formation.

1.1 Objectives

The objective of this project was to use a combination of measurements and model predictions to better understand the response of O_3 formation to NO_x and VOC perturbations in California. Direct measurements using transportable smog chambers were used as an independent check on the accuracy of model calculations. The altered emissions during COVID-19 shutdown periods were used as a real-world check on the aforementioned measurements and model predictions. The fully evaluated modeling system were used to predict how O_3 concentrations would respond to a range of NO_x and VOC emissions controls in Los Angeles, San Francisco, Sacramento, and Fresno.

Activities under the current project were carried out in coordination with projects funded by the California Air Resources Board (Project 19RD012) to make measurements during the RECAP-CA field campaign and the Coordinating Research Council (Project A-121 and A-121-2) to make complimentary VOC measurements alongside the chamber experiments. Under this expanded program, measurements were made during the years 2020 and 2021. The present report focuses on measurements collected in the year 2021, since these are most directly aligned with the funding support provided by Project 2021-07.

Model simulations were performed for all measurement periods in 2020 and 2021. Model simulations were also extended to cities without measurements to more fully evaluate O_3 control strategies across California in 2020.

All of the project objectives were accomplished as discussed in the following report.

1.2 Report Scope and Organization

Sections 2 and 3 in this report each contain their own Introduction, Methods, Results, Discussion, and Conclusions. Sections 2 and 3 are preceded by this current section, an overall Introduction (1), and followed by an overall Conclusions section (4) and Future Work section (5) apply to the entire study. Section 2 describes the photochemical smog chamber measurements made at two sites in Southern California for 16 weeks overlapping with the RECAP-CA field campaign. O_3 formation regimes are illustrated as a function of season. Full O_3 isopleths are developed for each measurement location, and source contributions to O_3 formation from emissions of VCPs, traffic pollutants, and biogenics are quantified. The expected amount of NO_x control needed to reach NO_x-limited conditions is estimated.

Section 3 extends the model analysis to major cities across California. Results are generated for the spring of 2020 when shutdown orders reduced mobile emissions, and for August 2020 when mobile emissions had

substantially recovered. The seasonal cycles observed in the measurements detailed in Section 2 are used to better understand the O_3 response to changing traffic emissions.

2. Ozone Response to NO_x and VOC Perturbations in Los Angeles

2.1 Introduction

Regulators in the South Coast Air Basin (SoCAB) surrounding Los Angeles has been working to mitigate Ozone (O_3) pollution for seven decades. Extensive reductions in precursor emissions of volatile organic compounds (VOCs) and nitrogen oxides (NO_x) have greatly decreased O_3 concentrations over that time, but our evolving understanding of O_3 health effects has translated to a commensurate reduction in target O_3 concentrations to protect public health. As a result, the current O_3 concentrations in the SoCAB still exceed the National Ambient Air Quality Standards (NAAQS), and researchers continue to search for ways to better understand the present-day sources and formation mechanisms of O_3 formation to further reduce concentrations.

The CalNex 2010 field campaign (*8*) comprehensively analyzed precursors of O_3 formation in the SoCAB. Initial measurements suggested that NO_x and VOCs concentration were significantly reduced in previous decades due to the extensive emission control program on transportation, but that mobile sources were still the dominant source of VOCs in the Los Angeles atmosphere (*3*, *4*, *9*). Subsequent studies highlighted the growing importance of non-transportation sources of VOC emissions. McDonald et al. (*6*) showed that volatile chemical products (VCPs) were an important source of O_3 precursors in Los Angeles. Follow-on studies have confirmed that VCPs are an important VOC emission source (*5*, *10*, *11*) that may contribute to elevated O_3 concentrations in multiple urban areas (*12*, *13*). The question of which VOC emissions source(s) contribute(s) most strongly to O_3 formation in the SoCAB is still being investigated by multiple research groups.

Recent trends highlight the urgent need to better understand present-day sources of O_3 formation in California. Between 2010 and 2020, the trend of reduced O_3 design values (the 4th highest daily maximum 8-hour average concentration, averaged over a 3-year period) that had held for decades in the SoCAB stalled, and O_3 concentrations even increased in some locations (*14*). This suggests that the O_3 chemical regime and/or dominant emission sources of O_3 precursors may have changed in recent years. New O_3 control strategies may be needed to further reduce O_3 pollution. Therefore, it is essential to conduct new field measurements and new modeling studies to understand the O_3 chemical regime and emissions of O_3 precursors in the SoCAB.

Recent studies (*2*, *15*) indicate that the O_3 sensitivity in central Los Angeles is in a VOC-limited regime. Observations during the COVID-19 shutdown period demonstrate that sufficiently large emissions changes can transfer the O_3 chemical regime in Los Angeles from VOC-limited to NO_x-limited conditions (*1*). Progress towards this transition is reflected in the shrinking area of the VOC-limited region over time due to the action of NO_x emissions controls (*16*). These types of observations illustrate the importance of continuous monitoring of the O_3 chemical regime throughout the SoCAB.

Our past study (*14*) developed a smog chamber system to directly measure the O_3 chemical regime in Sacramento, CA, by measuring O_3 response to NO_x and VOC perturbations. Long-term measurements at Sacramento observed a seasonal trend of O_3 sensitivity that moved from VOC-limited to NO_x-limited from spring to summer, and from NO_x-limited to VOC-limited from summer to winter. Here we extend those observations using two parallel systems to measure O_3 sensitivity at two sites in the SoCAB during the RECAP-CA field campaign. Seasonal trends in the O_3 chemical regime are shown from July to October 2021. The O_3 chemical regimes on the days with the highest recorded O_3 concentrations are summarized. A chamber model is created to generate O_3 isopleth diagrams at both measurement sites. The amount of NO_x control needed to transition to NO_x-limited conditions is estimated based on these isopleths. Source apportionment features (*17*) in the chamber model are further used to quantify VOC source contributions to O_3 formation. Finally, the combined measurements and model predictions are used to recommend optimized control strategies for further O_3 reductions in the SoCAB.

2.2 Methods

2.2.1 Measurement Locations

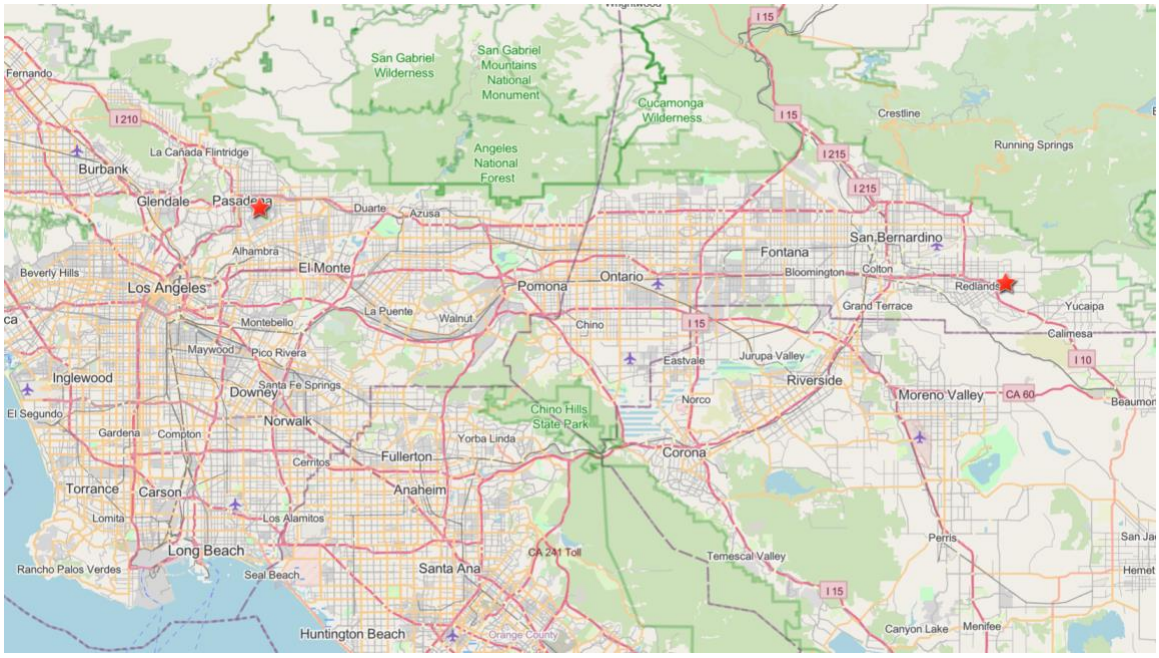

Figure 1. Map of measurement location (red star) in SoCAB. (Map data © OpenStreetMap contributors, Microsoft, Facebook, Inc. and its affiliates, Esri Community Maps contributors, Map layer by Esri).

O_3 sensitivity measurements were made in Pasadena and Redlands in the SoCAB surrounding Los Angeles (Figure 1). The Pasadena sampling site (34.140716, -118.122426) was located on the campus of the California Institute of Technology (CIT). Measurements at CIT began on July 17, 2021 and ended on October 31, 2021.

Nearby emissions sources include the university power plant, cafeteria plus other facilities, and the residential/commercial sources in the surrounding city of Pasadena. A major freeway is located ~1.2 km north of the CIT measurement site. Additional measurements were made by NOAA researchers and CARB staff at the CIT measurement site during August 2021 as part of the RECAP-CA field campaign.

The Redlands sampling site (34.059671, -117.147304) was located at the Dearborn Reservoir monitoring site maintained by the South Coast Air Quality Management District in the city of Redlands, CA. Measurements in Redlands started on July 10, 2021 and ended on October 31, 2021. Emissions sources close to the Redlands site include residential neighborhoods and a mixture of commercial and industrial land uses. The University of Redlands is located approximately 1 km west of the Redlands monitoring site (prevailing upwind direction). A major freeway is located approximately ~1.5 km southwest of the Redlands sampling site.

2.2.2 Chamber Measurements

2.2.2.1 Measurement description

Two transportable smog chamber systems with similar configurations were used to measure O_3 sensitivity to NO_x and VOC perturbations in ambient air at each study site in the SoCAB. The configuration, operation, and performance for a single transportable smog chamber system was previously characterized for measurements made at Sacramento in 2020 (*14*). Here, we will briefly summarize the configuration and operation of the O_3 sensitivity measurement made by the two mobile smog chamber systems deployed in the SoCAB.

Mobile chamber systems are based on three identical 1 m^3 fluorinated ethylene propylene smog chambers. All three smog chambers within a mobile system are filled with ambient air during a typical operation cycle. One chamber is perturbed by adding NO_2, a second chamber is perturbed by adding a mixture of VOCs representative of an urban atmosphere (*18*), and the third chamber acts as a base case for comparison to the first two. All chambers are suspended inside a support frame with reflective polished aluminum wall panels. UV lamps above and below the chambers irradiate the trapped atmosphere with UV intensity similar to mid-day conditions in California during the summer (100 W m^{-2}). Ambient air is circulated around the chambers to maintain the chamber temperature close to the ambient temperature. Incoming chamber air is not filtered and therefore contains all gas-phase and particle-phase species found in the ambient atmosphere. All chambers are flushed with clean air and irradiated after each measurement to mitigate possible carry-over effects from perturbation gases.

In the current study, smog chambers were filled with ambient air between 10:00 AM to 12:00 PM PDT on each measurement day. NO_x (8 ppb NO_2) and VOC (4.4 ppb ethylene, 2.8 ppb n-hexane, and 0.8 ppb m-xylene) was added at approximately 11 AM to encourage mixing of the perturbation gases with ambient air in the perturbation chambers. NO_x, NO_y, O_3, temperature and relative humidity (RH) were measured in each dark chamber immediately after filling over a time period of 30 min (10 min for each chamber). UV lights were then turned on for 180 min while chamber measurements continued in 30 min cycles (10 min for each chamber). Final O_3 concentrations after three hours of UV exposure were calculated for each chamber by fitting a regression curve to the O_3 concentrations during the preceding measurement period. The difference between

final O_3 concentrations in the NO_x-perturbed chamber and the base case chamber quantified the O_3 sensitivity to NO_x ($\Delta O_3^{+NO_x}$). The difference between the final O_3 concentrations in the VOC-perturbed chamber and the base case chamber quantified the O_3 sensitivity to VOC (ΔO_3^{+VOC}).

2.2.2.2 Consistency of smog chamber systems

Side-by-side comparisons of O_3 sensitivity measurements were made in Davis in mid-June 2021 before deployment to the SoCAB and in Pasadena in early November 2021 after the measurements ended. Davis was expected to be in the NO_x-limited chemical regime in June, while Pasadena was expected to be in the NO_x-rich chemical regime in November (*14*). This allowed the consistency checks to be performed at multiple locations with differing O_3 chemical regimes.

Figure 2 shows the consistency of final O_3 concentration measured in co-located but separate mobile smog chamber systems after three hours of UV exposure. The average correlation coefficient (R^2) between the co-located measurements of final O_3 concentrations is 0.996. The average slope of the least-squares linear regression line between co-located measurements of final O_3 concentrations is 0.94 ± 0.021. The slight bias between the O_3 measurements may be caused by differential monitor response. O_3 monitors are rated for 2% noise and 3% sensitivity drift per year. Slight differences in the location and ventilation conditions of the trailers could also introduce small differences in these co-located ambient measurements. Accounting for all the potential uncertainties, the final O_3 formation is still generally consistent between the two systems.

Figure 3 shows the consistency of O_3 sensitivity measurements ($\Delta O_3^{+NO_x}$ and ΔO_3^{+VOC}) made by the co-located smog chamber systems. O_3 sensitivity is measured using the same O_3 monitor, which potentially reduces the effect of minor bias in absolute O_3 readings. The O_3 sensitivity is calculated as the difference between two similar O_3 concentrations, which potentially increases the relative uncertainty in the calculation. The average correlation coefficient (R^2) between the co-located O_3 sensitivity measurements was 0.966. The average slope of the least-squares linear regression line between the co-located O_3 sensitivity measurements was 1.01 ± 0.062. Overall, the co-located O_3 sensitivity measurements indicate consistent behavior between the two mobile systems. Random errors in the measurements should be mitigated by the statistical methods that combine measurements across multiple days. This level of agreement will not alter the interpretation of the chemical regime for O_3 formation.

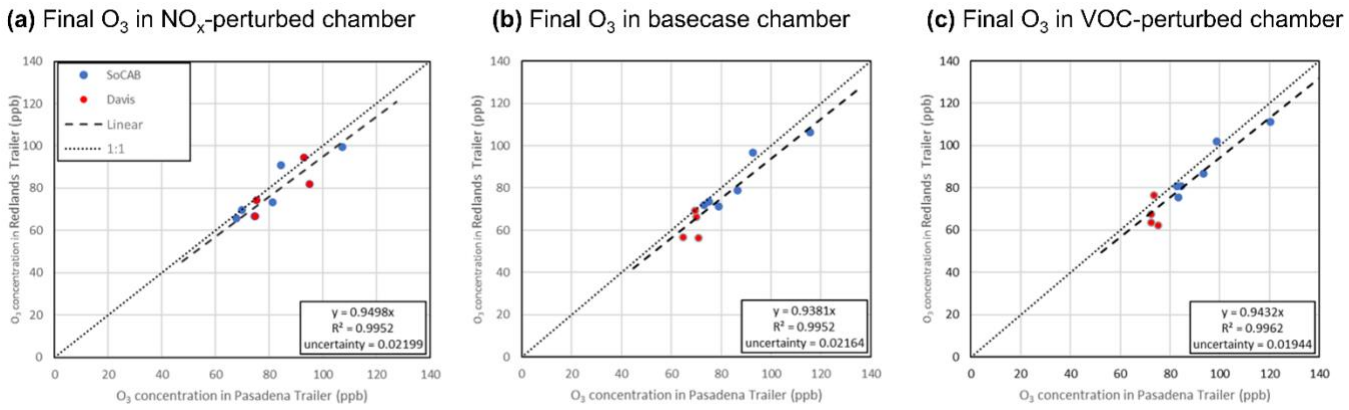

Figure 2. Consistency of projected O_3 concentrations after 3-hour UV exposure in 3 smog chambers between two smog chamber systems.

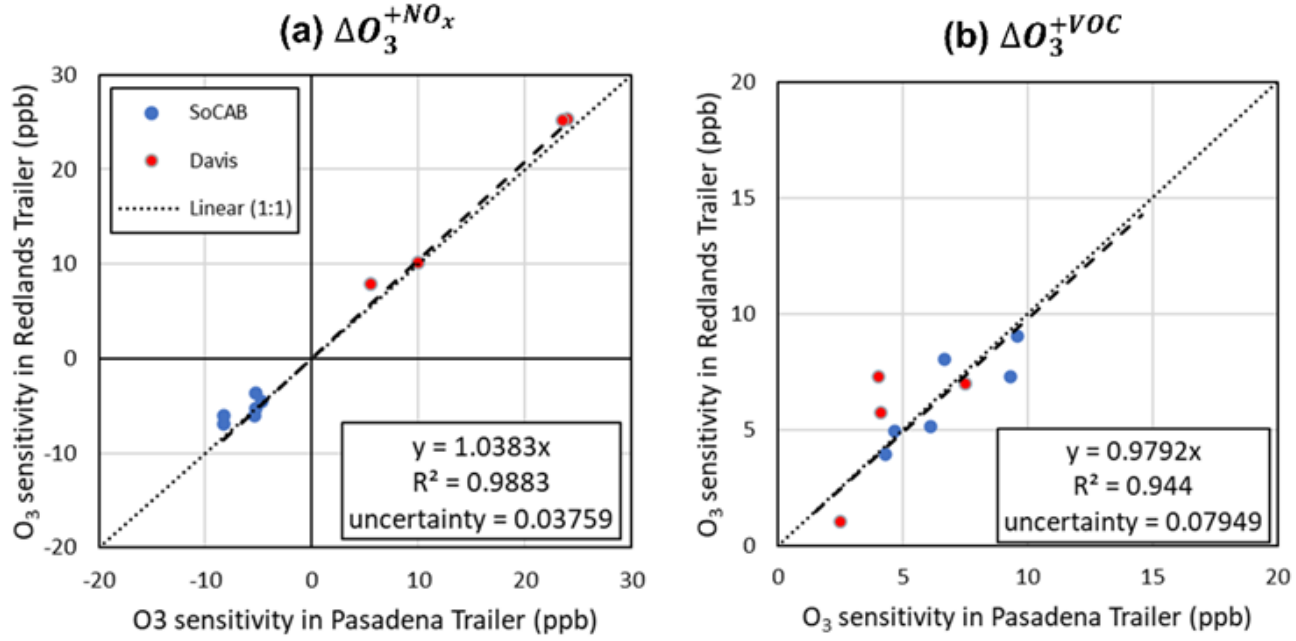

Figure 3. Consistency of O_3 sensitivity results from O_3 sensitivity experiments made by two smog chamber systems.

2.2.2.3 Consistency of chamber O_3 concentrations and ambient O_3 concentrations

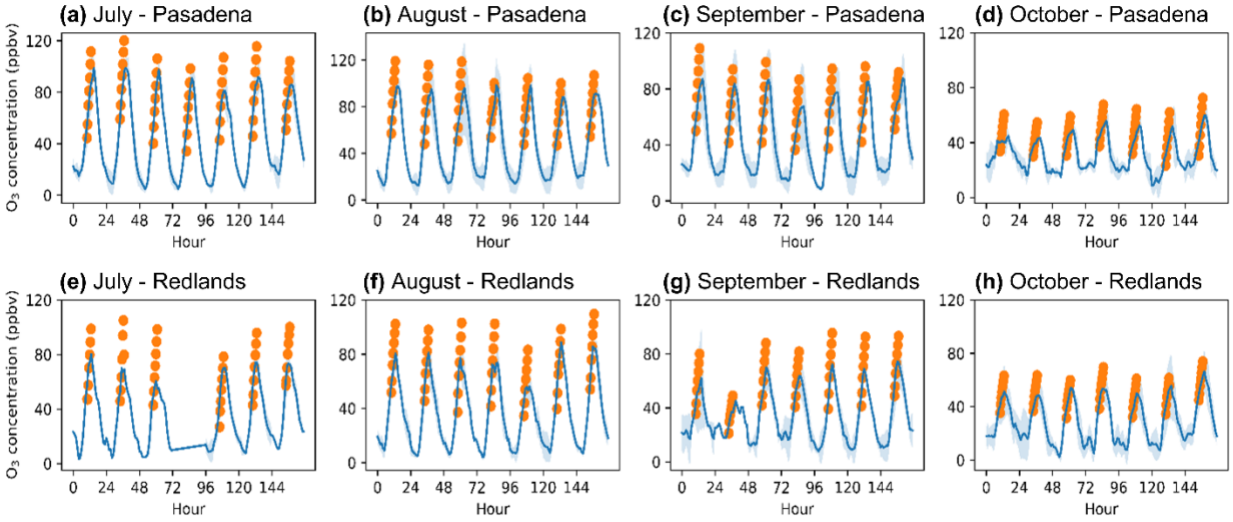

Figure 4. Weekly averaged ambient (solid line) vs. chamber (solid circles) O_3 concentrations measured in Redlands and Pasadena for July to October 2021. The shaded area indicates one standard deviation of the ambient O_3 concentration. Chambers were filled over a ~2-hr period followed by a 30-min dark measurement period before UV lights were turned on. Hour is relative to the start of the experiment.

Figure 4 illustrates the time-series of O_3 concentrations measured in the base case chambers in Pasadena and Redlands and at nearby ambient monitors. Results for the average week in each month are displayed separately. Initial chamber concentrations are identical to ambient concentrations. The rate of O_3 formation in the chambers and the final O_3 concentration at the end of the three-hour UV exposure period are greater than the ambient concentrations because the ambient air is being diluted by a rising boundary layer throughout the mid-day period. The chamber measurement captures the O_3 chemical formation potential of the ambient air, which is a key component of the ambient O_3 formation behavior. The consistency checks summarized in Figure 4 confirm that all chamber measurements operated under atmospherically relevant conditions.

2.2.3 VOC Measurements

2.2.3.1 VOC measurements in Redlands

Atmospheric VOC concentrations were measured each day in Redlands from 10 AM to 12 PM in parallel with chamber filling operations to better understand O_3 formation in the chamber experiment. A detailed description of the VOC collection and analysis methods has been provided previously by Kleeman et al. (*19*) and so only a brief summary is provided here. VOC samples were collected using Markes Universal Thermal Desorption tubes and 2,4-dinitrophenylhydrazine tubes. Collected samples were immediately sealed and refrigerated for short term-storage (1-3 days) before shipping back to the UC Davis laboratory for analysis. VOC concentrations were measured using a gas chromatograph + mass spectrometer (GC-MS) system and a liquid chromatograph + mass spectrometer (LC-MS) system following a rigorous protocol of multi-point

calibrations using authentic standards. Airborne carbonyl compound concentrations, including those of methyl ethyl ketone and cyclohexanone, were determined using a modified version of the US EPA method TO-11 (*20*). Concentrations for all other organic species were determined using a modified version of the US EPA method TO-17 (*21*). A total of 95 VOC species were measured above detection limits, including hydrocarbon, halogenated and oxygenated VOCs, and siloxanes.

CARB staff made additional VOC measurements in Redlands using a Proton Transfer Reaction Time-of-Flight Mass Spectrometer (PTR-ToF-MS, Vicus-Scout, Aerodyne Research Inc.) with 1-second time resolution. The PTR-MS ionized VOCs using H_3O^+ and then detected compounds with a high-resolution time-of-flight analyzer. The instrument was calibrated every four hours for fourteen VOC species, including ethanol, acetonitrile, acetone, acrylonitrile, isoprene, methyl vinyl ketone, methyl ethyl ketone, benzene, m-xylene, alpha-pinene, beta-caryophyllene, 1,2,4-trimethylbenzene, octamethylcyclotetrasiloxane (D4), and decamethylcyclopentasiloxane (D5). The background PTR-MS signals were determined by passing ambient air through a catalytic converter. The PTR-MS was housed in a stationary van (engine off) with an inlet located approximately 3 m above ground level. PTR-MS data from Redlands was processed using the Tofware (version 3.2.3, Tofwerk Inc.) and the final concentrations were averaged to 1-min intervals for subsequent analysis. All VOC concentrations measured in Redlands were averaged from 10 am to 12 pm in the current analysis to better understand initial chamber concentrations.

2.2.3.2 VOC measurements in Pasadena

NOAA staff made VOC measurements in Pasadena, CA, from August to September 2021 using multiple state-of-the-science instruments. General VOC measurements were made using a real-time gas chromatograph-mass spectrometer system (*22*) and a Tofwerk Vocus long time-of-flight mass spectrometer (*23*). Formic acid (HCOOH), HNO_2, HNO_3, N_2O_5, and peroxyacyl nitrates (PAN) were measured with an iodide chemical ionization mass spectrometer (I-CIMS) (*24*). Further details of I-CIMS measurements are discussed by Robinson et al. (*25*), Veres at al. (*26*), and Veres and Roberts (*27*). HCHO was measured by CARB using the Picarro (Picarro Inc., Santa Clara, CA) G2307 HCHO analyzer. This analyzer uses cavity ring-down spectroscopy (CRDS) to quantify the mixing ratio of HCHO in real time. The CRDS compares the time of decay of the laser light in an empty cavity and a cavity with HCHO to calculate the absorption intensity of HCHO. The absorption intensity is then converted to concentration using external calibration. The HCHO analyzer was calibrated in the factory and checked using the surrogate method (methane) as recommended by the manufacturer. During the measurement, the instrument was housed in a stationary van (engine off) with an inlet located approximately 3 m above ground level. The recorded 1-second data were averaged to 1-min intervals for data analysis. All VOC concentrations measured in Pasadena were averaged from 10 am to 12 pm in the current analysis to better understand initial chamber concentrations. Table 1 summarizes all the ambient measurement instruments made by three different groups throughout the experiment period.

Table 1. Summary of measurements in Pasadena and Redlands.

No.	Instruments	Species measured	Location	Sample duration/frequency	Institution	Reference
1	Transportable smog chamber system	O_3, NO, NO_2, NO_y, Temperature, Relative humidity, O_3 sensitivity	Pasadena, Redlands	2 s (O_3), 1 s (others)	UC Davis	(*28*)
2	Markes Universal Thermal desorption (TD) tube + GC-MS	TO-15 compounds, C3-C5 hydrocarbon	Redlands	10 min, 30 min, 70 min	UC Davis	
3	TD tube + LC-MS	Aromatic VOCs, siloxanes, glycols, glycol ethers, and other SVOCs.	Redlands	10 min, 30 min, 70 min	UC Davis	
4	2,4-dinitrophenylhydrazine tube + LC-MS	Aldehydes and ketones	Redlands	70 min	UC Davis	
5	PTR-ToF-MS	Ethanol, acetonitrile, acetone, acrylonitrile, isoprene, MVK, MEK, benzene, m-xylene, alpha-pinene, 1,2,4-trimethylbenzene, siloxanes	Redlands	1 s	CARB	
6	GC-MS	C2-C10 alkanes, C2-C5 alkenes, Acetone, benzene, terpenes, etc.	Pasadena	1 min	NOAA CSL	(*29*)
7	I-CIMS	$ClNO_2$, HCOOH, HNO_2, HNO_3, PANs, N_2O_5	Pasadena	1 min	NOAA CSL	(*30–32*)
8	CARB mobile platform (Picarro G2401, G2307, G2103)	CO, CO_2, CH_4, H_2O, NH_3, HCHO	Pasadena	1-5 min	CARB	
9	PTR-ToF-MS	Aromatics, monoterpenes, isoprene, OVOCs, siloxanes, etc.	Pasadena	1 s	NOAA CSL	(*23*, *33*)

GC-MS, gas chromatography mass spectrometer; I-CIMS, iodide chemical ionization mass spectrometer, LC-MS, liquid chromatography mass spectrometer; NOAA CSL, NOAA Chemical Sciences Laboratory; PTR-ToF-MS, proton transfer reaction time-of-flight mass spectrometer; SVOC, semi-volatile organic compound; TD, thermal desorption

2.2.4 Model Calculations

A photochemical chamber model was applied to better understand the VOC sources that control the O_3 chemical regime and to predict the amount of NO_x control required to transition from NO_x-rich conditions to NO_x-limited conditions in Pasadena and Redlands. The chamber model was based on the SAPRC11 chemical mechanism (*34*) with source apportionment capabilities (*17*). Wall loss rates were specified at 5% per hour based on measured concentration decreases (*14*). The UV spectrum used in the calculation was adjusted to match the lights used in the chamber (*14*). Initial concentrations were based on measured values of O_3, NO, NO_2, and the majority of VOC species and/or chemical transport model simulations of ambient concentrations with additional details discussed below.

2.2.4.1 Correction of measured aldehyde concentrations

Formaldehyde and acetaldehyde concentrations measured in Redlands were lower than previous measurements made at Riverside and Pasadena (Figure 5). An internal quality assurance/quality control audit suggests that the flow rate through the aldehyde collection device may have been too low at the Redlands site. Formaldehyde and acetaldehyde concentrations in Redlands were therefore corrected based on trends at the Pasadena site. Historical Photochemical Assessment Monitoring Stations (PAMS) measurements show that aldehydes concentrations measured at upwind and downwind locations in the SoCAB are correlated. Figure 6 shows that aldehyde concentrations measured at central Los Angeles and Riverside have a relatively constant ratio. Figure 7 shows that chemical transport model (CTM) simulations for aldehyde concentrations predict a similar ratio at Los Angeles and Riverside, albeit predicted absolute aldehyde concentrations are lower than measured values, possibly due to dilution introduced by the 4km grid cell resolution. The measurements and model predictions suggest that the ratio of aldehyde concentrations in Pasadena and Redlands should also be relatively constant. CTM simulations predict the ratio of concentrations in Redlands/Pasadena is 0.9 for formaldehyde and 0.66 for acetaldehyde. These ratios were used to scale the measured aldehyde concentrations in Redlands so that they have the expected average values in comparison to the measured aldehyde concentrations in Pasadena. The corrected aldehyde concentrations in Redlands are shown in Figure 5.

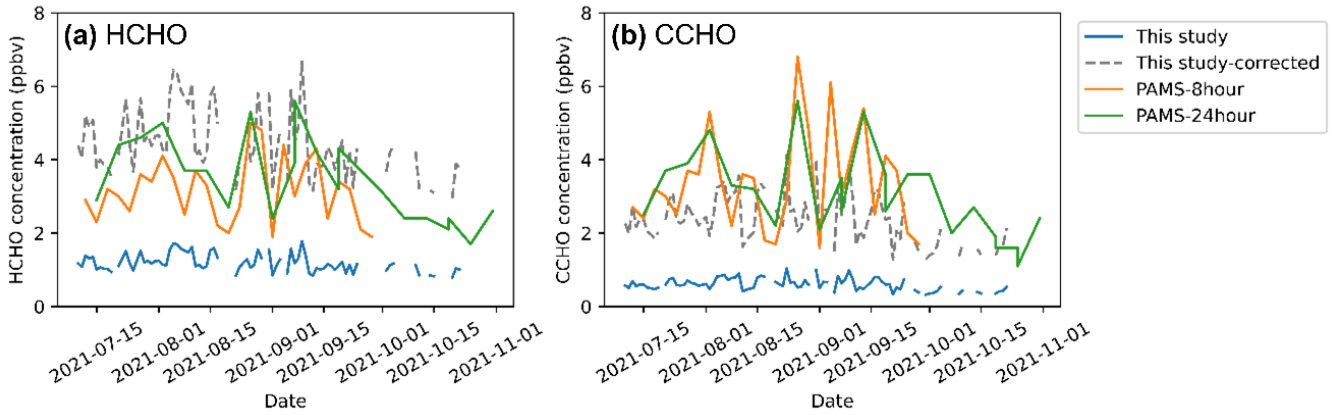

Figure 5. Time series of formaldehyde (HCHO) and acetaldehyde (CCHO) concentrations measured in Redlands (this study) and Riverside photochemical assessment monitoring stations (PAMS) in 2021. The dashed line shows the HCHO and CCHO concentration after correction.

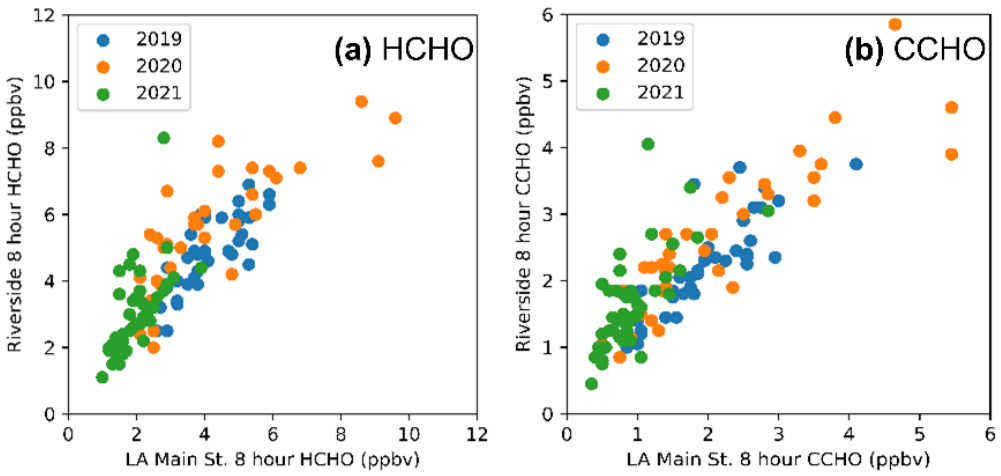

Figure 6. Formaldehyde and acetaldehyde concentrations measured at PAMS sites at Riverside and central Los Angeles in 2019, 2020, and 2021.

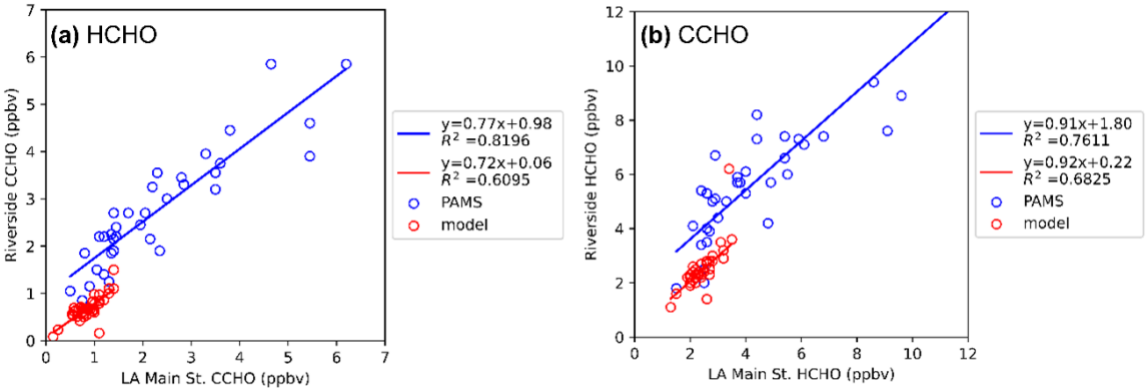

Figure 7. Formaldehyde and acetaldehyde concentrations measured at PAMS sites and predicted by CTM simulations at Riverside and central Los Angeles in 2020.

2.2.4.2 Chamber model initial concentrations

The initial concentrations for the species used in the chamber-model SAPRC11 chemical mechanism were obtained from a combination of measurements and CTM predictions. Preference was given to measurements made during the chamber-filling period (10 AM–12 PM) when these data were available. CTM predictions at 11 AM (reflects the averaged value between 10 AM–12 PM) on the appropriate day of the week and week of the year were used to initialize chamber concentrations when measurements were missing. This approach captures

day of week and seasonal emissions trends but does not perfectly account for meteorological conditions because CTM simulations were only available for the year 2020, not for the year 2021 when the field study was conducted. Additional corrections were therefore applied to CTM concentration to reflect day-specific conditions.

Hydrogen peroxide (H_2O_2, also referred as HO_2H in SAPRC11) is produced as a photochemical reaction product in urban atmospheres. H_2O_2 was not measured in Redlands during RECAP-CA, and the measurements in Pasadena were not available at the time of the present analysis. H_2O_2 predictions from CTM calculations were corrected for day-specific temperature trends based on the predicted relationship between H_2O_2 and ambient temperature in Pasadena and Redlands (Figure 8).

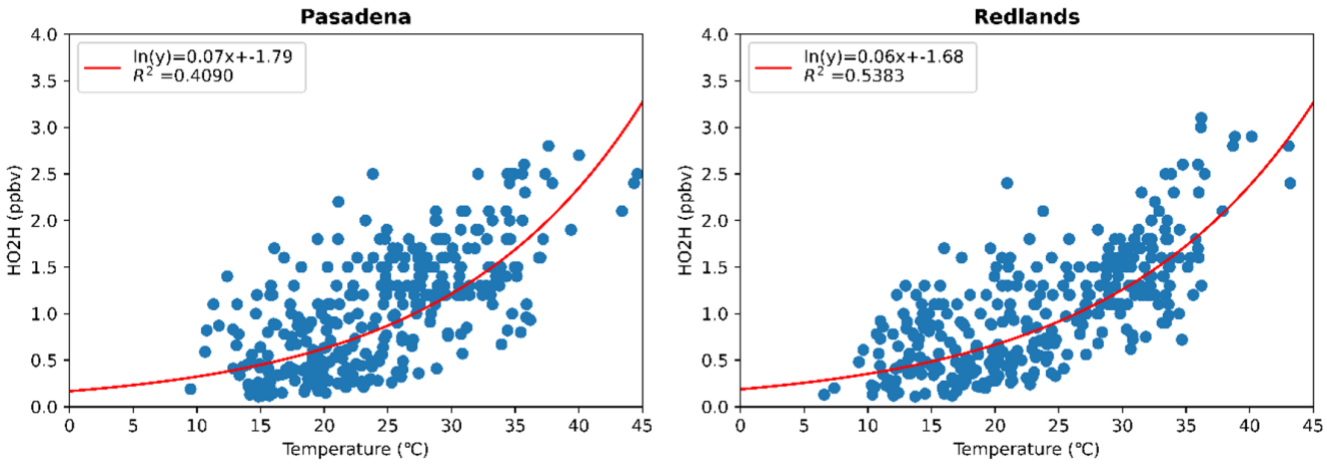

Figure 8. Predicted relationship between temperature and hydrogen peroxide concentrations in Pasadena and Redlands in the year 2020.

Ethene (ETHENE in SAPRC11) and acetylene (ACETYLEN in SAPRC11) are generally emitted from combustion sources in urban areas. Ethene and acetylene were not measured at the Redlands site during RECAP-CA. CTM predictions of ethene and acetylene in Redlands were corrected for day-specific conditions using the relationship with carbon monoxide illustrated in Figure 9.

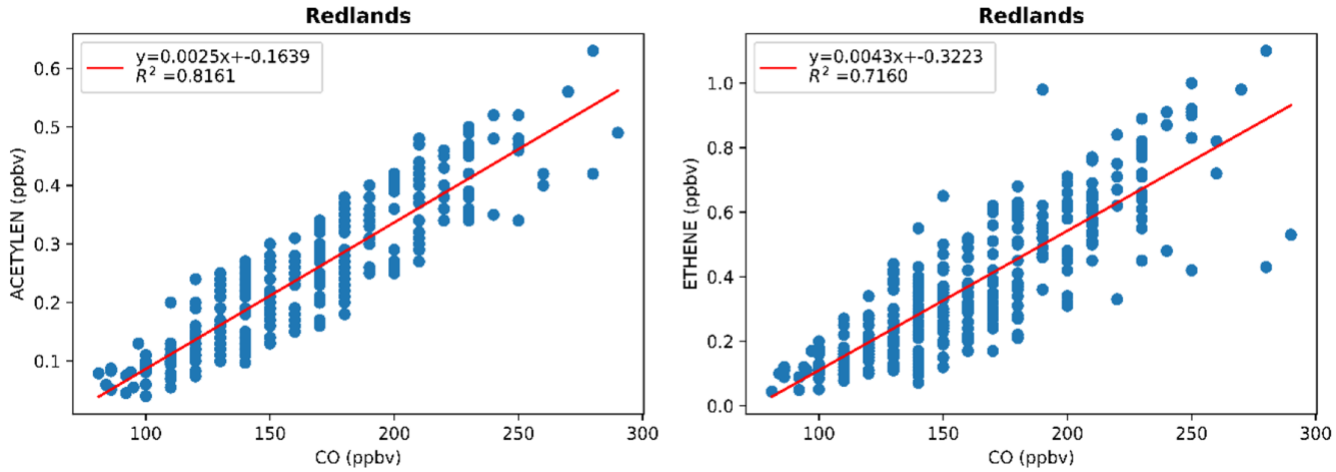

Figure 9. Predicted relationship between (a) acetylene and CO and (b) ethene and CO in Redlands, CA.

The VOC measurement in Redlands did not include compounds in the ALK1 and ALK2 lumped species that contain important short-chain alkanes (primary Ethane for ALK1, and Propane for ALK2). CTM predictions of ALK1 and ALK2 in Redlands were therefore estimated using measured compounds within the ALK3 lumped species based on the predicted relationships shown in Figure 10.

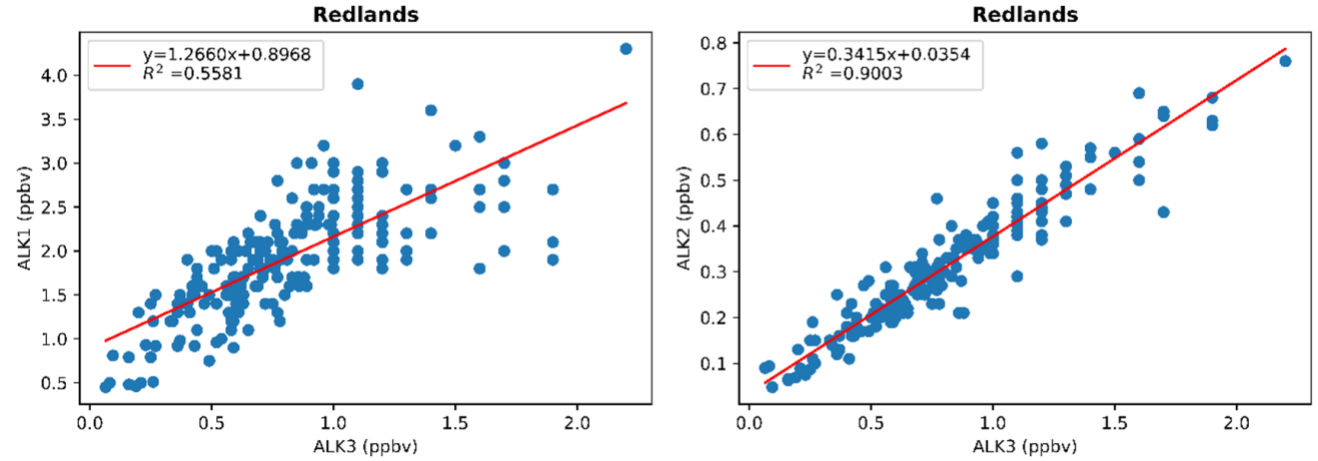

Figure 10. Predicted relationship between (a) ALK1 and ALK3 and (b) ALK2 and ALK3 in Redlands, CA.

TERP is the lumped species to represent all monoterpenes in SAPRC11. Only a single monoterpene (α-pinene) was measured in Redlands using PTR-MS. The ratio of total monoterpenes to α-pinene measured in Pasadena (~10) was used to scale day-specific α-pinene to TERP concentrations in Redlands.

PTR-MS measurements of ISOPRENE, TERP, and methyl vinyl ketone (MVK) are only available for limited days in the current study. Emission rates for these biogenic compounds are highly dependent on ambient

temperature. Figure 11 displays this non-linear relationship based on PTR-MS measurements in the current study. The best-fit curves illustrated in Figure 11 were used to predict concentrations of ISOPRENE, TERP, and MVK on days when PTR-MS measurements were not available.

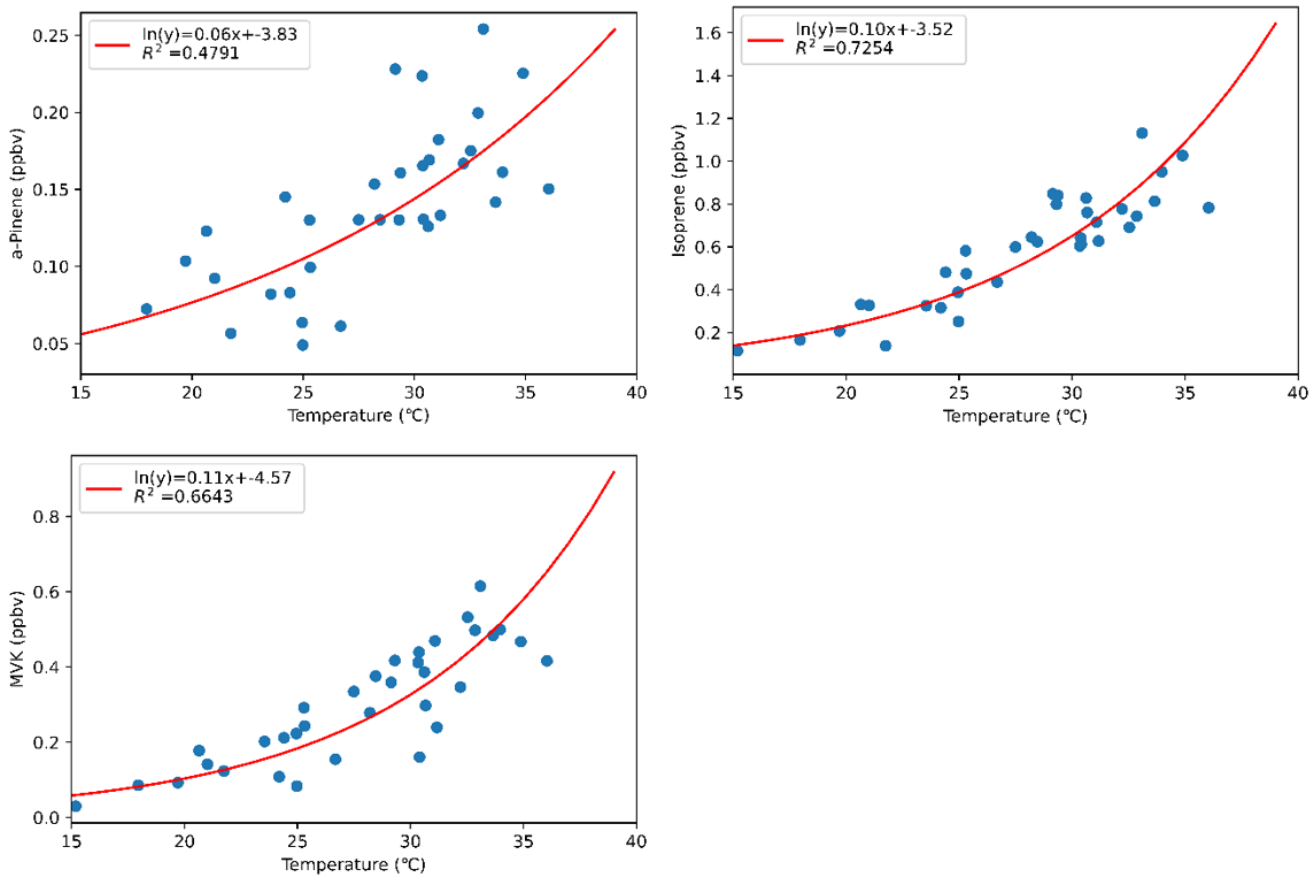

Figure 11. Relationship between temperature and (a) α-pinene, (b) isoprene, and (c) methyl vinyl ketone measured using PTR-MS.

A full list of measured VOC compounds, and their assigned SAPRC11 species in Pasadena and Redlands is included in Table 2 and Table 3. Concentrations for lumped VOC species are calculated based on the sum of all the measured individual VOC species in the lumped category.

Table 2. List of VOCs measured in the Pasadena site, the statistics of the mixing ratio (minimum, maximum, median, mean, standard deviation) and the group name in SAPRC11.

	Compounds	Min	Max	Median	Mean	std	SAPRC
Alkanes							
	Ethane	1.799717	13.11953	4.95875	5.432181	2.70921	ALK1

	Compounds	Min	Max	Median	Mean	std	SAPRC
	Propane	0.72965	5.223117	1.800571	2.058937	1.11373	ALK2
	n-Butane	0.300783	2.138325	0.584	0.685034	0.38843	ALK3
	Isobutane	0.154183	1.0126	0.339238	0.40821	0.20044	ALK3
	n-Pentane	0.13635	0.995525	0.283853	0.331119	0.18775	ALK4
	Isopentane	0.225117	2.5073	0.513368	0.659446	0.47827	ALK4
	Cyclopentane	0.012333	0.110425	0.027978	0.03409	0.02182	ALK4
	2,2-Dimethylpropane	0.00366	0.03195	0.00888	0.01052	0.00654	ALK2
	n-Hexane	0.091417	0.58775	0.193258	0.254978	0.141333	ALK4
	Cyclohexane	0.021583	0.203825	0.04916	0.057511	0.040332	ALK5
	2-Methylpentane	0.0583	0.388175	0.125483	0.139227	0.076567	ALK4
	3-Methylpantane	0.053983	0.35995	0.109288	0.133709	0.07295	ALK4
	2,2-Dimethylbutane	0.01285	0.11235	0.02639	0.034334	0.022573	ALK4
	Methylcyclopentane	0.0802	0.48955	0.155475	0.188439	0.100726	ALK4
	n-Heptane	0.021683	0.16195	0.05646	0.068693	0.038524	ALK4
	2,4-Dimethylpentane	0.022	0.148883	0.055925	0.064377	0.035129	ALK4
	Methylcyclohexane	0.016267	0.135717	0.044175	0.055578	0.032744	ALK5
	n-Octane	0.013683	0.15255	0.044233	0.051499	0.033318	ALK5
	C8 cycloalkanes	0.008081	0.068459	0.021838	0.024318	0.012065	ALK5
	2-Methylheptane	0.013817	0.131775	0.041858	0.051188	0.031542	ALK5
	3-Methylheptane	0.0096	0.0863	0.026292	0.033092	0.020267	ALK5
	2,2,4-Trimethylpentane	0.0513	0.3247	0.132125	0.147265	0.076218	ALK3
	2,3,4-Trimethylpentane	0.01335	0.11995	0.038108	0.047424	0.029371	ALK4
	n-Nonane	0.007867	0.1262	0.030333	0.034291	0.025528	ALK5
	n-Decane	0.025117	0.21815	0.061442	0.071773	0.043523	ALK5
Alkenes							
	Ethene	0.357783	2.111517	0.736208	0.882529	0.470922	ETHENE

	Compounds	Min	Max	Median	Mean	std	SAPRC
	Acetylene	0.381833	1.6411	0.656017	0.736061	0.300278	ACETYLEN
	Propene	0.04915	0.439125	0.127165	0.14501	0.085116	OLE1
	1-Butene	0.008283	0.0887	0.017475	0.022894	0.01671	OLE1
	cis-2-Butene	0.00115	0.0249	0.003317	0.004754	0.005073	OLE1
	trans-2-Butene	0.00136	0.014283	0.003325	0.00402	0.002909	OLE2
	1,3-Butadiene	0.00175	0.046125	0.00966	0.010892	0.008879	OLE2
	1-Pentene	0.00365	0.039325	0.007205	0.009879	0.007326	OLE1
	cis-2-pentene	0.0005	0.00875	0.001783	0.0022	0.001769	OLE1
	trans-2-Pentene	0.00058	0.0139	0.003108	0.003693	0.002874	OLE2
	2-Methyl-1-butene	0.003183	0.03275	0.007575	0.009456	0.006352	OLE2
	2-Methyl-2-butene	0.0036	0.020825	0.007342	0.009111	0.005063	OLE2
	3-Methyl-1-butene	0.00165	0.0237	0.004015	0.00527	0.004408	OLE1
	Hexadienes	0.032423	0.224865	0.075441	0.083483	0.038926	OLE2
Aromatics							
	Benzene	0.0768	0.569153	0.196844	0.214839	0.099265	BENZENE
	Toluene	0.148162	1.322297	0.337863	0.430715	0.257631	ARO1
	Xylenes and Ethylbenzene	0.074432	0.688	0.181775	0.224783	0.131186	ARO1
	Styrene	0.003224	0.136142	0.014276	0.024067	0.031125	OLE2
	C9 aromatics	0.032658	0.268595	0.075578	0.088528	0.049908	ARO1
	Indane, MethylStyrene, propenyl benzene, methyl ethenyl benzene	0.001705	0.04821	0.004689	0.010637	0.012181	ARO2
	C10 aromatics	0.010631	0.082604	0.024847	0.029079	0.015557	ARO2
	Tetrahydronaphthalene	0.003865	0.024523	0.008714	0.009848	0.004876	ARO2
	methyl naphthalene	0.001934	0.026883	0.005274	0.008061	0.006206	ARO2
	Benzonitrile	0.001752	0.011784	0.003469	0.00455	0.002838	ARO1

	Compounds	Min	Max	Median	Mean	std	SAPRC
	benzothiazole	0.00418	0.029523	0.012111	0.012355	0.005391	ARO1
Biogenic-related VOCs							
	Methacrolein (MAC)	0.032533	1.4509	0.445767	0.499263	0.399223	MACR
	Methyl vinyl ketone (MVK)	0.03304	2.16606	0.47835	0.569802	0.517401	MVK
	Isoprene	0.338291	5.008459	2.170406	2.285412	1.310086	ISOPRENE
	Monoterpenes	0.07885	0.45045	0.168667	0.186419	0.085687	TERP
	α-Pinene	0.004633	0.0881	0.017683	0.023342	0.01767	NaN
	β-Pinene	0.00225	0.04235	0.009242	0.012412	0.008867	NaN
OVOCs							
	Nitromethane	0.002505	0.020117	0.009198	0.008361	0.00378	NROG
	Methanol	2.462593	12.23888	5.603631	5.870127	2.3691	MEOH
	Formic Acid	1.436535	8.153899	3.128441	3.357751	1.653584	HCOOH
	Formamide	0.034527	0.241019	0.078375	0.087325	0.045427	NROG
	Methyl nitrate	0.028767	0.081767	0.051383	0.053655	0.014558	NROG
	Nitromethane	0.0237	0.09935	0.056127	0.059029	0.023238	NROG
	Ethanol	3.838818	29.41297	8.791394	10.10755	5.162942	ETOH
	Acetaldehyde	1.026291	9.530324	3.492468	3.634008	1.74977	CCHO
	Acetic Acid	0.939109	4.710072	2.167346	2.276082	0.913622	CCOOH
	Hydroxy Or Peroxyacetic Acid	0.100077	0.304009	0.16967	0.17628	0.057284	RCOOH
	Etheneamine	0.002215	0.020279	0.006915	0.008017	0.004742	ALK5
	Acetonitrile	0.146615	0.59618	0.262621	0.294334	0.115817	NROG
	Acetamide	0.028257	0.104802	0.049288	0.054457	0.02091	ALK5
	Methyl Isocyanate, Hydroxy Acetonitrile, Glycolonitrile	0.003602	0.010081	0.005786	0.006059	0.001792	ALK5
	Ethyl nitrate	0.007833	0.0252	0.015062	0.015101	0.004497	ALK2

Compounds	Min	Max	Median	Mean	std	SAPRC
Peroxyacetyl nitrate (PAN)	0.099601	1.781545	0.797427	0.869416	0.464937	PAN
Isopropanol	0.3243	6.92145	0.656675	0.924668	1.255235	ALK4
Acrolein, Hexenal Fragment	0.096297	0.720712	0.284531	0.281929	0.134038	MACR
Acetone	2.694317	11.36173	5.698175	6.171351	2.426566	ACET
Propanoic Acid, Hydroxyacetone, Methyl Acetate, Ethyl Formate, Methoxy Acetaldehyde	0.240545	1.694505	0.767358	0.79962	0.359373	RCOOH
Propanoic Acid water cluster	0.0214	0.107775	0.055452	0.052818	0.020916	RCOOH
Hydroxy Or Peroxypropanoic Acid	0.031036	0.160189	0.083442	0.08393	0.029651	RCOOH
C3 Amides	0.009739	0.043198	0.017216	0.019075	0.006909	ALK5
Nitropropenes, Oxazolidone	0.002451	0.017667	0.007205	0.007511	0.00349	OLE1
Isopropyl nitrate	0.007083	0.041183	0.023683	0.022656	0.009653	ALK4
n-Propyl nitrate	0.00315	0.0139	0.0077	0.007891	0.002965	ALK4
Peroxy propionyl nitrate (PPN)	0.013508	0.215086	0.109963	0.102535	0.053464	PAN2
C4 Alcohol Water Cluster	0.00201	0.049571	0.005705	0.008832	0.011116	ALK5
Butane Diols, C4 Carbonyl Water Cluster	0.031564	0.282766	0.08566	0.097207	0.051723	ALK5
C4 Acid Water Cluster	0.008836	0.048856	0.025661	0.024295	0.00951	RCOOH
C4 Tetrols	0.003	0.011757	0.00664	0.006822	0.002375	ALK5
Butanal And MEK	0.0013	1.421432	0.343559	0.386542	0.335033	MEK
Ethyl Acetate, Butryic Acid, Hydroxy Butanone, Acetoin	0.074255	0.690523	0.279837	0.320766	0.167255	ALK2
Hydroxy Or Peroxy Butanoic Acid	0.018109	0.101045	0.048739	0.050388	0.020114	RCOOH

Compounds	Min	Max	Median	Mean	std	SAPRC
Sum Of 2-3-Butanedione And Fragments	0.098527	0.626856	0.281404	0.292476	0.12054	BACL
Acetic Anhydride	0.016545	0.103658	0.047128	0.051491	0.020912	NROG
Malic Acid	0.002106	0.015216	0.006788	0.006813	0.002792	RCOOH
Furans	0.022018	0.163054	0.062577	0.068354	0.029982	ARO2
Sum Of 2-(3H)Furanone 2-(5H)Furanone And Fragments	0.026764	0.183559	0.086784	0.088151	0.033951	ARO2
C4 2-Oxy 4-Dbe	0.002067	0.032505	0.015404	0.01523	0.006866	OLE2
Maleic Anhydride	0.007623	0.07236	0.034948	0.032609	0.014123	OLE2
C2 Acetamides	0.002324	0.12784	0.005009	0.01076	0.023019	ALK5
2-Methyl-3-Buten-2-Ol	0.032418	0.250378	0.101441	0.105065	0.045811	OLE1
Pentane Diols	0.006582	0.048505	0.017644	0.020107	0.008993	ALK5
Pentanoic Acids, Methyl Butanonate	0.009036	0.068315	0.027637	0.026875	0.01233	RCOOH
Hydroxy Or Peroxy Pentanoic Acid	0.001091	0.040832	0.012963	0.016891	0.01165	RCOOH
C5 Ketones	0.029091	0.266667	0.099587	0.104051	0.049375	MEK
Methyl Methacrylate, Pentanedione, Propenyl Ester Acetic Acid , Acetylacetone	0.089655	0.54	0.240633	0.246387	0.098075	OLE2
C5 Di-Acids	0.004345	0.034784	0.016872	0.017549	0.006916	RCOOH
Sum 2-Methylfuran, 3-Methylfuran, Isomers, And Fragments	0.030091	0.268027	0.107294	0.112716	0.057592	ARO2
Methyl Furanone , Methanol Furan	0.0382	0.252027	0.131936	0.133922	0.054927	ARO1
Sum Of Furfural, Isomers, And Fragments	0.014559	0.102126	0.035463	0.03821	0.01699	ARO1
Hexanals, Hexanones	0.010088	0.070324	0.027058	0.028567	0.013019	MEK

Compounds	Min	Max	Median	Mean	std	SAPRC
Ethyl Butyrate, Isobutyl Acetate, Acids	0.008351	0.094283	0.022569	0.027445	0.017481	ALK4
C6 Hydroxy Or Peroxy Acid	0.00523	0.04173	0.016009	0.016552	0.007617	RCOOH
C6 Saturated Diols	0.001047	0.01501	0.002862	0.005501	0.004447	ALK5
C6 Diketone Isomers	0.034239	0.226973	0.103685	0.10264	0.043045	MEK
Dimethylfuranone	0.007028	0.051324	0.023658	0.024289	0.009416	OLE2
C6 Di-Acids	0.003527	0.018712	0.008425	0.008564	0.003499	RCOOH
Benzene Nitrophenol	0.002704	0.021117	0.011165	0.009752	0.004593	XYNL
C6 Diacids	0.0019	0.017208	0.007857	0.008625	0.003526	RCOOH
Phenol, Vinyl Furan	0.0302	0.160288	0.064575	0.074306	0.029504	PHEN
Dimethylfuranone	0.021681	0.149784	0.065947	0.065323	0.02696	ALK5
C6 Diacid	0.00413	0.026955	0.011624	0.011943	0.004714	RCOOH
Sum Of 2,5-Dimethylfuran (Dominant Isomer) 2-Ethylfuran And Fragments	0.016221	0.125829	0.056955	0.053191	0.022561	ARO2
Heptanal	0.005045	0.035784	0.013628	0.014704	0.007201	RCHO
Ethyl Cyclopentanone	0.009545	0.099423	0.034091	0.03753	0.018572	MEK
Allyl Ester Isobutyric Acid	0.013566	0.116829	0.045962	0.047796	0.022137	RCOOH
C3 Substituted Furan	0.007143	0.072586	0.023917	0.025691	0.01485	ARO1
Salicyladehyde	0.004704	0.035252	0.015101	0.016136	0.006138	BALD
Guaiacol, Propionylfuran , Acetylmethylfuran	0.011099	0.086726	0.035568	0.037477	0.018894	CRES
3-Methoxycatechol	0.0054	0.031721	0.014663	0.014792	0.006154	XYNL
C7 Diacids	0.002407	0.012721	0.006927	0.006894	0.002377	RCOOH
Benzaldehyde	0.020855	0.218802	0.050513	0.061533	0.043321	BALD
Octanal	0.026487	0.193099	0.06677	0.072466	0.035582	RCHO
Cyclooctanone	0.004126	0.067748	0.020465	0.022612	0.013455	MEK

	Compounds	Min	Max	Median	Mean	std	SAPRC
	C8 2-Oxy 3-Dbe	0.005212	0.036559	0.014339	0.015316	0.006824	ALK5
	C8 3-Oxy 3Dbe	0.001858	0.016252	0.006301	0.006656	0.003579	ALK5
	C4 Substituted Furan	0.005345	0.038414	0.015229	0.015712	0.007505	ARO1
	4-Ethylphenol	0.001703	0.025153	0.007083	0.007307	0.004576	XYNL
	Sum Of Creosol Isomers (Hydroxytoluene)	0.005883	0.038234	0.015622	0.016164	0.007173	CRES
	Syringol	0.002218	0.013234	0.006009	0.005982	0.002432	XYNL
	Phenyl Ester Of Acetic Acid	0.002642	0.015523	0.005192	0.006428	0.003428	ARO1
	Methyl Salicylate, Vanillin	0.003685	0.023829	0.009407	0.009865	0.004396	BALD
	Tolualdehyde	0.0088	0.070685	0.025604	0.027281	0.013536	BALD
	Phthalic Acid	0.001623	0.021225	0.008568	0.009191	0.004872	ARO1
	Phthalic Anhydride	0.001909	0.029622	0.012875	0.013082	0.006873	ARO1
	Nonanal	0.016694	0.153613	0.051761	0.055059	0.028141	RCHO
	C9 Carbonyl	0.002891	0.02773	0.009361	0.010041	0.005151	MVK
	Nopinone	0.006055	0.050739	0.019646	0.021796	0.011194	IPRD
	C9 2-Oxy 4-Dbe	0.003956	0.026523	0.010346	0.010629	0.004802	ARO1
	3-Methylacetophenone	0.002782	0.029559	0.008826	0.010275	0.00563	MEK
	Linalool, Borneol, Citronellal, Eucalyptol, Others	0.002486	0.019505	0.006909	0.007319	0.003661	OLE2
	Pinonaldehyde	0.00315	0.022991	0.00877	0.008949	0.004214	RCHO
	Apinene Oxide	0.006956	0.039892	0.014522	0.017011	0.007631	OLE2
	C10 2-Oxy 4-Dbe	0.002035	0.014694	0.006044	0.006167	0.002746	ARO1
	Pinonaldehyde	0.002903	0.023613	0.009074	0.009416	0.004846	RCHO
	Texanol	0.010099	0.105847	0.032856	0.034388	0.018917	ALK5
Halogenated VOCs							
	Dichloromethane	0.1107	0.771483	0.230958	0.308336	0.184981	ALK1

	Compounds	Min	Max	Median	Mean	std	SAPRC
	Chloroform	0.023067	0.112	0.050692	0.054515	0.021486	NROG
	CFC-11	0.019569	0.040874	0.027805	0.029492	0.005074	NROG
	Trichlorofluoromethane	0.147933	0.3552	0.199183	0.209849	0.050726	NROG
	1,2-Dichloroethane	0.013867	0.021367	0.01665	0.01644	0.002277	ALK1
	1,1-Dichloroethene	0.0001	0.00155	0.000267	0.00035	0.000283	ALK3
	dichloroethene	0.009418	0.025541	0.013931	0.014142	0.002903	NROG
	Trichloroethene	0.001433	0.022333	0.004313	0.005525	0.004425	NROG
	Tetrachloroethene	0.009267	0.043	0.020871	0.020718	0.00815	NROG
	1,2-Dichlorotetrafluoroethane	0.01128	0.027425	0.01675	0.01725	0.004185	NROG
	1,1,2-Trichlorotrifluoroethane	0.050567	0.119475	0.071225	0.074908	0.017573	NROG
	p-dichlorobenzene	0.001127	0.026279	0.007477	0.008336	0.005021	ARO1
	Parachlorobenzotrifluoride (PCBTF)	0.024345	0.233459	0.073266	0.085612	0.049349	NROG
Others							
	Carbon disulfide	0.003867	0.028175	0.007717	0.00935	0.00546	NROG
	Acetonitrile	0.146615	0.59618	0.262621	0.294334	0.115817	NROG
	butanenitrile	0.001883	0.026547	0.005628	0.006123	0.004414	ALK5
	pyridine	0.007212	0.032766	0.013143	0.015682	0.007604	ARO1
	D4-siloxane	0.003686	0.028171	0.008775	0.009242	0.00492	NROG
	D5-siloxane	0.013164	0.100414	0.032453	0.035915	0.018901	NROG

Table 3. List of VOCs measured in Redlands site, the statistics of the mixing ratio (minimum, maximum, median, mean, standard deviation) and the group name in SAPRC11.

Compounds	Min	Max	Median	Mean	Std	SAPRC
Alkanes						

	Compounds	Min	Max	Median	Mean	Std	SAPRC
	n-Butane	0.068	1.988273	0.447064	0.514378	0.294419	ALK3
	Isobutane	0.007	0.925545	0.301045	0.30115	0.16785	ALK3
	n-Pentane	0.002	0.435455	0.1039	0.123181	0.086519	ALK4
	Isopentane	0.025	1.180455	0.399773	0.424395	0.257717	ALK4
	n-Hexane	0.32352	7.34944	1.2056	1.592633	1.470749	ALK4
	Isohexane	0.028371	1.23013	0.413533	0.427202	0.266424	ALK4
	n-Heptane	0.06976	0.370944	0.12752	0.145852	0.066723	ALK5
Alkenes							
	Propylene	0.182	2.198545	0.44655	0.575347	0.40116	OLE1
	1-Butene + Isobutylene	0.089	0.768	0.2441	0.273321	0.122436	OLE1
	1,3-Butadiene	0.00096	0.111253	0.03152	0.036356	0.03934	OLE1
	cis-2-Pentene	0.0039	0.0378	0.012	0.013263	0.006356	OLE2
Aromatics							
	Benzene	0.20192	1.258676	0.3736	0.44583	0.240305	BENZENE
	Toluene	0.04128	1.259898	0.361047	0.381083	0.241457	ARO1
	p-Butylm	0.006944	0.18752	0.066385	0.073347	0.042715	ARO2
	o-Butylo	0.00608	0.140509	0.052131	0.055634	0.032725	ARO2
	Ethylbenzene	0.00608	0.149062	0.057018	0.059489	0.035521	ARO1
	1,2,4-Trimethylbenzene	0.02528	0.12992	0.03584	0.041465	0.021348	ARO2
	4-Butyl4-ethyltoluene	0.00352	3.850967	0.67088	0.850876	0.82396	ARO2
	n-Butylbenzene	0.0032	0.045696	0.005264	0.008218	0.008721	ARO1
	tert-Butylbenzene	0.001344	0.119467	0.014187	0.024733	0.030148	ARO1
	Propylbenzene	0.00352	0.031564	0.012768	0.014437	0.007313	ARO1
	Isopropylbenzene	0.092288	0.33152	0.14308	0.15356	0.061809	ARO1
	Styrene	0.00736	0.08736	0.01408	0.017167	0.014343	ARO2
	p-Cymene	0.00544	0.04032	0.01008	0.011539	0.006275	ARO2

	Compounds	Min	Max	Median	Mean	Std	SAPRC
	Naphthalene	0.00608	0.06888	0.026656	0.028192	0.01245	ARO2
	1-Methylnaphthalene	0.001037	0.009507	0.001695	0.002094	0.001272	ARO2
	2-Methylnaphthalene	0.001688	0.011641	0.002985	0.003326	0.001541	ARO2
	Azobenzene	0.046043	0.17365	0.065514	0.072526	0.026339	ARO1
Biogenic-related VOCs							
	Isoprene*	0.114864	1.131562	0.624298	0.58873	0.259808	ISOPRENE
	α-Pinene*	0.048977	0.254069	0.133166	0.141292	0.054529	TERP
	Limonene	0.01472	0.26768	0.03264	0.050748	0.052751	TERP
	Methyl vinyl ketone (MVK)*	0.030149	1.539817	0.297522	0.335372	0.259159	MVK
OVOCs							
	Methanol	0.15904	1307.242	57.35072	144.7257	233.8232	MEOH
	Ethanol	0.18	26.81	5.26	5.947569	6.0392	ETOH
	2-Propanol	64.72704	445.984	84.7168	142.9751	119.4396	ALK4
	Benzyl alcohol	0.02432	0.133728	0.0368	0.041226	0.020182	ARO1
	Formaldehyde	0.78813	1.778982	1.134229	1.17516	0.24017	HCHO
	Acetaldehyde	0.324096	1.041042	0.586452	0.591849	0.164294	CCHO
	Propanal	0	0.144011	0.0747	0.078063	0.023601	RCHO
	Butanal	0.036456	0.127183	0.049973	0.057509	0.020424	RCHO
	Hexanal	0.054679	0.881462	0.162502	0.226448	0.181965	RCHO
	3-Methylbutyraldehyde	0.025686	0.272158	0.068093	0.08278	0.048318	RCHO
	Acrolein	0.001071	0.006071	0.002052	0.002319	0.001292	MACR
	Bis(2-chloroethyl) ether	0.003422	0.189037	0.012253	0.021699	0.030913	ALK5
	Bis(2-chloroethoxy)methane	0.022526	0.144053	0.052346	0.057154	0.023523	ALK5
	Benzaldehyde	0.029444	0.59724	0.202726	0.203183	0.159685	BALD
	m,p-Tolualdehyde	0.001164	0.00345	0.001913	0.001923	0.000493	BALD
	Phenylacetaldehyde	0.116574	0.391765	0.188194	0.206019	0.069635	BALD

	Compounds	Min	Max	Median	Mean	Std	SAPRC
	Acetone	10.81035	52.03983	15.62261	20.88379	10.97754	ACET
	2-Butanone	0.111926	0.282303	0.115936	0.136071	0.049742	MEK
	Methyl ethyl ketone (MEK)*	0.000335	8.798581	0.005774	0.812687	1.980416	MEK
	Cyclohexanone	0.000714	0.007381	0.002381	0.002642	0.001247	PROD2
	Methyl acetate	0.039936	0.951998	0.28404	0.305855	0.207319	ALK2
	n-Butyl acetate	0.009785	0.695099	0.139777	0.173739	0.132866	ALK2
	Phenol	0.157264	0.924313	0.401992	0.436592	0.172924	PHEN
	2,4-Dimethylphenol	0.00614	0.035083	0.018828	0.017834	0.006468	XYNL
	m-Cresol	0.005161	0.035118	0.011122	0.016393	0.010586	CRES
	o-Cresol	0.000151	0.072336	0.00438	0.009799	0.012413	CRES
	p-Cresol	0.004587	0.286562	0.076542	0.074758	0.056216	CRES
	Isophorone	0.000688	0.101506	0.010387	0.013025	0.012707	IPRD
	Nitrobenzene	0.070613	0.542836	0.201344	0.205022	0.099087	NROG
	2-Nitrophenol	0.027022	0.066699	0.0293	0.034854	0.013076	NPHE
	Dibenzofuran	0.004087	0.027442	0.004512	0.005576	0.003624	ARO1
	Diethylphthalate	0.014369	0.688478	0.216091	0.251654	0.193044	ARO1
	Dimethylphthalate	0.006976	0.035242	0.007838	0.010925	0.00833	ARO1
	N-Nitrosodipropylamine	0.048528	1.085604	0.134289	0.209601	0.200514	NROG
	N-Nitrosodimethylamine	0.00727	0.343626	0.038766	0.068913	0.072412	NROG
Halogenated VOCs							
	Carbon Tetrachloride	0.019264	0.19656	0.076949	0.081524	0.029674	NROG
	Chloroform	0.009775	0.078604	0.025689	0.030125	0.016263	NROG
	Dichloromethane	0.054432	0.469789	0.13088	0.153147	0.079494	ALK1
	Dichlorodifluoromethane	0.0756	1.2992	0.437818	0.461654	0.158426	NROG
	Bromochloromethane	0.00032	0.04256	0.010052	0.014313	0.013473	ALK1
	Bromodichloromethane	0.0016	0.03584	0.003808	0.006786	0.007277	NROG

	Compounds	Min	Max	Median	Mean	Std	SAPRC
	Chlorodibromomethane	0.00064	0.007331	0.00224	0.002313	0.001157	NROG
	Trichlorofluoromethane	0.0592	0.73528	0.257193	0.28536	0.117083	NROG
	Bromoform	0.00224	0.006272	0.0032	0.003498	0.000933	NROG
	1,1,1,2-Tetrachloroethane	0.00096	0.0112	0.00336	0.003902	0.002236	NROG
	1,1,1-Trichloroethane	0.000747	0.00512	0.00256	0.00261	0.000966	ALK1
	1,1,2,2-Tetrachloroethane	0.00224	0.0336	0.006613	0.011618	0.009843	NROG
	1,1,2-Trichloroethane	0.00224	0.04704	0.02768	0.024988	0.015855	NROG
	CFC-113	0.03136	0.21336	0.082575	0.089841	0.031448	NROG
	Dichlorotetrafluoroethane	0.00224	0.04536	0.018124	0.019155	0.006138	NROG
	Trichloroethene	0.00096	0.01792	0.00336	0.004481	0.003825	ALK3
	Tetrachloroethylene	0.0016	0.016698	0.007648	0.007595	0.00324	NROG
	Allyl chloride	0.166507	17.0992	1.11272	3.701834	5.50138	ALK2
	(Z)-1,3-Dichloropropene	0.002016	0.0112	0.00448	0.005164	0.002549	ALK5
	1,1-Dichloropropene	0.50752	3.71168	0.712	1.066276	0.898547	ALK5
	4-Chloro-3-methylphenol	0.003458	0.128734	0.056548	0.059944	0.033928	XYNL
	1,2-Dichloropropane	0.0032	0.03808	0.007253	0.00929	0.007837	ALK2
	1,2,3-Trichloropropane	0.010453	0.02688	0.01736	0.017917	0.005676	ALK2
	1,3-Dichloropropene	0.0016	0.0112	0.004256	0.005005	0.002728	ALK5
	Chlorobenzene	0.01248	0.13216	0.030342	0.035776	0.028105	ARO1
	1,2-Dichlorobenzene	0.000163	0.036051	0.005772	0.009671	0.008886	ARO1
	1,3-Dichlorobenzene	0.000442	0.012228	0.004397	0.004672	0.002398	ARO1
	1,4-Dichlorobenzene	0.000325	0.097207	0.004713	0.015633	0.02453	ARO1
	PCBTF	0.000489	0.050549	0.0134	0.01564	0.010838	NROG
Others							
	Acetonitrile*	0.116745	0.285546	0.17229	0.176158	0.035255	NROG
	Acrylonitrile*	0.000014	0.010235	0.000014	0.001235	0.002576	NROG

Compounds	Min	Max	Median	Mean	Std	SAPRC
D4-siloxane	0.00832	0.076608	0.04192	0.041241	0.020888	NROG
D5-siloxane	0.00096	0.3536	0.141527	0.14353	0.07669	NROG

2.3 Results

2.3.1 Time Series of Relative Humidity (RH) and Temperature

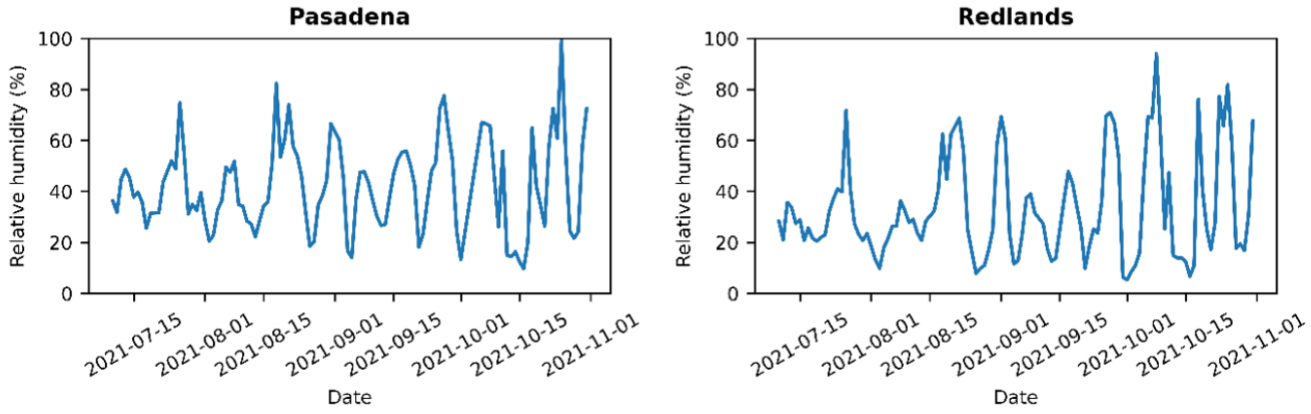

Figure 12. Time series of daily ambient relative humidity in Pasadena and Redlands, CA averaged between 10 AM and 12 PM from July to October 2021.

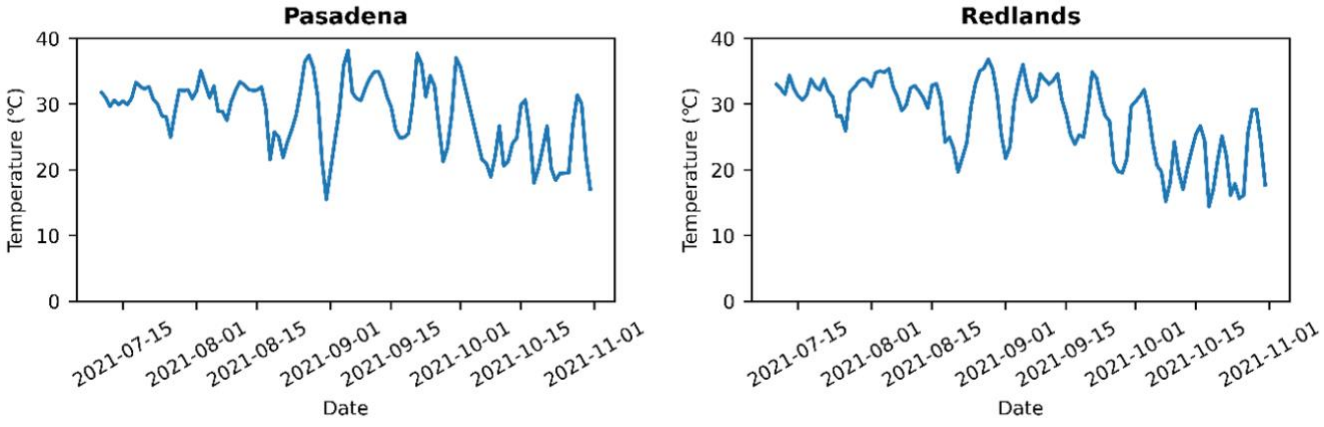

Figure 13. Time series of daily ambient temperature in Pasadena and Redlands, CA averaged between 10 AM and 12 PM from July to October 2021. Data source: https://www.arb.ca.gov/aqmis2/aqmis2.php.

Figure 12 and Figure 13 show the measured time series of relative humidity (RH) and temperature in Redlands and Pasadena between July and October 2021. The RH and temperature at the two sites have similar range and seasonal patterns. Peak daily temperatures declined noticeably starting in mid-September during the transition to the fall season. Corresponding RH increased over this period. Decreasing temperature is expected to reduce biogenic VOC emissions and evaporative emissions of semi-volatile organic compounds (SVOCs) (e.g., from motor vehicles). Decreasing temperature will also decrease gas-phase chemical reaction rates.

2.3.2 Time Series of Ambient NOx and O3

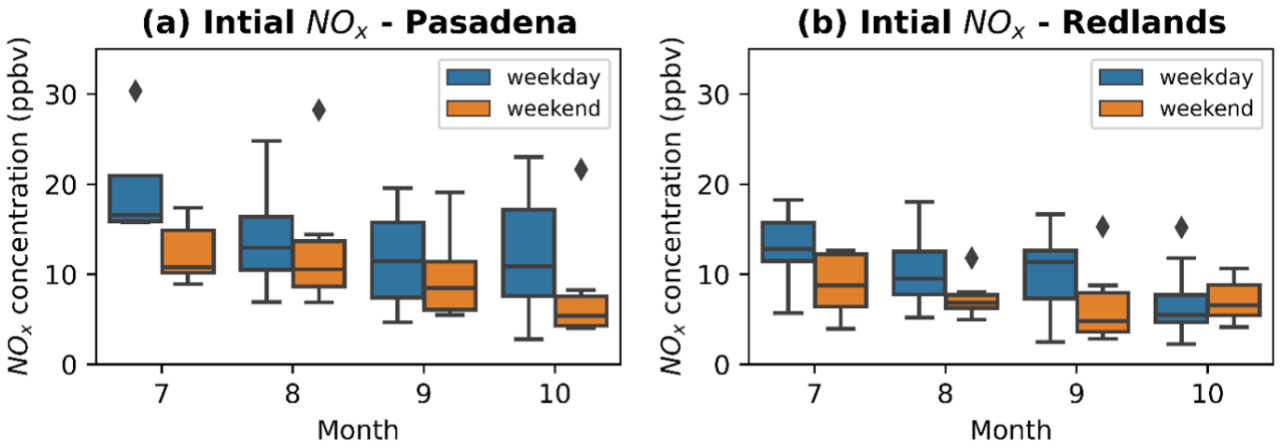

Figure 14. Monthly trend of daily initial NO_x concentration in base case chamber in Pasadena and Redlands, CA from July to October 2021. Ambient NO_x concentrations were measured in smog chamber systems in Pasadena and Redlands. The box shows the quartiles and median of the dataset, whiskers show the maximum and minimum of the dataset excluding outliers shown as diamonds. (same for the following boxplot).

Figure 14 shows initial ambient NO_x concentrations and final base case chamber O_3 concentrations measured in chamber systems in Pasadena and Redlands. Initial NO_x concentrations were ambient NO_x measurements averaged between 10 AM and 12 PM. Traffic emissions have a large impact on ambient NO_x concentration in the SoCAB (*35*, *36*). The diurnal patterns of measured NO_x concentrations (Figure 13) suggest that partially diluted emissions from traffic influenced initial chamber NO_x concentrations in the current study. NO_x concentrations had greater variability and higher peak values in Pasadena (range from 5–30 parts per billion by volume [ppbv]) than in Redlands (below 20 ppbv) (Figure 1). Previous studies have also observed higher NO_x concentrations in Pasadena than Redlands (*15*, *37*).

A strong weekday/weekend pattern was observed for NO_x concentrations. The weekend-to-weekday ratio (WE/WD) of initial NO_x was 0.79 in Pasadena and 0.87 in Redlands averaged across the entire measurement period. Redlands had higher median weekend NO_x concentrations in October, possibly because the atmosphere happened to be more stagnant on weekends than weekdays during three out of five weeks in this month. The effects of this stagnation were also observed in higher ambient temperature on weekends in October.

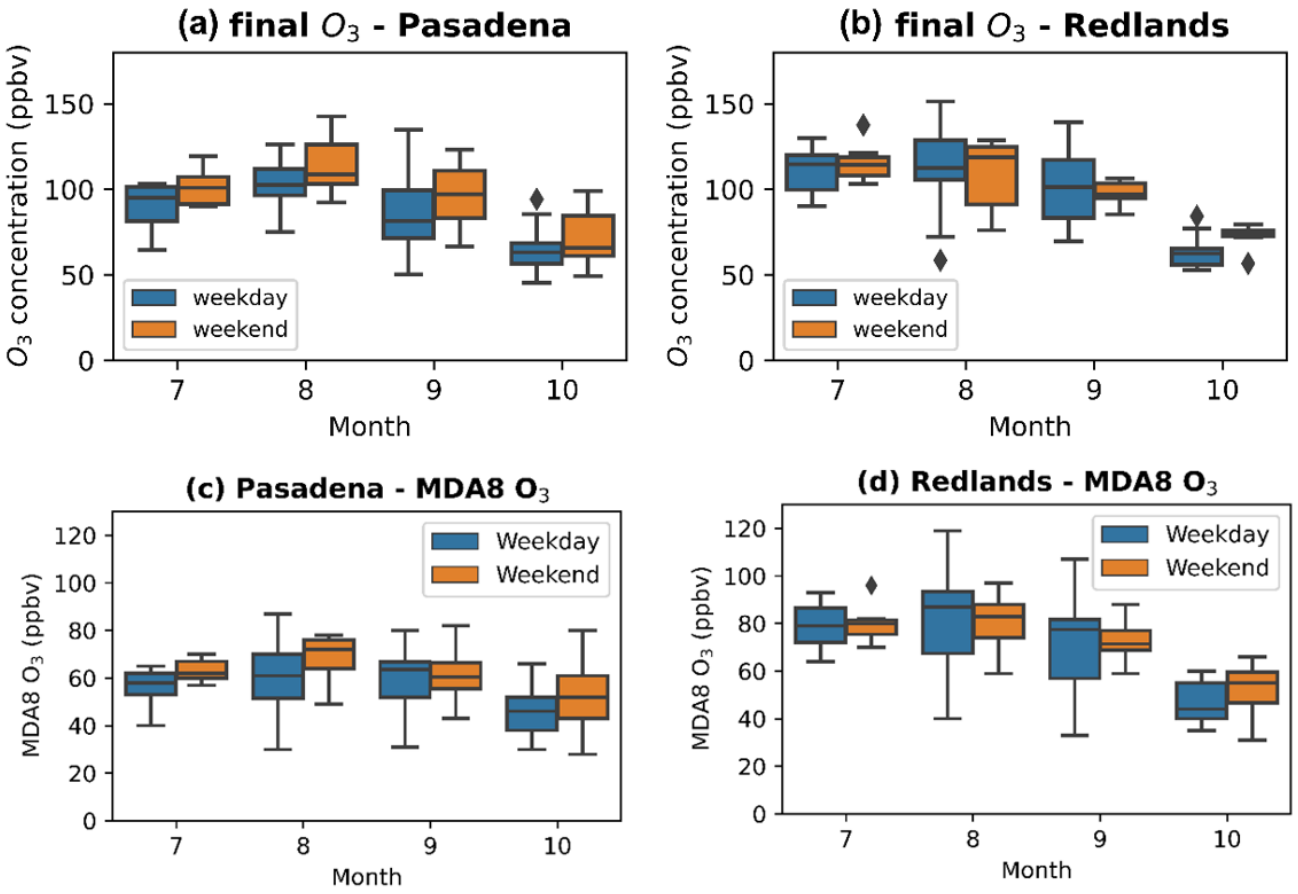

Figure 15. Monthly trend of final O_3 concentration in the base case chamber, and MDA8 O_3 concentrations in Pasadena and Redlands, CA, from July to October 2021. Data source: https://www.arb.ca.gov/aqmis2/aqmis2.php.

The final O_3 concentrations in the base case chamber were higher than ambient peak O_3 concentrations because atmospheric concentrations undergo dilution as the mixing height increases throughout the day. Chamber concentrations reflect the chemical production of O_3 from reactions of NO_x and VOCs drawn from the atmosphere between 10 AM and 12 PM. Measured final base case chamber O_3 concentrations in Redlands were greater than or equal to O_3 concentrations in Pasadena (Figure 15a and b). These chamber results are consistent with trends found in ambient O_3 measurements. Redlands has days with maximum daily 8-hour average (MDA8) O_3 larger than 90 ppbv, while all MDA8 O_3 concentrations measured in Pasadena were less than 90 ppbv (Figure 15c and d). Higher MDA8 O_3 in the downwind site (Redlands) partially reflects transport of O_3 and its precursors from upwind urban areas in addition to formation of O_3 from local emissions. The O_3 formation within the chamber system is driven by the reaction of VOCs either emitted locally or transported to the site from upwind sources during the preceding time period. Chamber experiments cannot account for pollutant transport on the day of the experiment that occurs after the fill period. The different initial NO_x concentrations in Redlands and Pasadena may also influence the chemical regime, which may lead to different

levels of O_3 production. A detailed discussion of the chamber perturbation measurements and the O_3 chemical regime is presented in Section 2.4; O_3 source apportionment calculations are presented in Section 2.5.3.

2.3.3 Time Series of Volatile Organic Compounds (VOCs)

The chemical regime for O_3 formation depends on the concentrations of VOCs that react to form peroxy radicals in the atmosphere. Three general categories of VOCs are suspected to play significant roles in O_3 formation in Southern California: biogenic volatile organic compounds (BVOCs) (plants), benzene / toluene / ethylbenzene / xylene (BTEX) compounds (mobile sources), and volatile chemical products (VCPs). Concentrations for specific compounds within each of these categories were measured using a combination of methods (see Section 2.2.3).

Species with statistically significant seasonal trends were identified using hypothesis tests applied to the results of the least squares linear regression with time as the independent variable and concentration as the dependent variable. Each test used a null hypothesis that the slope of the regression line was zero. Species with a significant seasonal trend had p-values less than 0.05.

Concentration trends for characteristic compounds in the BVOC, BTEX, and VCP categories are discussed in the following sections.

2.3.4 Time Series of Biogenic VOC (BVOC): Isoprene & Monoterpenes

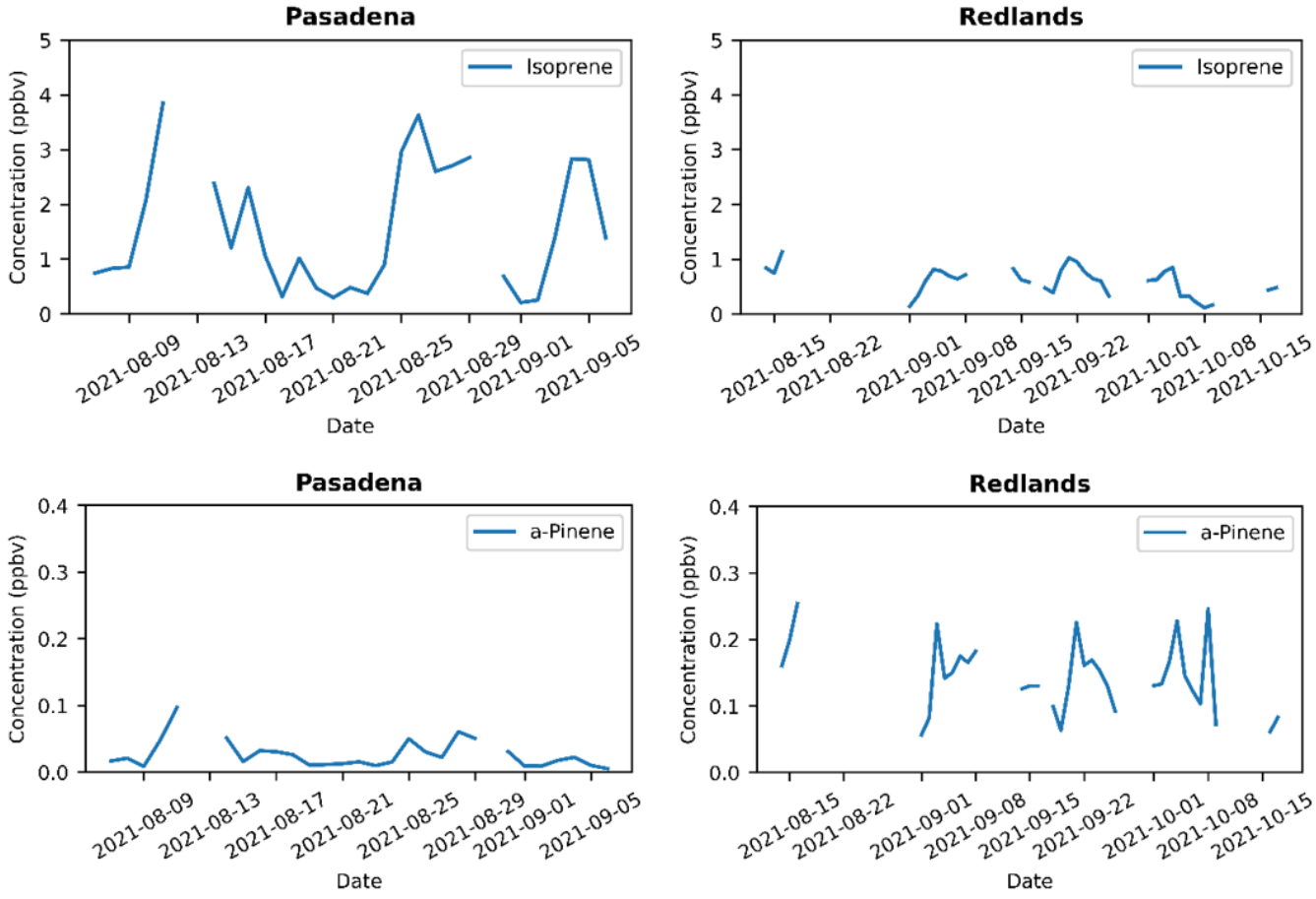

Figure 16. Time series of ambient BVOCs (isoprene, α-pinene) concentration in Redlands and Pasadena between 10 AM–12 PM. Redlands data is from PTR-MS, and Pasadena data is from GC-MS.

Figure 16 displays the time series of BVOC concentrations measured in Pasadena and Redlands. Isoprene concentrations in Pasadena were two to three times higher than isoprene concentrations measured in Redlands, while α-pinene concentrations measured in Pasadena were two to three times lower than α-pinene concentrations measured in Redlands. In general, α-pinene concentrations were an order of magnitude lower than isoprene concentrations. The difference in isoprene concentrations at the different sites may reflect the prominence of irrigated landscaping in Pasadena, as landscape plants can be an important source of BVOC emission in urban areas (*38*). These trends may also be caused by VOC aging in air masses as they are transported downwind from Pasadena to Redlands.

2.3.5 Time Series of BTEX

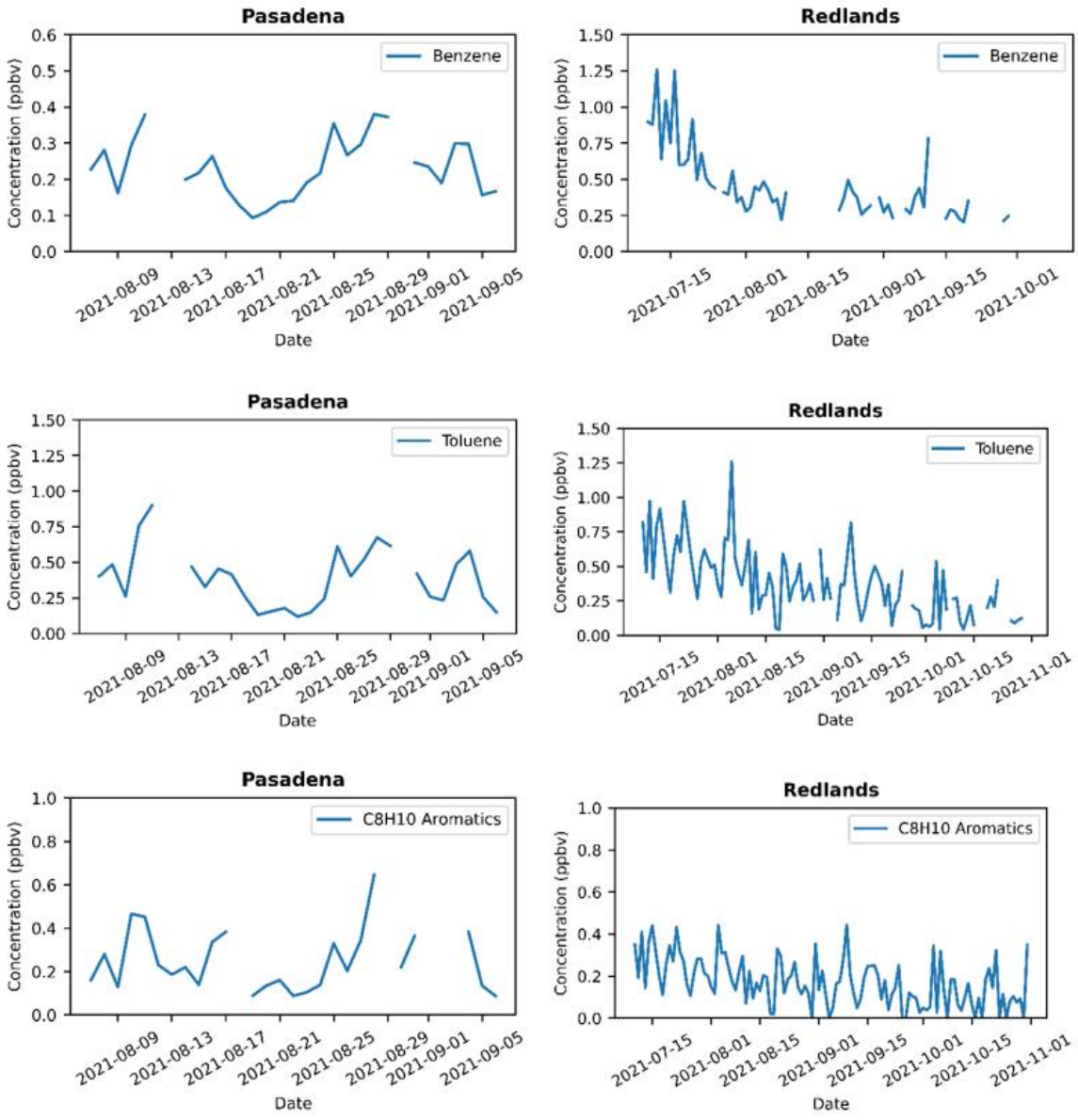

Figure 17. Time series of ambient BTEX concentration in Redlands and Pasadena between 10 AM–12 PM. Redlands benzene, toluene, ethylbenzene and xylenes data is from tube measurement, and Pasadena benzene, toluene data is from GC-MS, Pasadena ethylbenzene + xylenes data is from PTR-MS.

Figure 17 displays the time series of for BTEX compound concentrations in Pasadena and Redlands. VOC measurements in Pasadena are only available in August, so seasonal trends cannot be diagnosed at this site. Daily BTEX concentrations in Pasadena follow the trend of temperature that reflects evaporative losses (e.g., from gasoline used in vehicles). The time series of these emissions is similar to BVOC concentrations that also respond positively to increasing temperature.

Strong seasonal trends (p-value < 0.05) are apparent for BTEX concentrations in Redlands. The seasonal pattern for these compounds is qualitatively consistent with higher evaporative losses from motor vehicles in the middle of summer followed by decreasing evaporative losses as temperatures decrease in the fall.

The composition of gasoline used in California changes between summer and fall. Summer blends have lower concentrations of butane and other "light" compounds, to reduce evaporation during warm summer months. The butane content of gasoline increases during other seasons. Trends in BTEX concentrations did not exhibit a step-change during the transition from summer-blend gasoline to winter-blend gasoline, perhaps because BTEX concentrations are consistent in these blends. California sets limits for aromatics (25% by volume) and benzene (0.8% by volume) in Phase 3 Reformulated Gasoline (CaRFG3) (*39*). There is no evidence that the aromatic content of gasoline changes strongly between summer and winter blends. A previous study (*40*) showed that the toluene and xylene concentration in the headspace vapor of liquid gasoline changes by less than 10% between summer and winter blends.

2.3.6 Time Series of VCPs

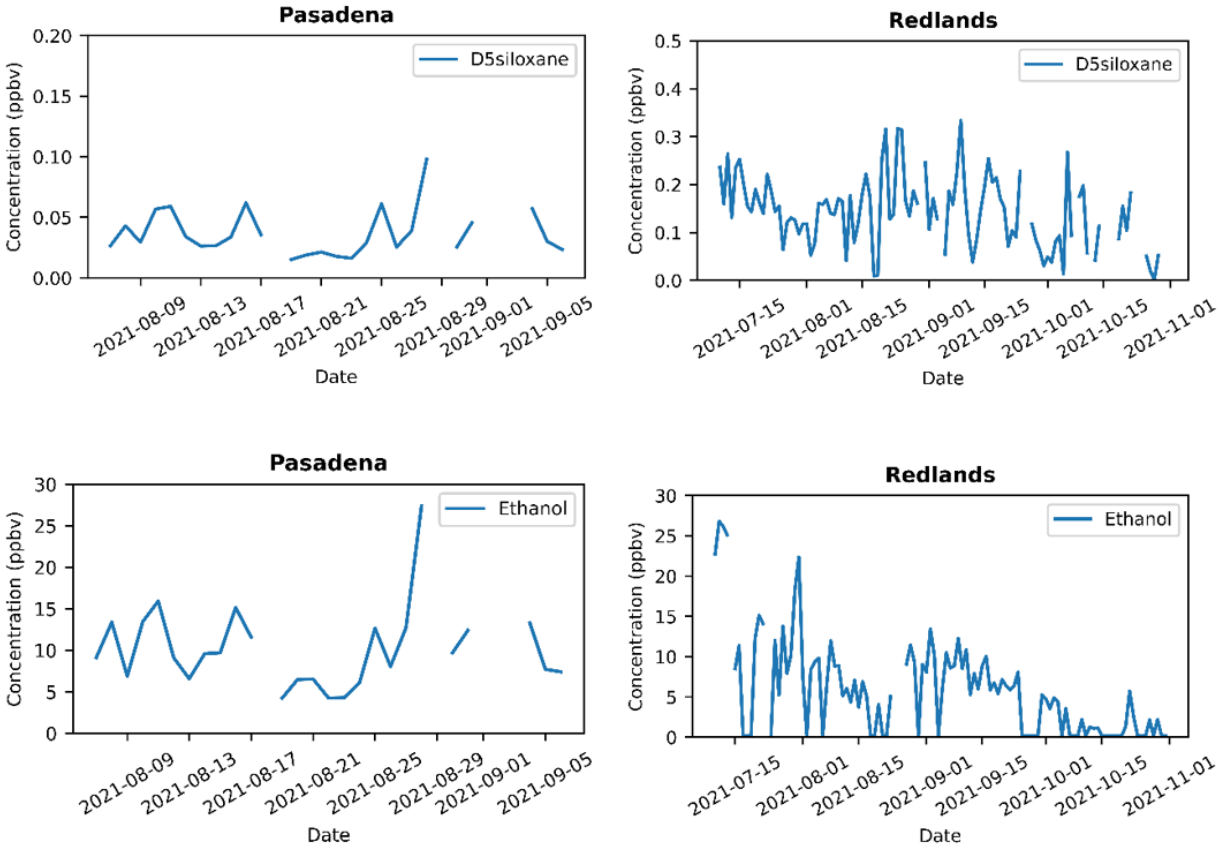

Figure 18. Time series of ambient D5-siloxane and ethanol concentration in Redlands and Pasadena between 10 AM–12 PM. Redlands D5-siloxane data is from tube measurement, and Pasadena D5-siloxane and ethanol data are from PTR-MS.

Figure 18 shows the time series of D5-siloxane and ethanol concentrations in Redlands and Pasadena. D5-siloxane is widely used as a tracer for VCPs (especially personal care products), and ethanol concentrations have been shown to have large contributions from VCPs (in addition to ethanol used in gasoline blends) (*12*, *41*). No seasonal trend is apparent in the D5-siloxane concentrations measured in Redlands, but ethanol followed a seasonal pattern of decreasing concentrations with temperature. The divergence of the trends suggests that ethanol and D5-siloxanes in Redlands may be influenced by different sources. Ethanol and D5-siloxane concentrations in Pasadena have similar trends, indicating that they may originate from the same source(s).

2.4 Chamber Measurement Results

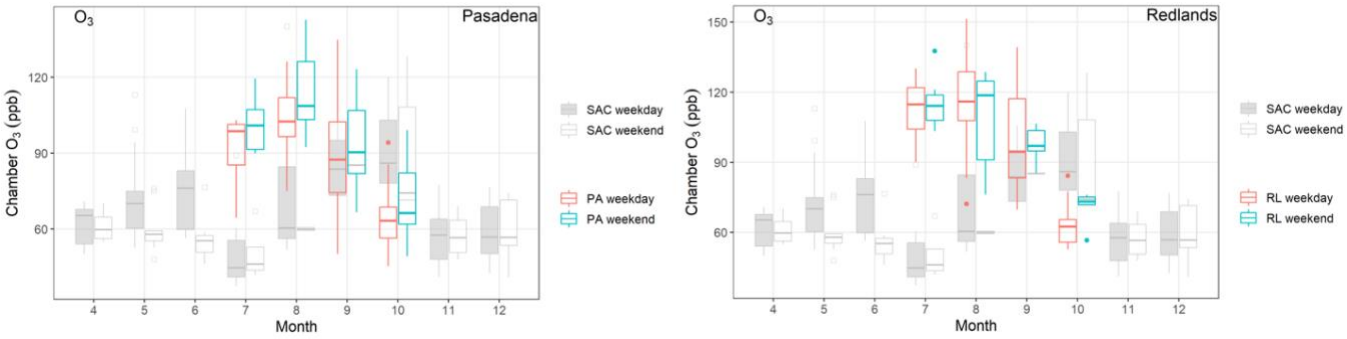

Figure 19. Time series of final O_3 concentrations in the base case chamber from daily chamber experiments in Pasadena and Redlands, CA from July to October 2021. The background box and whisker plot are the time series of measured O_3 sensitivity in Sacramento, CA in 2020 (*14*).

Figure 19 shows the final O_3 concentration in the base case chamber after three hours of UV exposure. Final O_3 concentrations in Pasadena were higher on weekends than on weekdays due the consistently NO_x-rich chemical regime at this site combined with lower NO_x concentrations on weekends. Final O_3 concentrations in Redlands were significantly higher on weekends than weekdays in October, suggesting that the chemical regime was NO_x-rich during this month. Final O_3 concentrations in Redlands did not exhibit a consistent pattern between weekdays and weekends from July to September, suggesting that the O_3 chemical regime was close to the ridgeline on the isopleth diagram.

Figure 20 shows O_3 sensitivity in the chamber studies carried out in Pasadena and Redlands. Pasadena had negative median $\Delta O_3^{+NO_x}$ sensitivity throughout the study (Figure 20a). This indicates that the O_3 chemical regime in Pasadena was mostly VOC-limited with very little seasonal trend compared to similar measurements made in Sacramento in 2020 (background boxplot in Figure 20). The upper quartile of $\Delta O_3^{+NO_x}$ was in the NO_x-limited regime on weekends in July and August, but quickly transitioned to the VOC-limited regime thereafter. Pasadena is adjacent to the VOC-limited urban core of Los Angeles(*28*, *42*). The significant anthropogenic NO_x and VOC emissions in this region are relatively insensitive to temperature-driven seasonal changes compared

to more rural regions with stronger biogenic influence(*28*). As expected, ΔO_3^{+VOC} was inversely correlated with $\Delta O_3^{+NO_x}$ in Pasadena. Addition of the VOC surrogate increased O_3 formation by an amount that was greater on weekdays than weekends. The VOC-limited regime in Pasadena has a larger weekend-weekday difference for ΔO_3^{+VOC} than $\Delta O_3^{+NO_x}$.

Median O_3 sensitivity in Redlands was in the VOC-limited regime in July, transitioned towards the NO_x-limited regime (especially on weekends) during August, and then transitioned back to VOC-limited conditions in September-October. A similar seasonal pattern was observed in Sacramento during a previous study in 2020 (background boxplot in Figure 20). The seasonal change in O_3 sensitivity may be influenced by the seasonal trends in biogenic VOC emissions(*28*) and the increased evaporative emissions of SVOCs (e.g., from mobile sources) on hotter days(*43*).

The O_3 sensitivity pattern observed in Pasadena and Redlands reflects the transition from a VOC-limited urban core towards a more NO_x-limited downwind area(*28*, *44–46*). Overall, the trends in the O_3 chemical regime observed in Pasadena and Redlands are consistent with recent observations of O_3 chemistry in urban and downwind suburban areas(*28*, *47*).

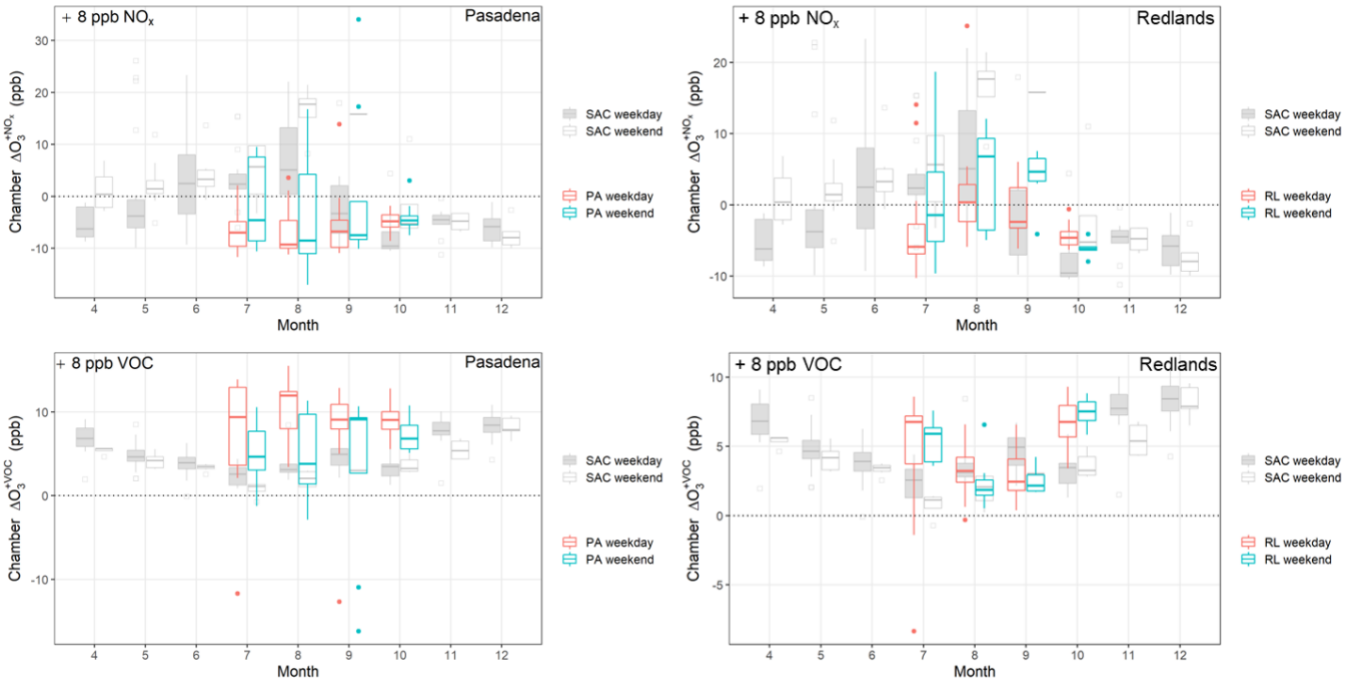

Figure 20. Time series of daily O_3 sensitivity results ($\Delta O_3^{+NO_x}$ and ΔO_3^{+VOC}) in weekdays and weekends from chamber measurements in Pasadena and Redlands, CA from July to October 2021. The background box and whisker plot are the time series of O_3 sensitivity results from chamber measurements in Sacramento, CA in 2020.

The days with the highest measured O_3 concentrations are of particular interest in the current study since emissions control programs are traditionally tailored to reduce the O_3 design value, which is determined by the 4th highest MDA8 O_3 averaged over a three-year period. Figure 3 illustrates boxplots of measured $\Delta O_3^{+NO_x}$, and ΔO_3^{+VOC} in Redlands and Pasadena binned according to the MDA8 O_3 concentration measured at nearby monitoring stations.

Pasadena has O_3 sensitivity in the VOC-limited regime on days with MDA8 O_3 < 70 ppbv (Figure 21a). The O_3 chemical regime in Pasadena was evenly distributed between NO_x-limited regime and VOC-limited regime on days with MDA8 O_3 > 70ppbv. The ΔO_3^{+VOC} (Figure 21c) in Pasadena had an inverse trend compared with $\Delta O_3^{+NO_x}$. The weakening response of VOC addition on days with higher MDA8 O_3 may be related to higher ambient VOC concentrations (see Figure 5) since the magnitude of the VOC perturbation was constant across all measurements. This may also be caused by increasing loss rates of NO_x under a higher radical production environment on higher MDA8 O_3 days. $\Delta O_3^{+NO_x}$ had greater variability on days with higher MDA8 O_3 in Pasadena, although it should be noted that fewer sample measurements were available in the highest MDA8 O_3 range. Even though median sensitivity was in the transition regime between NO_x-limited and VOC-limited conditions, the O_3 sensitivity in Pasadena could be either strongly NO_x-limited or VOC-limited on any given day with O_3 concentration above 70 ppbv.

Redlands had negative $\Delta O_3^{+NO_x}$ on more than 90% of days with MDA8 O_3 less than 50 ppbv. As MDA8 O_3 concentrations increased, the probability of observing negative $\Delta O_3^{+NO_x}$ decreased. NO_x-saturated conditions were only measured on 47% of the days with MDA8 O_3 above 90 ppbv (Figure 21b). The trend of more NO_x-limited conditions on higher MDA8 O_3 days in Redlands may be related to both higher VOC emission and higher radical production rates. Variability in the $\Delta O_3^{+NO_x}$ increased at higher O_3 concentrations. Overall, Redlands had an almost equal probability of O_3 sensitivity in the VOC-limited (56%) and NO_x-limited (44%) regime on O_3-nonattainment days (MDA8 O_3 > 70 ppbv). The measured O_3 sensitivity trends illustrated in Figure 21 suggest that VOC emission controls should be coupled with NO_x emission controls to mitigate O_3 concentrations in Pasadena and Redlands until NO_x-limited conditions can be achieved.

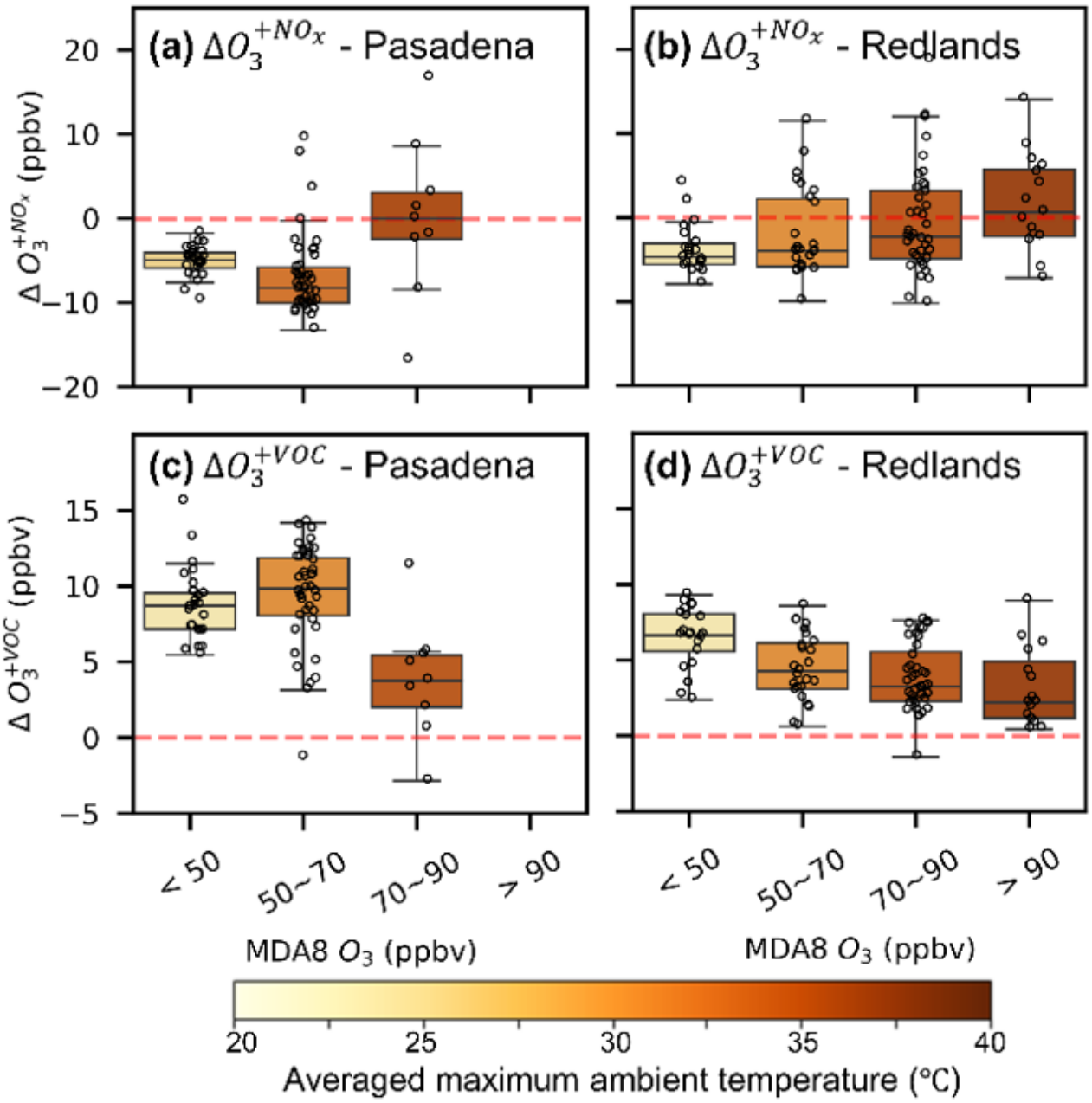

Figure 21. Boxplot of O_3 sensitivity to NO_x and VOC as a function of MDA8 O_3 concentration. Points indicate the data point in each range of MDA8 O_3 concentration. The color of each box represents daily maximum ambient temperature averaged within that concentration bin.

2.5 Chamber Modeling

2.5.1 Model Performance

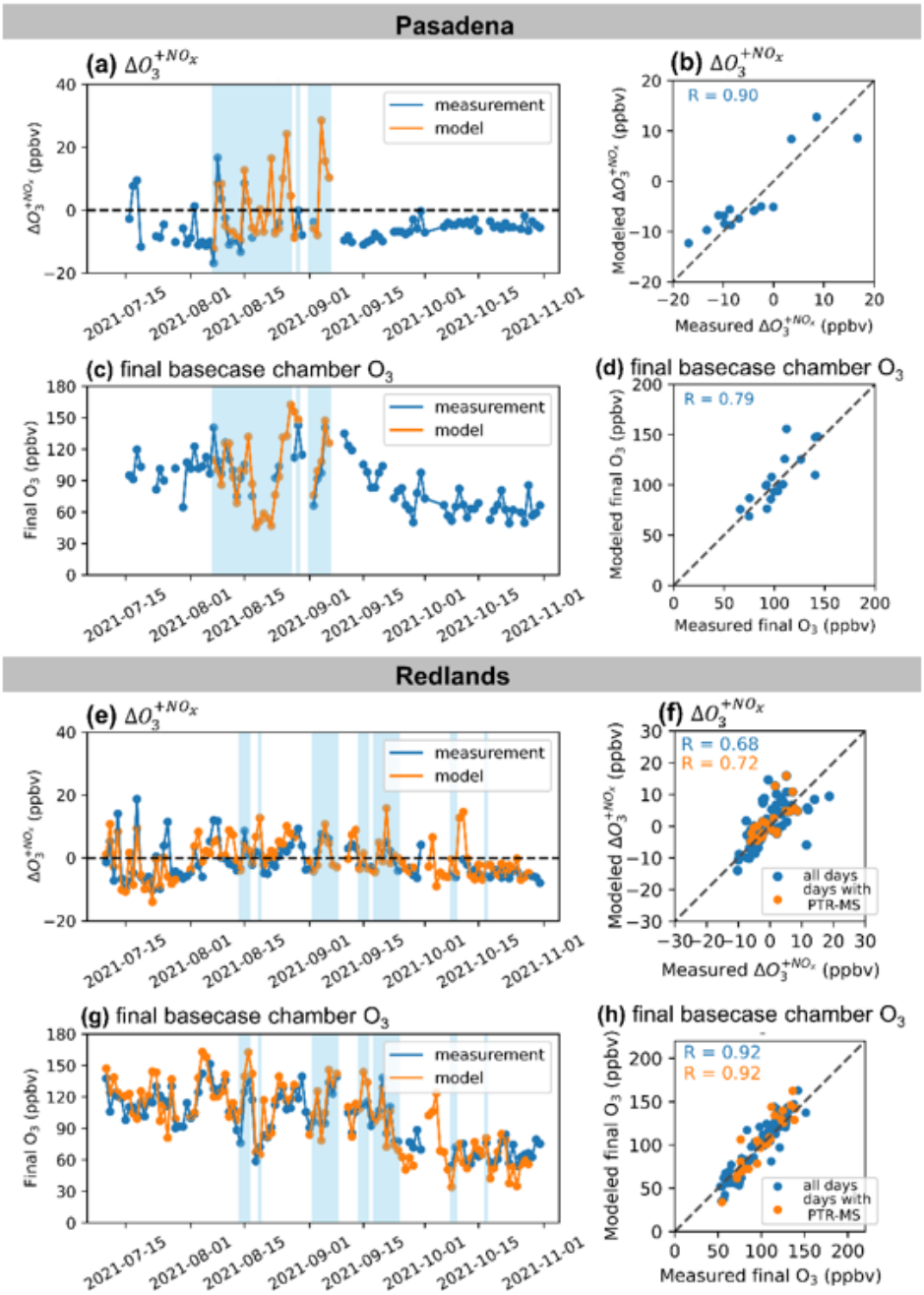

Figure 22. Time series of modeled and chamber measured O_3 concentration and O_3 sensitivity in chambers in Pasadena and Redlands, CA between July and October 2021. Shaded regions correspond to periods when the most complete VOC measurements were available.

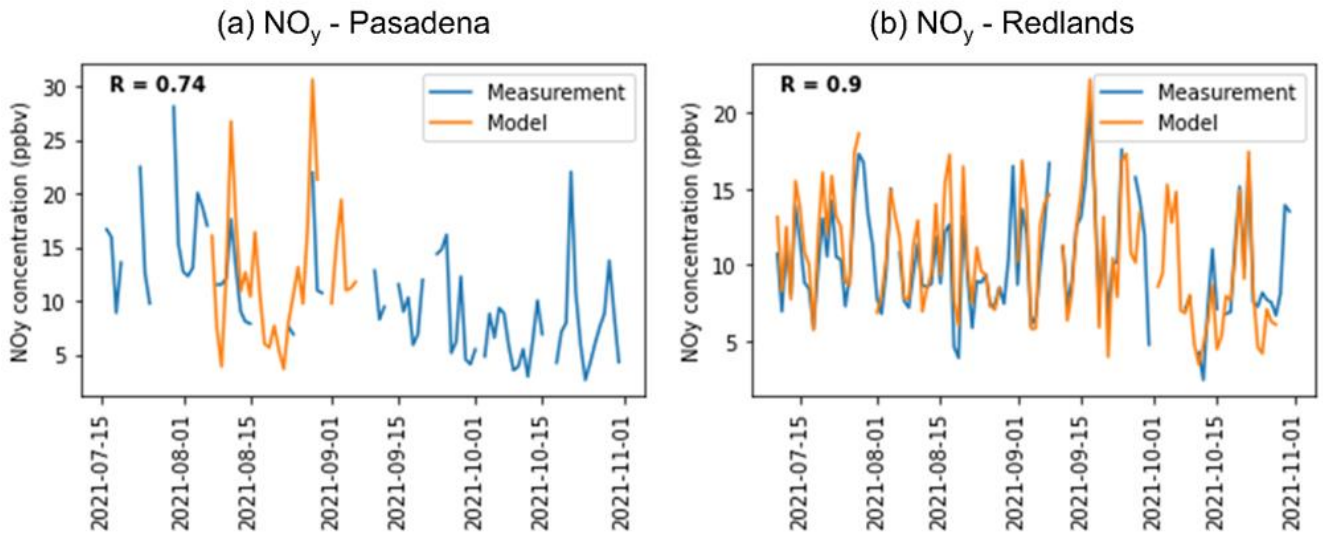

Figure 23. Time series of modeled and measured NO_y concentration in chambers in Pasadena and Redlands, CA between July and October 2021.

Each chamber experiment was simulated using a photochemical box model initialized with concentrations that were directly measured and predicted with a regional chemical transport model. Figure 22 shows the predicted/measured final O_3 concentration and the $\Delta O_3^{+NO_x}$ in Pasadena and Redlands, respectively. Simulations are restricted to days when VOC measurements were available, which especially restricts the number of days that can be evaluated in Pasadena. Despite the more limited input data, Pasadena simulations span periods with a wide range of O_3 formation and with several transitions between VOC-limited and NO_x-limited conditions. These simulations provide insights into O_3 sources and chemical regimes in Pasadena even though it was not possible to simulate the transition into the fall season. Simulations in Redlands span the full measurement time period, tracking the seasonal decline in base O_3 concentrations and multiple transitions between VOC-limited and NO_x-limited regimes. Days with the most complete initial VOC data including PTR-ToF-MS measurements (blue shading) have higher correlation (R value) between model predictions and measurements. Overall, the good correlation between predicted and measured final O_3 concentration in the base case chamber and $\Delta O_3^{+NO_x}$ in the perturbed chamber shows that the box model can reproduce the behavior of the chamber experiments in Pasadena and Redlands. NO_y concentrations predicted by model calculations were also in good agreement with chamber measurement (Figure 23). Sensitivity tests show that use of chamber temperature vs. ambient temperature has little influence on the comparison between predicted and measured final O_3 concentration in the base case chamber and $\Delta O_3^{+NO_x}$ in the perturbed chamber (Figure 24). Ambient temperature profiles are therefore used to predict the O_3 isopleth in the remainder of the analysis.

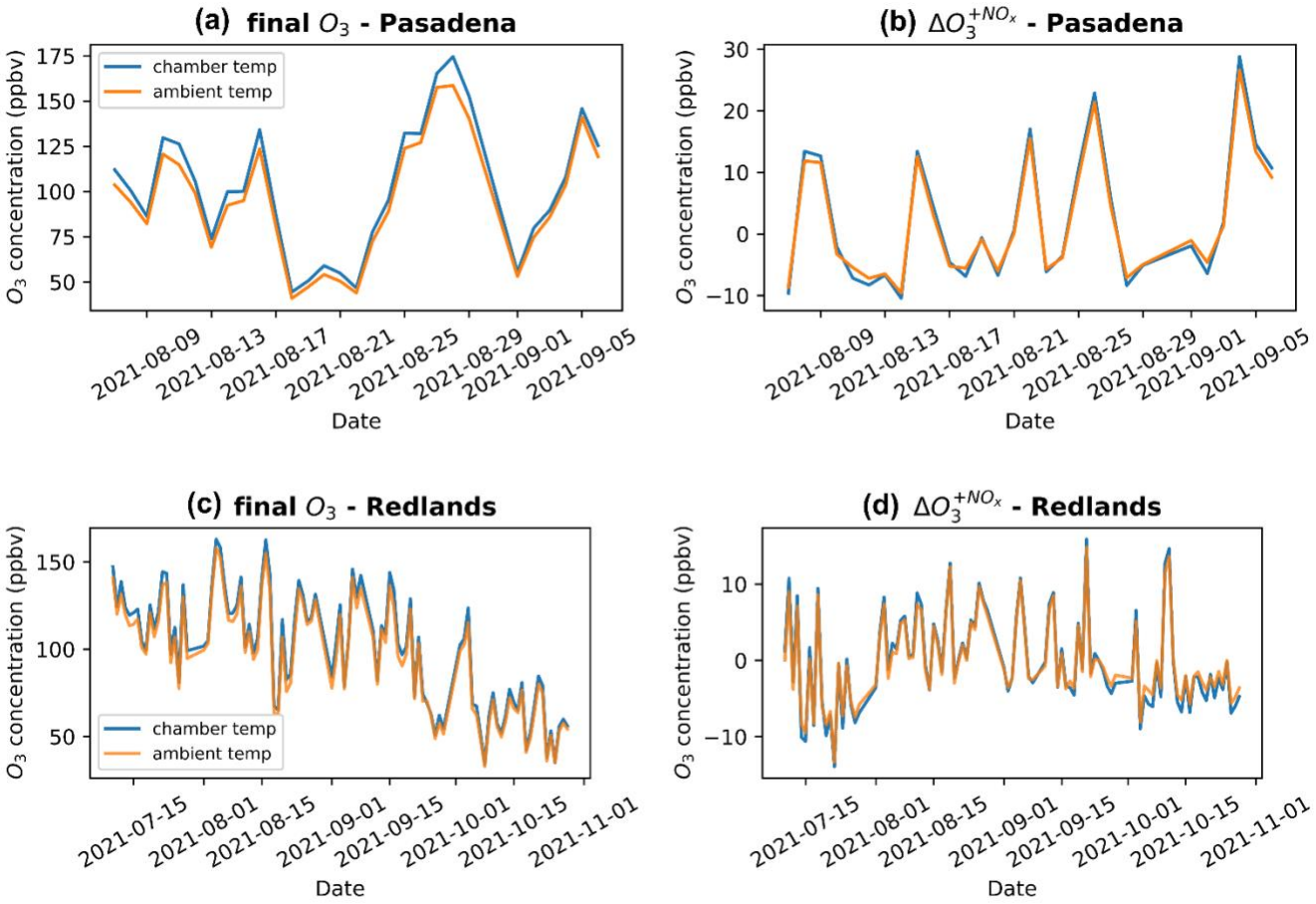

Figure 24. Time series of modeled results at chamber temperature (blue line) and ambient temperature profile (orange line).

2.5.2 Ozone Isopleth

O_3 isopleth diagrams succinctly summarize the non-linear relationship between O_3 formation and precursor NO_x / VOC concentrations. Traditional O_3 isopleth diagrams are based exclusively on model predictions. In the current study, it is possible to add direct measurements of O_3 sensitivity to the isopleths calculated with the chamber model to verify both the base O_3 concentration and the response in O_3 concentrations caused by perturbations in NO_x / VOC levels.

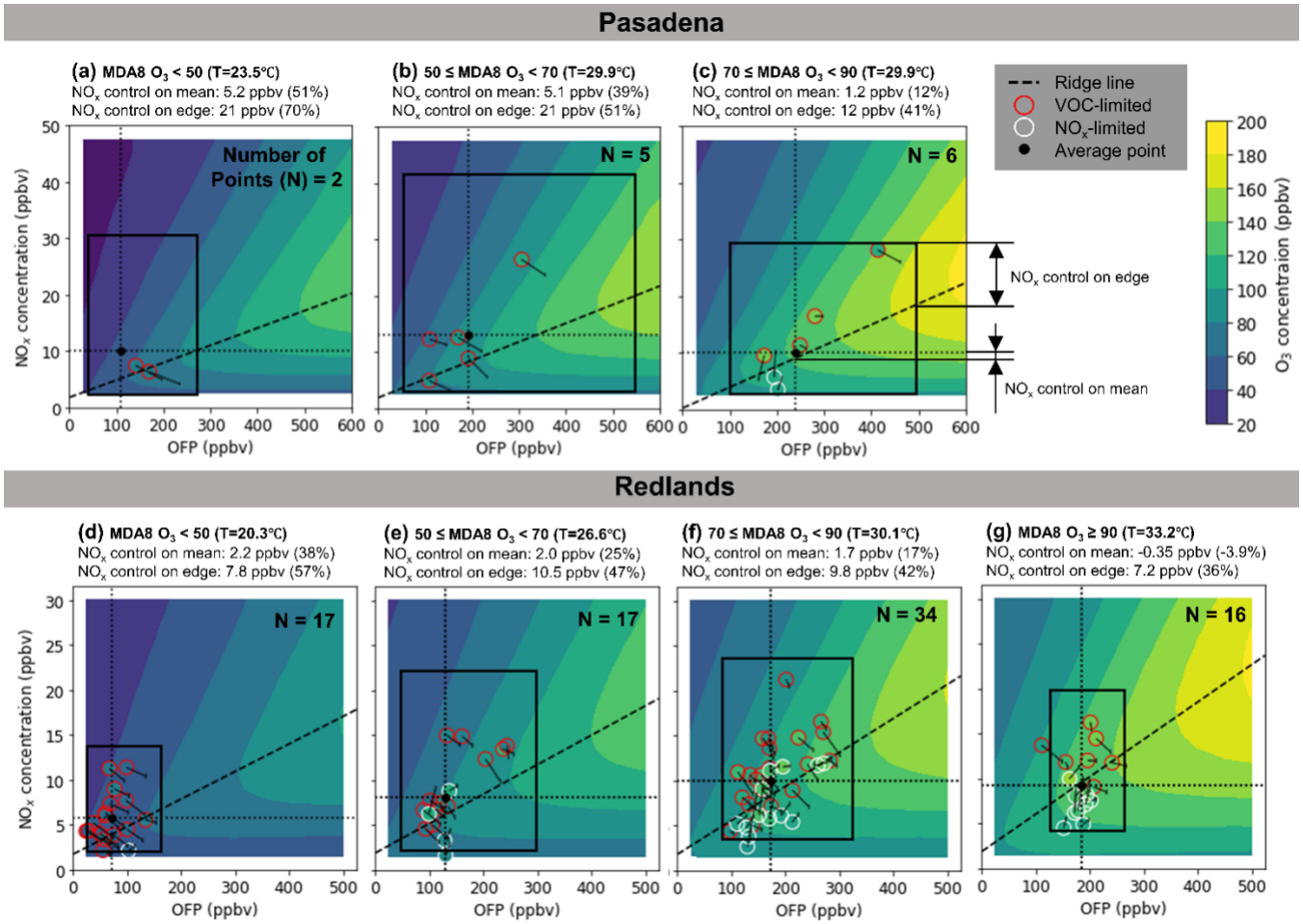

Figure 25. O_3 isopleth in Pasadena and Redlands, over four MDA8 O_3 concentration ranges experienced during the study. Simulated O_3 concentrations are based on measured concentrations of NO_x and VOC (represented by O_3 formation potential [OFP]) scaled to cover the full range of possible conditions. The intersection of light dotted lines represents the average measured NO_x and VOC levels in the indicated MDA8 O_3 range. The box around the average represents the standard deviation of the measured values. The heavy dashed line represents the ridgeline of isopleth. Open circles represent chamber measurements for comparison to model predictions. Arrows indicate the O_3 response to NO_x or VOC addition.

O_3 isopleths were generated each day by simulating the O_3 formation at multiple scaled NO_x and VOCs levels around the base concentrations measured for that day. Measured VOC concentrations are expressed on the basis of their O_3 formation potential (OFP), which is the sum of individual VOC concentrations weighted by their maximum incremental reactivity (MIR)(*48*, *49*). Separate isopleths are averaged based on the MDA8 O_3 range. Each averaged O_3 isopleth in Figure 5 therefore represents the averaged O_3 chemistry for multiple days within the target MDA8 O_3 concentration range. Increasing MDA8 concentrations generally corresponds to higher average temperature (see values in each subpanel title).

Measured final O_3 concentrations are plotted as open circles in Figure 25 using the same color key as the modeled O_3 isopleth. The location of each observation circle is based on measured NO_x and VOC concentrations. Most measurements of final O_3 concentrations are in agreement with model predictions as indicated by the similarity between the color of each circle and the background color of the isopleth. The measured O_3 chemical regime is indicated by the outline color of each dot (red =VOC-limited regime; white = NO_x-limited regime). Most of the measurements match the O_3 sensitivity regime in the predicted O_3 isopleth. The few measurement points that fall in the wrong O_3 sensitivity regime in Figure 25 are located in the transition regime (very close to the ridge line). The arrow attached to each measurement point indicates the measured O_3 sensitivity to NO_x and VOC perturbation ($\Delta O_3^{+NO_x}$ and ΔO_3^{+VOC}). Arrows pointing to the bottom-right indicate that NO_x addition decreased the O_3 concentration, while arrows pointing to the upper-right indicate that NO_x addition increased the O_3 concentrations. Arrows should be orthogonal to the background isopleth lines. Overall, the generally accurate model performance over most of the study period supports a deeper understanding of how much NO_x reduction is needed to achieve the NO_x-limited regime.

The average NO_x and VOC concentrations measured during the study period are shown at the intersection of the dotted lines in Figure 25. All NO_x and VOC measurements available during the experimental window were used to calculate the average to maximize the sample size. The averaged-NO_x in Pasadena and Redlands were based on 80 and 100 days of ambient measurements, respectively. The averaged-OFP was based on 30 days of VOC measurements in Pasadena and 100 days of VOC measurement in Redlands. Average VOC concentrations were higher on days with higher MDA8 O_3 (and temperature). Average O_3 sensitivity in Pasadena is slightly NO_x-limited on O_3-nonattainment days. Averaged O_3 sensitivity in Redlands is slightly VOC-limited on days with MDA8 O_3 between 70 and 90 ppbv, and NO_x-limited on days with MDA8 O_3 > 90 ppbv. The averaged O_3 sensitivity calculated in each O_3 isopleth has the same O_3 sensitivity regime as the median measurements summarized in Figure 21.

The vertical distance between the intersection of the dotted lines to the ridge line in Figure 25 indicates the amount of NO_x reduction that is needed to reach NO_x-limited conditions for the averaged O_3 sensitivity regime based on the composition of the atmosphere between 10am and 12pm. NO_x concentrations in Pasadena would need to be reduced by 12% (assuming VOC is stable) before the average O_3 chemical regime reaches NO_x-limited conditions on O_3-nonattainment days (MDA8 O_3 > 70 ppbv). NO_x concentrations in Redlands would need to be reduced by 17% before the average O_3 chemical regime reached NO_x-limited conditions in Redlands when MDA8 O_3 is between 70 and 90 ppbv.

Each confidence interval box shown in Figure 25 assumes that the NO_x and OFP concentrations follow a log-normal distribution(*50*). The interior region of the black box represents the O_3 chemistry corresponding to 95% of the ambient measurements. The vertical distance between the upper-right edge of the confidence interval to the ridge line represents the amount of NO_x control needed to move 95% of the observations with the highest O_3 concentrations to the NO_x-limited chemical regime in the absence of any VOC controls. The calculations summarized in Figure 25 indicate that NO_x concentrations need to decrease by ~40% to reach NO_x-limited condition on 95% of the days in Pasadena and Redlands based on the composition of the atmosphere between

10am and 12pm. The 40% NO_x reduction only barely reaches the NO_x-limited regime on peak O_3 days. Further NO_x control is still needed to reduce the O_3 design values. Perdigones et al. (*46*) reported a comparable or larger amount of NO_x reduction (40–60%) in SoCAB that could reduce the number of O_3-nonattainment days to 20–10%, respectively. The State Implementation Plan from South Coast Air Quality Management District (*51*) estimated that a 67% NO_x reduction would be needed in the SoCAB to comply with the O_3 NAAQS by 2037. All of the evidence suggests that NO_x reductions greater than 40% are required to control O_3 concentrations in the SoCAB.

While the O_3 isopleths predicted in the current study are consistent with multiple observations, limitations in both measurements and model calculations should be noted. The chamber methods used in the current study quantify the chemical production of O_3, but they do not consider the effects of dilution, mixing, and deposition. The chamber measurements focus on the time of day that characterizes peak O_3 production relevant for the design of O_3 control programs, but measurements were not made at other times of the day that may fall into different chemical regimes. Box-model calculations carried out to gain a deeper understanding of the measurements suggest that these issues do not alter the overall conclusions of the study, but those same box model calculations have uncertainty associated with initial VOC concentrations on days when only partial measurements were available. Overall, the novel comparisons between measurements and model predictions carried out in the current study improve our understanding and confidence in the emissions control programs designed to reduce O_3 concentrations in Southern California.

The findings in the current study help to explain the atmospheric impacts of the COVID-19 stay-at-home order in California (March to June 2020) that decreased traffic by as much as 50% in the SoCAB(*45*, *52*). NO_x concentrations decreased by 26% in Pasadena and 8% in Redlands as a result. Parker et al.(*53*) analyzed ambient data and concluded that the western portion of the SoCAB remained VOC-limited despite these significant reductions in ambient NO_x concentrations. Likewise, the results of the current study indicate that the urban cores of major cities in Los Angeles remain VOC-limited in all seasons(*28*). This further supports the conclusions of the current analysis that ~30% NO_x reductions are not sufficient to transition to the NO_x-limited regime and consequently reduce O_3 concentrations in polluted urban core areas in the SoCAB. Additional analyses compared the ambient air quality data between the weekdays and weekends, which experience natural variabilities in traffic activities. These analyses provide an alternative approach to understanding the O_3 chemical sensitivities in SoCAB. However, the results did not pass statistical confidence measures due to the low number of data points available for comparison during the heavily modified traffic conditions following the shelter-in-place order. The inconsistencies in meteorological conditions also contributed to significant uncertainties in this analysis. This demonstrates the strength and the need for tools like chamber experiments that yield an understanding of the O_3 chemical regimes at daily intervals.

2.5.3 O_3 Source Apportionment

Figure 26 shows predictions, using the chamber model, of the contribution of different VOC categories to O_3 formation in Redlands and Pasadena. O_3 contributions from twelve types of VOCs were tracked based on SAPRC11 mechanism (see Table 4 below). Some VOCs are directly emitted from a limited number of sources and so O_3 formation from these compounds can be directly interpreted as a source contribution. Other VOCs (and O_3 itself) can form in the atmosphere over multiple days of chemical reaction. The day-specific box model calculations used in the current study cannot explicitly identify the source-origin of these secondary VOCs, although results from previous CTM and receptor-oriented studies can suggest source contributions for several important species.

Odd oxygen present in O_3, NO_2, and other oxygenated compounds at the start of each day contributed to over half of total O_3 concentrations at both Redland and Pasadena during the current study. Approximately 30–60 ppb of this background O_3 originated upwind of California, while the remainder formed over land on days prior to the measurement day.

Chamber model calculations predict that the top four VOCs that contribute significantly to O_3 formation on the measurement day in Redlands are: biogenics, aromatics, alcohols, and aldehydes (see Figure 27). The top four VOCs that contribute to O_3 production in Pasadena are: biogenics, aldehydes, alkanes, and alcohols. Biogenic VOCs (mainly isoprene and monoterpenes) made the largest contribution to the O_3 formation on the measurement day at both sites. Past studies that performed multi-day source apportionment calculations for aldehydes suggest that biogenic VOCs are the dominant ambient source of these compounds (*54*). This suggests that biogenics plus aldehydes derived from biogenics may contribute to 30–40% of the O_3 formation in Pasadena and Redlands.

Methanol and ethanol are the dominant alcohols in the current analysis. Methanol is a toxic alcohol that is used as a solvent in cleaning products, pesticide, fuel, and other industrial products. (https://comptox.epa.gov/dashboard/). Methanol can be emitted to atmosphere as a VCPs, but decomposition of terrestrial plants is the primary emission source of methanol in the atmosphere (Bates, 2021). Ethanol is used as an additive in gasoline and is a large component of VCPs in urban areas. These combined alcohols contributed to 8–17% of the O_3 formation in Pasadena and Redlands during the study period.

Aromatics mainly consist of BTEX compounds that originate from fossil transportation fuels in the SoCAB. Alkanes are emitted from multiple sources including evaporation of petroleum products and industrial solvents. Concentrations of butane in particular increased significantly at the Redlands measurement site during the transition from summer blend gasoline to winter blend gasoline. The chamber model results predict that fossil transportation fuels may contribute to approximately 15% of the O_3 formation in Pasadena and Redlands.

Table 4. VOC categories used in O_3 apportionment calculations.

Name of Categories	Contents (name is defined in SAPRC11)
Bio	ISOPRENE TERP SESQ
ARO	BENZENE ARO1 ARO2
Alcohol	MEOH ETOH
Alkane	ALK1 ALK2 ALK3 ALK4 ALK5
Aldehyde	HCHO CCHO RCHO
Alkenes	OLE1 OLE2 ETHENE ACETYLEN
Ketone	ACET MEK
H2O2	HO2H
CH4	CH4
PAN	PAN PAN2
Others	GLY MGLY MACR MVK IPRD CRES PHEN CATL XYNL BALD BACL PROD2
COOH	COOH CCOOH ROOH R6OOH RAOOH

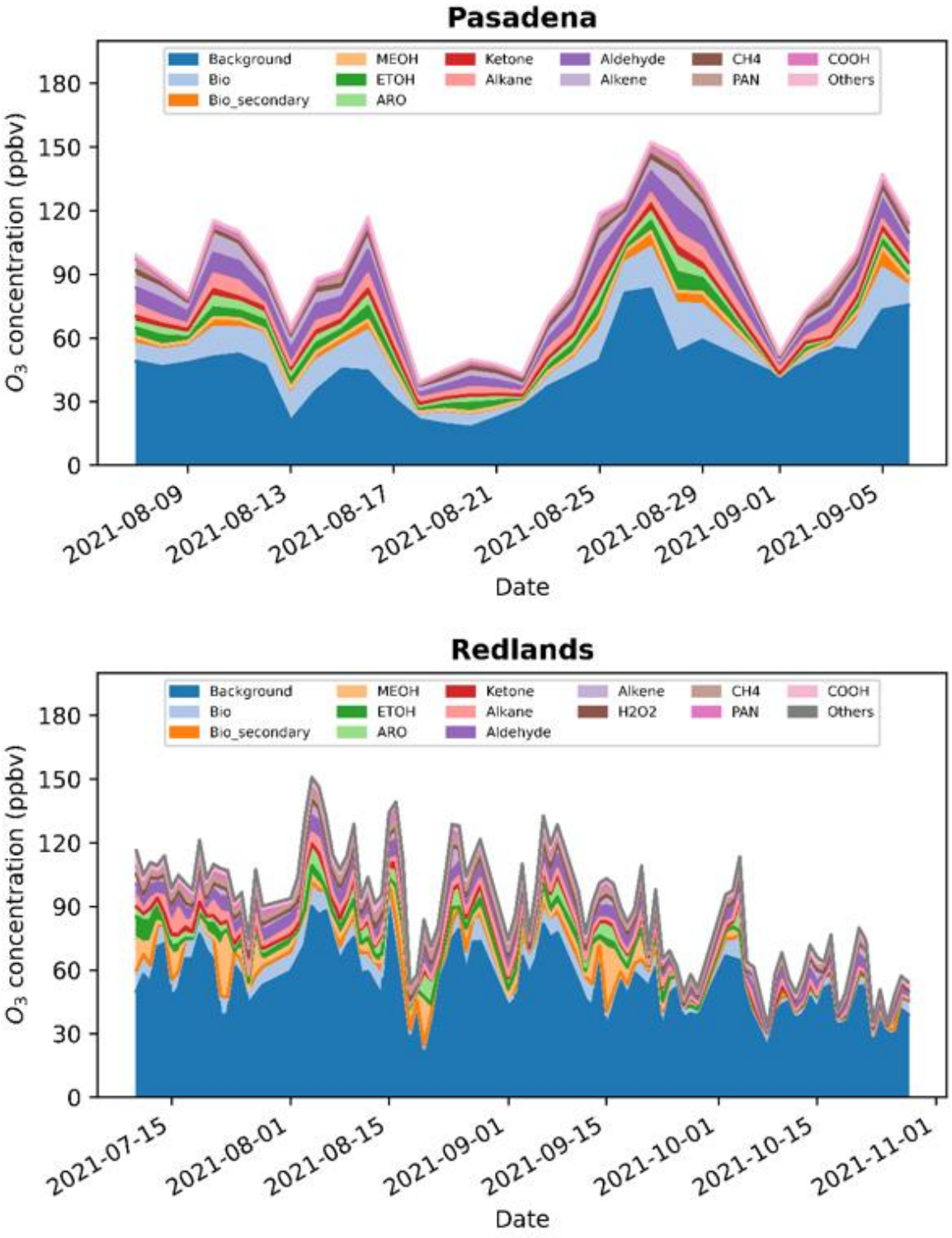

Figure 26. Time series of modeled final O_3 in base case chamber from different VOC sources using the O_3 source apportionment technique.

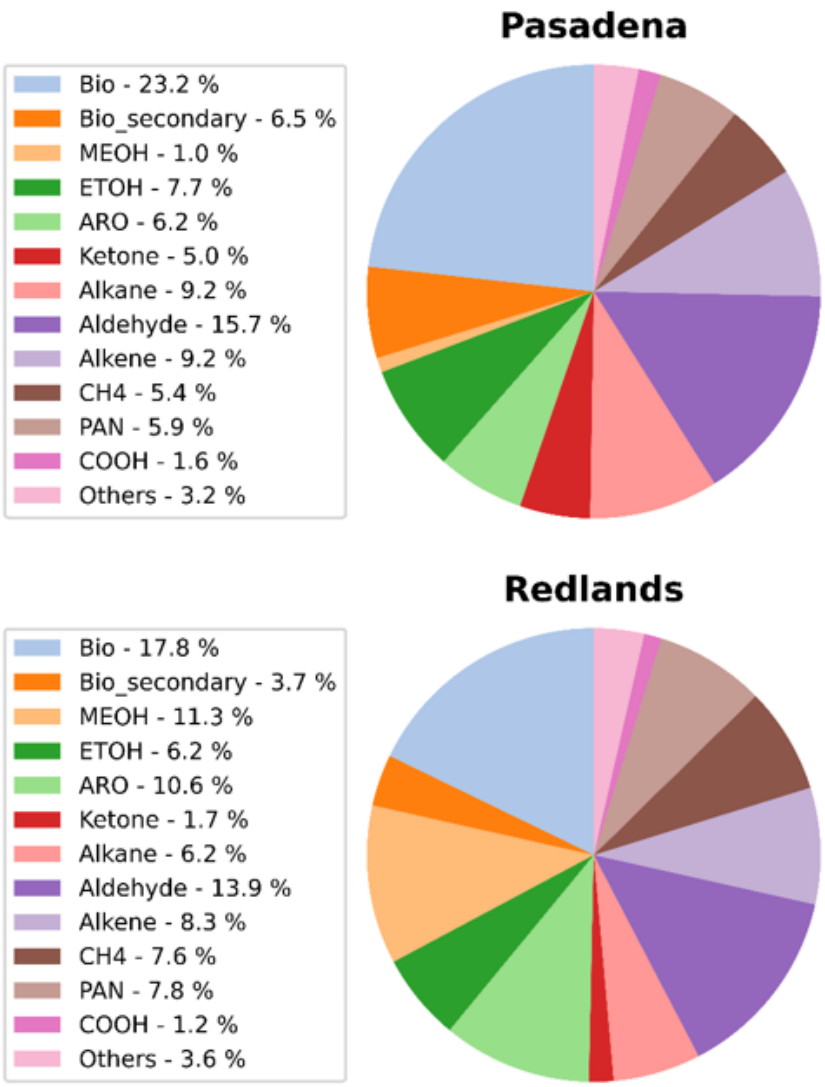

Figure 27. Contribution of 12 VOC types to O_3 formation in Pasadena and Redlands, CA.

2.6 Discussion

The measurements and model predictions presented in the preceding sections indicate that biogenic sources were the single largest VOC category that contributed to O_3 formation in Pasadena and Redlands during the summer of 2021. The upper limit of reasonable contributions to O_3 formation from VCPs and fossil transportation fuels suggest that each of these sources contributed roughly half as much as biogenic sources. The dominance of the natural sources over the anthropogenic sources reflects the success of decades of emissions control efforts that have reduced anthropogenic emissions of reactive VOCs in California.

Future progress on reducing ambient O_3 concentrations in California will need to acknowledge the magnitude of the natural vs. anthropogenic VOC source contributions in current conditions. Additional reductions in VOC emissions from both fossil transportation fuels and VCPs may achieve some short-term O_3 reductions, but it will likely not be possible to achieve full compliance with the O_3 NAAQS solely through a VOC emissions control program. NO_x controls will be the most efficient long-term strategy for continued O_3 reduction in the SoCAB.

The success of future emissions control programs for O_3 reductions will be determined by how well they work in the chemical regime governing O_3 formation. Measurements and model simulations both indicate that the current monthly-average O_3 chemical regime is NO_x-rich on 90% of the summer days in Pasadena and 70% of the summer days in Redlands. The days with the highest MDA8 O_3 concentration have the greatest probability of being NO_x-limited on average, but also the greatest variability in the O_3 formation regime. NO_x reductions of ~8% to ~17% would achieve monthly-average NO_x-limited conditions but NO_x reductions of ~40% would be needed to achieve NO_x-limited conditions on 95% of the days in each month. Modest NO_x controls will help reduce average O_3 concentrations in Pasadena and Redlands, but more significant NO_x reductions will be needed to reduce the most stubborn O_3 concentrations.

Given the balance of the contributions from various NO_x and VOC sources and the current chemical regime for O_3 formation, a combined strategy of NO_x and VOC controls seems optimal in the short term. This strategy could be achieved by continuing to transition away from traditional fossil-fueled motor vehicles since this would eliminate both NO_x and VOC emissions. Transition to zero-emission vehicles (ZEV) would also be consistent with California's greenhouse gas reduction plans in the coming years. Additional controls could focus on VCPs to help further mitigate the potential for NO_x reductions to increase O_3 concentrations. In the longer term, emissions control programs will need to focus heavily on NO_x controls once remaining anthropogenic VOC sources have been largely eliminated.

2.7 Conclusions

O_3 sensitivity to NO_x and VOC perturbations was directly measured using chamber experiments in Redlands and Pasadena, CA between July and October 2021. The median observed O_3 sensitivity was in the VOC-limited regime in Pasadena, but showed a seasonal trend in Redlands, where median O_3 formation was VOC-limited in July and October and transitioned towards the NO_x-limited regime in August and September. This seasonal pattern is consistent with the expected trends in both biogenic VOC (BVOC) emissions and evaporative emissions from fossil fuels. Pasadena and Redlands had O_3-nonattainment days under both NO_x-limited and VOC-limited conditions

Proximity to higher population density favors NO_x-rich conditions. Chamber measurements suggest that Pasadena was in the NO_x-rich chemical regime on 90% of the measurement days during the study period, while Redlands was NO_x-rich on 70% of the measurement days. The highest measured O_3 concentrations occurred more frequently on days that were NO_x-limited, but the variability in the O_3 chemical regime also increased on

high O_3 days. These ground-based direct chamber measurements are consistent with satellite observations of the HCHO/NO_2 ratio that suggest the urban core in Southern California is mostly NO_x-rich throughout the year, while suburban or remote areas have more NO_x-limited days and a clearer seasonal trend in O_3 sensitivity.

A model of O_3 chemical formation based on the SAPRC11 mechanism predicts O_3 behavior that is consistent with measurements. Both the model and the direct measurements suggest that ~12% to ~17% NO_x reductions will achieve NO_x-limited conditions on the average day in Pasadena and Redlands, but more aggressive NO_x controls of ~40% would be needed to achieve NO_x-limited conditions on 95% of the days. This suggests that VOC emission controls should be coupled with NO_x emission controls to mitigate any temporary increases in O_3 concentrations until consistent NO_x-limited conditions can be achieved.

Chamber model calculations suggest that BVOCs are the single-largest VOC source of O_3 formation in Pasadena and Redlands, followed by fossil transportation fuels and VCPs. Since BVOCs cannot be easily controlled, VOC controls should focus on fuels and VCPs to supplement NO_x controls in the short term. Given the magnitude of the VOC emissions from biogenic sources, long-term strategies will need to rely exclusively on NO_x reductions.

2.8 Appendix

Lower MDA8 O_3 concentrations were observed on Sunday than Wednesday across the SoCAB region during the COVID-19 period suggesting that the chemical regime had shifted to NO_x-limited conditions(*45*). The uncertainty in this analysis is very high, however, because the heavily modified traffic conditions lasted less than 12 weeks and the variability in O_3 concentrations due to meteorology was significantly larger than observed weekday-weekend differences. P-values for comparisons between MDA8 O_3 measurements on Sunday and Wednesday exceed 0.3. Statistical analysis of the monitoring data shows that more than 100 weeks of heavily modified traffic conditions would be required to detect a 2 ppb change in weekend ground-level O_3 concentrations at a significance level of 95% with a power of 80%. The COVID-19 shutdown period simply did not last this long in California.

The weight of evidence supports the conclusions of the current analysis that ~30% NO_x reductions are not sufficient to transition to the NO_x-limited regime and consequently reduce O_3 concentrations in polluted urban core areas in the SoCAB. It should be noted that the seasonal timing of the shutdown order (March to June) was earlier than the seasonal timing of the current measurement period. More NO_x-reduction may be needed to reach the NO_x-limited regime in the spring season when MDA8 O_3 concentrations are lower(*28*). The trends observed during the COVID-19 shutdown period support the conclusions of the current analysis that ~30% NO_x reductions are not sufficient to transition to the NO_x-limited regime and consequently reduce O_3 concentrations in polluted urban areas in the SoCAB.

3. Extended Ozone Isopleth Analysis

3.1 Introduction

Modern Ozone (O_3) control programs originated in Los Angeles, California, and this megacity continues to be a leading case study for designing and testing methods to reduce O_3 concentrations to levels that protect public health. As ambient O_3 concentrations have decreased towards background levels, the effects of O_3 control programs have become more difficult to detect against the backdrop of natural atmospheric variability. The lack of an obvious annual decrease in ambient concentrations has motivated direct measurement of O_3 responses to precursor perturbations to confirm the accuracy of model predictions (see Section 2.5.1). These new methods help guide appropriate decisions about future control programs in the presence of uncertainty.

Uncertainty about the design of O_3 control programs is not limited to Los Angeles. Multiple cities in California violate the National Ambient Air Quality Standards (NAAQS) for O_3 concentrations, despite years of modeling and control programs. As in Los Angeles, annual decreases in these cities of O_3 concentrations are difficult to identify in the presence of natural year-to-year variability. The persistence of high O_3 concentrations in these locations erodes confidence in the design of their emissions control programs, which increases resistance to those programs.

O_3 control programs are typically developed for a "design day" representing the highest O_3 concentrations within the target region. The theoretical understanding of O_3 formation chemistry under ideal controlled conditions can be difficult to reconcile with observed behavior in the real atmosphere, subject to random fluctuations in weather conditions and emissions. The results in Section 2 demonstrate that a statistical analysis of O_3 formation over a longer period than a single episode can yield a deeper understanding of the effectiveness of various O_3 control strategies under a wider range of conditions.

In this section, we construct O_3 isopleth diagrams for San Francisco, Sacramento, Fresno, and Redlands over multiple months in 2020. Each of these areas is in O_3-nonattainment status. The isopleth results are used to predict the amount of nitrogen oxides (NO_x) control necessary to achieve NO_x-limited conditions on 95% of the days with the highest O_3 concentrations at each location. The magnitude of this required NO_x reduction is compared to the NO_x reduction that occurred during spring 2020 due to reduced traffic during the "stay-at-home" policy during COVID-19. The combined model and measurement results improve our understanding of how future changes to traffic patterns may influence ambient O_3 concentrations.

3.2 Methods

3.2.1 Locations

Box model simulations are carried out for O_3 formation in March and August 2020 in four major cities across California: San Francisco, Sacramento, Fresno, and Redlands (eastern Los Angeles). Exact locations within each city were selected based on their proximity to monitoring sites operated by local air quality management districts and/or the California Air Resources Board (CARB). Table 5 shows the detailed location of each monitoring site and the measurements available at that site.

Table 5. Model locations corresponding to monitoring sites.

Site Name	Location (lat/lon)	O_3 attainment status	Measurements available
San Francisco-Arkansas Street	37.76595, -122.39902	Attainment	O_3, NO, NO_2, CO, Temperature, RH
Sacramento-T Street	38.56844, -121.49311	Non-attainment	O_3, NO, NO_2, Temperature, RH, chamber measurement (in August 2020)
Fresno- Garland	36.78538, -119.77321	Non-attainment	O_3, CO, NO_2, Temperature, RH
Redlands-Dearborn	34.05965, -117.14734	Non-attainment	O_3, temperature, RH, NO and NO_2 from San Bernadino 4th Street site, chamber measurement (in August 2021), VOC offline measurements (in August 2021)

The San Francisco Bay Area (abbreviated as Bay Area hereafter) is the second largest population center in California. The Bay Area has been designated as an O_3-nonattainment area. We chose the grid cell around the CARB monitoring station in downtown San Francisco (37.76595, -122.39902) as the target area for model simulation. This site has an O_3 design value below 70 ppbv in the past three years. However, the increased trend observed in the O_3 design value shows the importance of the O_3 sensitivity analysis in this area. The main NO_x sources in the Bay area are motor vehicles and other mobile sources. The volatile organic compounds (VOC) emissions from anthropogenic sources are greater than those from biogenic sources in the Bay Area, according to the CARB emissions inventory (*55*).

Sacramento is a major metropolitan area in the Central Valley of California. Measurements of O_3 sensitivity were made near the CARB monitoring station in downtown Sacramento (38.56844, -121.49311). This site is an O_3-nonattainment site, with an O_3 design value of ~80 ppbv in the past three years. Major NO_x emissions sources in the region include traffic, and commercial and residential buildings. The VOC reactivity that contributes to O_3 formation is dominated by biogenic VOC (BVOC) (*47*, *56*, *57*).

Fresno is the largest city in the San Joaquin Valley, which is an O_3 non-attainment area for the 2015 NAAQS 8hr O_3 standard. The grid cell around the CARB monitoring station in Garland (36.78538, -119.77321) was selected as the target area for model simulations. The mixing of local anthropogenic emissions and biogenic emissions from suburban or remote areas results in high O_3 concentrations during the summer and early fall.

The South Coast Air Basin (SoCAB) surrounding Los Angeles is the most populated area in California. The Redlands-Dearborn site (34.05965, -117.14734), in a downwind area within the SoCAB, typically records among the highest O_3 concentrations in the region due to a combination of meteorology, emissions, and chemical reactions that act on upwind and local emissions. Our field measurements of the O_3 sensitivity using the transportable smog chamber system were conducted in the Redlands-Dearborn site from July to October 2021.

3.2.2 Model Calculations

The formulation of the box model is described in Section 2.2.4, and so only a brief overview is provided here. Each box model calculation predicts the O_3 formation over a three-hour time period due to chemical reactions based on measured or predicted initial concentrations starting at approximately 10 AM to 12 PM. Chemical reactions are represented using the SAPRC11 mechanism (*34*). Since these calculations are designed to represent ambient conditions, the UV spectrum is tuned to atmospherically relevant values. Transport, vertical mixing, and dry deposition to the surface are not directly considered in the calculation, but these processes influence the concentrations used to initialize the box model calculations each day.

The initial conditions for box model calculations are based on measured values of NO, NO_2, and O_3 from nearby monitoring stations and predicted values of VOCs based on regional simulations using a chemical transport model (CTM) (*58*) coupled with a scaling factor that accounts for increased VOC concentrations at higher temperatures due to enhanced evaporative emissions from mobile sources and enhanced biogenic emissions from plants (*14*). Isopleths were calculated for each individual simulation day by scaling the NO_x and VOC concentrations over 3-hour simulation periods. Similar box model calculations carried out for Redlands and Pasadena in the summer of 2021 predict concentrations that are in good agreement with measurements, suggesting that model calculations capture the dominant features of the O_3 formation cycle at each location.

3.3 Results

Figure 28 compares the O_3 concentration from the box model with the ambient O_3 concentration in March and August in each study area. Ambient concentrations reflect chemical formation, atmospheric mixing, and deposition. The box model only predicts the effects of chemical reaction, so deviations between the measurements and model are expected (similar to deviations between chamber measurements and ambient measurements in Section 2.5.1). The O_3 formation rate in the box model calculations was generally linear, suggesting that the VOCs in the simulated atmosphere were not fully consumed over the three-hour analysis period. The rate of O_3 formation (slope) generally matches the observed rate of O_3 formation at ~10 AM. Initial O_3 formation rates in August are more rapid than initial O_3 formation rates in March, indicating that the VOC mixture is more reactive in the summer months. In all cases, the final O_3 concentrations were greater than the ambient concentrations because the ambient air was diluted by the rising boundary layer throughout the mid-day period. This divergence is expected since the box model does not account for the atmospheric mixing and dilution. Final O_3 concentrations at the end of the 3-hour simulation period are closer to measured ambient O_3 concentrations in March than in August, indicating that the composition of the atmosphere is more uniform with elevation in the spring months. The agreement between predicted O_3 formation rates and measured ambient rates shown in Figure 28 are similar to the agreement between the predicted O_3 formation rates and measured base case chamber rates discussed in Section 2.5.1. Overall, the box model represents the chemical formation rate of O_3, which is one of the dominant factors that determines the behavior of ambient O_3 concentrations.

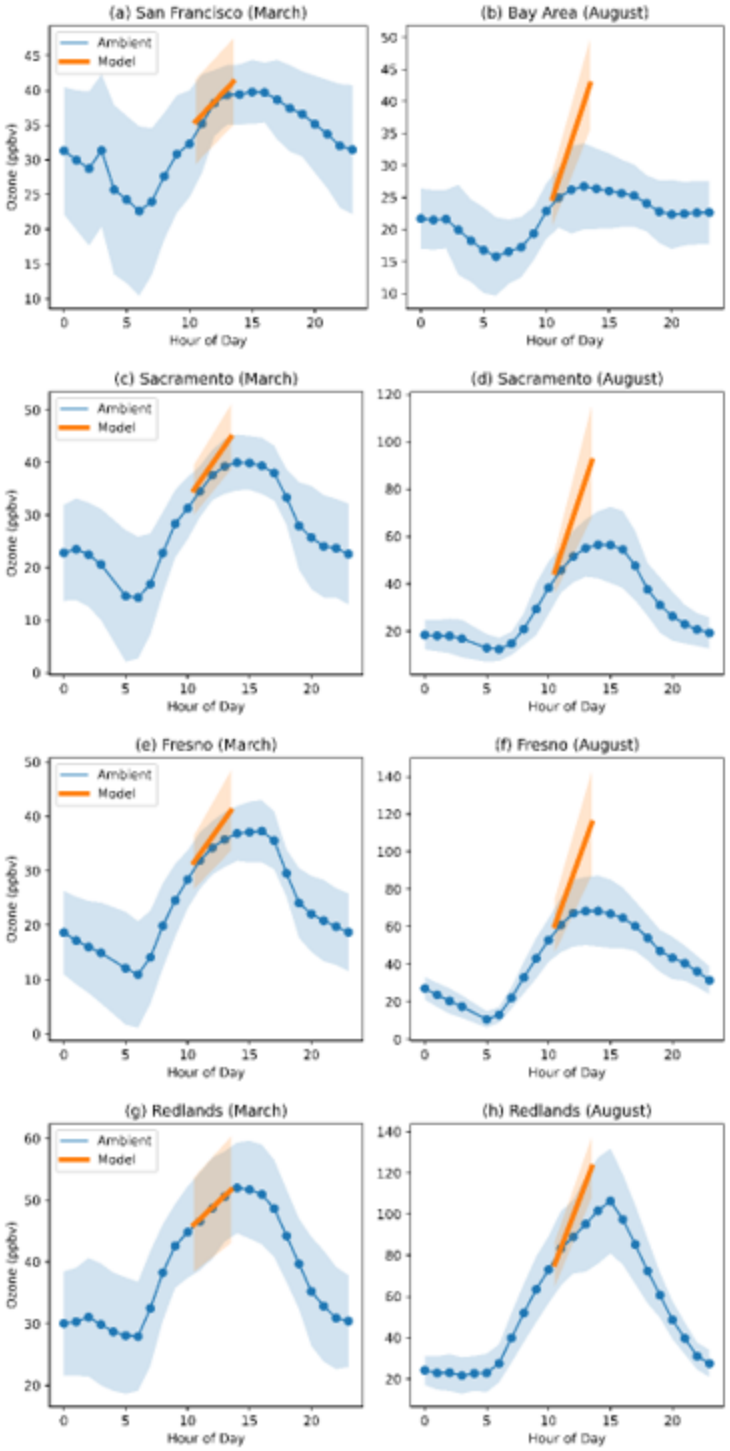

Figure 28. Averaged diurnal O_3 concentrations from Air Quality Management District monitoring stations in four locations in California and the modeled initial and final O_3 concentration from the box model for March and August 2020.

Summary O_3 isopleths in each study area were plotted by averaging the daily O_3 isopleth in March or August 2020 (Figure 29). Daily O_3 isopleths were generated by scaling the initial daily NO_x and VOCs (represented as ozone formation potential (OFP)) to multiple levels and simulating the final O_3 concentration using the box model. The dashed line in each plot indicates the ridge line of the O_3 isopleth, which separates the NO_x-limited O_3 chemical regime (under the ridge line) and the VOC-limited O_3 chemical regime (above the ridge line). The dots in Figure 29 represent the averaged initial NO_x and OFP condition during the study period. The 95% confidence interval of NO_x and OFP around the averaged value is shown as the black box. The vertical distance between the averaged dot to the ridge line in the O_3 isopleth indicates the amount of NO_x control that is needed to reach the NO_x-limited regime for the average day. The vertical distance between the upper right corner of the confidence interval box to the ridgeline indicates the amount of NO_x control that is needed to move 95% of the days with the highest O_3 concentration to the NO_x-limited regime.

Average O_3 sensitivity at the San Francisco-Arkansas Street site was predicted to be in the VOC-limited regime in March and August 2020 (Figure 29a and b). This means San Francisco may experience increased O_3 concentrations in the future as NO_x-control strategies advance. The O_3 design value at San Francisco has been lower than 70 ppbv over the past three years, so some amount of O_3 increase can be tolerated. NO_x concentrations decreased by approximately 30% in San Francisco at the beginning of the COVID-19 stay-at-home order (March) (*59*, *60*). The isopleth results calculated in the present study suggest that this level of reduction would not move the O_3 formation regime to NO_x-limited conditions. The highest O_3 concentration throughout the year occurs in the summer months (August). The stay-at-home order had a limited impact on the NO_x concentration throughout California in August 2020 (*1*), but even if the timing of the order had caused a 30% reduction in NO_x concentrations, O_3 formation would remain in the VOC-limited chemical regime. Figure 29b suggests that ~60 and ~80% of NO_x reduction is needed to move the averaged condition or the peak O_3 days to the NO_x-limited regime in August. Past studies of model simulation (*55*, *61*) showed that the Bay Area was in the VOC-limited regime in the urban core. The consistent result from this study suggests that more NO_x reduction is still needed to move the O_3 sensitivity regime to NO_x-limited in San Francisco.

Figure 29c and d show the predicted O_3 isopleth around the Sacramento-T Street site in March and August 2020. The O_3 chemical regime in Sacramento was VOC-limited in March and turned to NO_x-limited in August. The calculations predict that NO_x reductions of ~70% would be needed to reach NO_x-limited conditions in March. Peak O_3 conditions have already reached the NO_x-limited regime in August. This means further NO_x control can effectively reduce O_3 concentration in Sacramento during the summer O_3 season but may increase the O_3 concentration during spring. Past studies (*56*, *61*) found that the O_3 sensitivity regime in the urban core of Sacramento was in the VOC-limited regime with a trend of transitioning to the NO_x-limited regime. Direct measurements of O_3 sensitivity found that the O_3 sensitivity in Sacrament was NO_x-limited in the hottest months (August and September) and VOC-limited in cooler seasons in 2020 (*14*). The consistent results from modeled O_3 isopleths and the field measurements suggest that the NO_x control in Sacramento has already switched to the NO_x-limited O_3 formation regime in 2020.

Figure 29e and f show the predicted O_3 isopleth around the Fresno-Garland site in the San Joaquin Valley. As in Sacramento, the O_3 chemical regime near Fresno-Garland in March was mostly VOC-limited. Average

conditions transition to the NO_x-limited regime in August. The upper right edge of the confidence interval box suggests that NO_x reductions of ~27% would be needed to move to NO_x-limited conditions for peak O_3 concentrations in August. Past studies (*62–64*) found that the O_3 sensitivity in urban areas in Fresno transitioned between the VOC-limited regime and the NO_x-limited regime during the summer, which is consistent with this study. NO_x reductions of ~40% were observed in Fresno during the stay-at-home order in March 2020 (*59*). Based on the calculations performed in the current study, this level of reduction could have shifted conditions from VOC-limited to NO_x-limited in Fresno during the summer months (August), but they were not sufficient to shift the chemical regime in the spring (March).

Figure 29g and h show the predicted O_3 isopleth around the Redlands-Dearborn site in the SoCAB. Average conditions in Redlands were VOC-limited regime in March and transitioned towards NO_x-limited in August 2020. The averaged O_3 sensitivity regime in Redlands was close to the ridge line in August. NO_x reductions of ~13% and 29% would be required to move average conditions and peak conditions to the NO_x-limited regime, respectively. Direct chamber measurements in Redlands observed O_3 sensitivity transition between NO_x-limited regime and VOC-limited regime in August 2021, which is similar to the modeled O_3 isopleth in August 2020. NO_x reductions of ~30% were observed around the South Coast Air Basin during the COVID-19 shutdown period. The calculations performed in the current study suggest that this level of NO_x control would be sufficient to shift to the NO_x-limited regime for 95% of observed high O_3 days in Redlands during the summer (August) but not during spring (March).

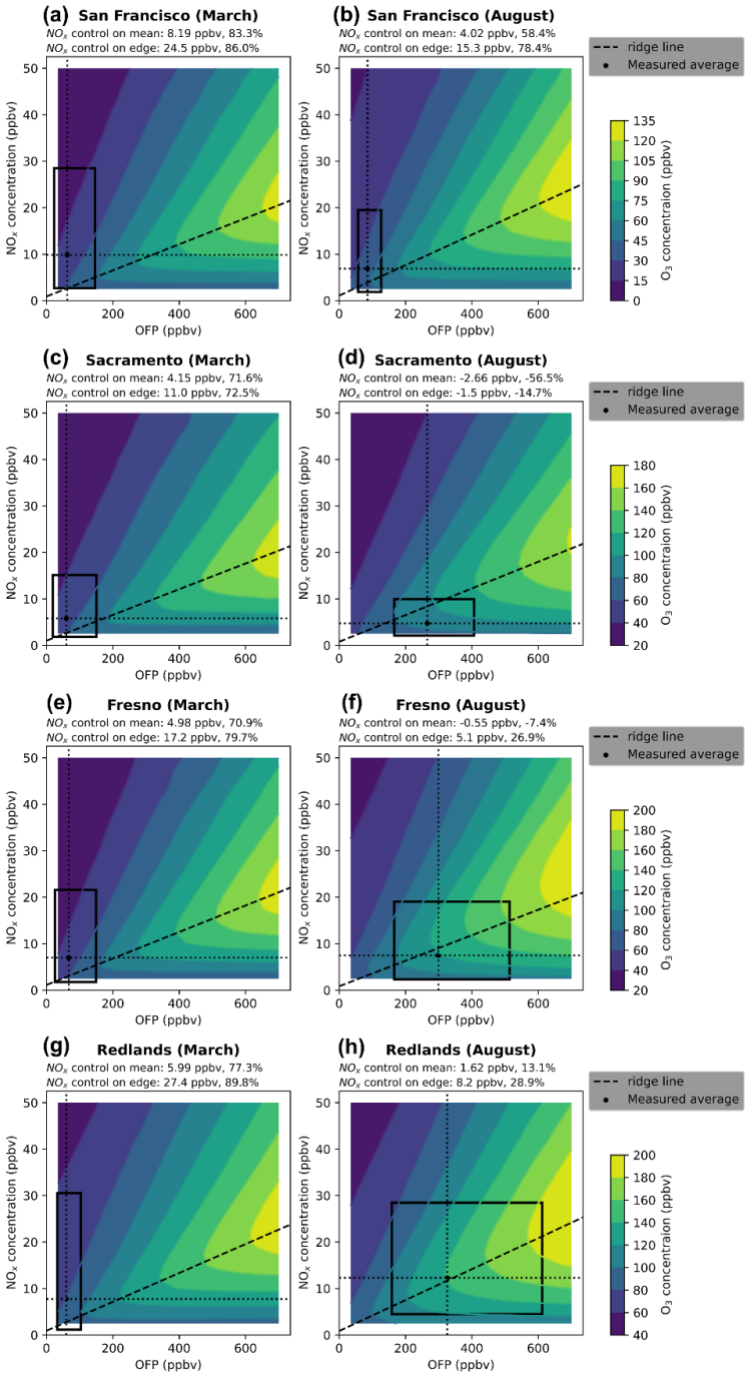

Figure 29. Monthly averaged O_3 isopleth for Bay Area, Sacramento, Fresno, and Redlands, CA.

Table 6 summarizes the amount of NO_x reduction required to reach the NO_x-limited O_3 regime at each site in the current study. Required NO_x reductions are lower in summer (August) than in spring (March) at all locations due to the seasonal cycle in biogenic and evaporative VOC emissions. Also shown in Table 6 is the

estimated NO_x reduction associated with the COVID-19 stay-at-home order issued in March 2020. In all cases, the magnitude of the NO_x reduction produced by removing the majority of the vehicle traffic is less than half of what would be required to transition O_3 chemistry to a NO_x-limited regime during the spring season. It is, therefore, not surprising that O_3 concentrations were observed to increase during the shutdown period.

The highest O_3 concentrations occur during summer months when the amount of NO_x control needed to reach NO_x-limited conditions is at a seasonal minimum. The analysis carried out in the current study suggests that the traffic reduction associated with the COVID-19 stay-at-home order would have been sufficient to reach NO_x-limited conditions for 95% of the days with the highest O_3 concentrations at Fresno and Redlands (see boxes shaded green in Table 6). Sacramento was already in the NO_x-limited regime during the summer months. San Francisco remains deep in the VOC-limited regime during the summer months, but it is noteworthy that San Francisco is currently in compliance with the O_3 NAAQS.

Table 6. Summary of NO_x Reduction Required to Reach NO_x-limited O_3 Regime.

Location	Month	NO_x Reduction Required to Reach NO_x-limited O_3 Regime*		Estimated NO_x Reduction during COVID-19 shutdown
		Average O_3	95th Percent O_3	
San Francisco	March	83%	86%	30%
San Francisco	August	58%	78%	
Sacramento	March	72%	72%	34%
Sacramento	August	-57%	-15%	
Fresno	March	71%	80%	40%
Fresno	August	-7%	27%	
Redlands	March	77%	90%	30%
Redlands	August	13%	29%	

*Boxes shaded green would be in the NO_x-limited regime under COVID-19 shutdown conditions

3.4 Discussion

O_3 sensitivity has been analyzed over short timescales in past studies using ratios of photochemical indicator species, including H_2O_2/HNO_3 and $HCHO/NO_2$ (*65*). The TROPOspheric Monitoring Instrument (TROPOMI) on the Sentinel-5 Precursor (Sentinel-5P) satellite measures the H_2O_2 and NO_2 in the tropospheric. TROPOMI has

the capability to analyze the O_3 sensitivity regime over broad geographical regions (*16*, *66–69*). Our previous study (*14*) analyzed the TROPOMI HCHO/NO_2 across California from April to December 2020. The spatial distribution of HCHO/NO_2 suggests that the O_3 chemical regime tends to be more VOC-limited in urban cores and transitions towards NO_x-limited conditions in rural and remote areas. In this study, the San Francisco site is located in the urban core, and average O_3 sensitivity remains VOC-limited in August. Sites in Redlands, Sacramento, and Fresno are either out of the urban cores or surrounded by rural areas with heavy vegetation. These locations transition to NO_x-limited conditions in August. Therefore, the spatial and seasonal trends in the predicted O_3 sensitivity regime match the spatial distribution of O_3 sensitivity analyzed from satellite data at the four study sites.

3.5 Conclusions

Photochemical box model calculations were carried out during March and August 2020 at four sites (San Francisco, Sacramento, Fresno, Redlands) across California to statistically analyze the amount of NO_x control required to reach NO_x-limited conditions for O_3 formation. Model calculations represented the contribution to O_3 formation attributable to chemical formation and were consistent with past simulations that showed good agreement with direct chamber measurements of O_3 sensitivity in the atmosphere.

The amount of NO_x reduction required to reach NO_x-limited conditions changed by season. Summer periods require less NO_x control to reach NO_x-limited conditions compared to other seasons, likely due to increased biogenic and evaporative VOC emissions during summer. O_3 concentrations are highest in summer months, however, so these targets should be the immediate priority for the emissions control program. NO_x reductions needed to reach NO_x-limited O_3 conditions during summer months are greater in dense urban cities like San Francisco (78%) than in smaller cities like Fresno (27%) and Redlands (29%). Calculations predict that Sacramento is already in the NO_x-limited regime in summer months so any additional NO_x control will immediately reduce O_3 concentrations.

The NO_x reductions associated with COVID-19 stay-at-home orders were at least a factor of two smaller than the reductions required to achieve NO_x-limited chemistry during March–April 2020. A reduction of similar magnitude during August would have achieved NO_x-limited conditions for 95% of the days with the highest O_3 concentrations at Sacramento, Fresno, and Redlands. San Francisco would require NO_x reductions across multiple sectors in addition to transportation before reaching NO-limited conditions.

The results of the current study highlight that reduced traffic emissions can play a role in achieving healthy air quality in California, but these controls will need to be coordinated with broader reductions across multiple economic sectors to succeed in all locations.

4. Conclusions

Two transportable smog chamber systems were deployed in the South Coast Air Basin (SoCAB) to directly measure the O_3 chemical formation regime during the RECAP-CA field campaign. Each smog chamber system consisted of three fluorinated ethylene propylene chambers (1 m^3 each) irradiated by UV lights. Chambers were filled with ambient air between 10 AM and 12 PM each day. One chamber was perturbed by adding ~8 ppb of NO_x (as NO_2), a second chamber was perturbed by adding ~8 ppb of a VOC representing urban atmospheres (4.4 ppb ethylene, 2.8 ppb n-hexane, and 0.8 ppb m-xylene), and the third chamber was used as a base case comparison point. After being filled, the chambers were exposed to UV lights (100 W m^{-2}) for 3 hours to simulate conditions typical for the California atmosphere. O_3, NO, NO_2, NOy, T, and RH were measured continuously from chambers throughout the experiment. Comparisons between the chamber concentrations determine if O_3 formation chemistry is in the NO_x-limited or VOC-limited chemical regime. The median observed O_3 sensitivity in Pasadena was stable in the VOC-limited regime, but showed a seasonal trend in Redlands, where median O_3 formation was VOC-limited in July and October and transitioned towards the NO_x-limited regime in August and September. The variability of the O_3 chemical regime increased at higher O_3 concentrations. Both Pasadena and Redlands had O_3 nonattainment days with O_3 sensitivity in the strongly NO_x-limited regime and strongly VOC-limited regime.

A photochemical chamber model initialized with measured concentrations at the beginning of each study day successfully predicted the final O_3 concentration and the O_3 chemical regime in the measurement chambers. The chamber model was used to predict O_3 formation under a range of NO_x and VOC conditions. O_3 isopleths created with the chamber model predict that average conditions in Pasadena and Redlands are in the NO_x-rich chemical regime, and that ~40% NO_x control would be required to transition to NO_x-limited conditions on 95% of the days with the highest O_3 concentrations in the absence of simultaneous VOC controls. NO_x controls smaller than this level will cause O_3 concentrations to increase at both locations.

Tagging features inherent in the chamber model were used to quantify VOC source contributions to O_3 formation during the measurement period in Pasadena and Redlands. Biogenic VOCs and aldehydes that likely formed from biogenic VOCs were the largest daily contributors to O_3 formation identified in Pasadena and Redlands. Fossil transportation fuels and VCPs each contributed roughly half as much as biogenic VOCs to O_3 formation under the study conditions. Background O_3 and NO_2 that form before the start of each measurement day significantly contributed to final O_3 concentrations, but these untagged compounds form from sources similar to those identified on measurement days.

Photochemical box model calculations were extended to statistically analyze the O_3 formation regime at San Francisco, Sacramento, Fresno, and Redlands in March and August 2020. Average conditions at each location were VOC-limited during March 2020 due to the natural seasonal cycle of biogenic VOC emissions. The level of NO_x reduction experienced due to COVID-19 “stay-at-home” orders was not sufficient to shift the days with the highest O_3 formation to the NO_x-limited regime. If a similar “stay-at-home” order had been issued in

August 2020, then the days with the highest O_3 formation at Fresno and Redlands would have shifted from VOC-limited to NO_x-limited. Sacramento was already in the NO_x-limited regime during August 2020, and San Francisco remained in the VOC-limited regime even in the presence of the hypothetical NO_x reductions.

The results of the current study demonstrate that reductions in motor vehicle emissions can play an important role in improving air quality in California, but they will need to be coordinated with controls in other sectors to succeed at all locations. Removing a large fraction of the vehicle traffic during the COVID-19 shutdown period during spring 2020 significantly reduced ambient NO_x concentrations but even this drastic intervention was not sufficient to shift O_3 formation chemistry into a new NO_x-limited regime. Future emissions control strategies could focus on replacing fossil-fueled mobile sources with electric vehicles (reduces both NO_x and VOC) in coordination with other control strategies, such as reducing VCP emissions. Ultimately, NO_x reductions from mobile sources will need to be combined with reductions from other sectors, such as off-road vehicles, agricultural equipment, and ships to fully transition to NO_x-limited O_3 chemistry across California.

5. Future Work

The combined approach of smog chamber measurements and model calculations produced consistent results in Sacramento, Pasadena, and Redlands. Similar measurements and model calculations should be performed for sites in the San Joaquin Valley to help design optimized O_3 control strategies.

Multi-day simulations with chemical transport models should confirm the efficiency of proposed emissions control programs targeting mobile sources and stationary sources combined with VCP reductions.

6. References

1. Schroeder, J. R., C. Cai, J. Xu, D. Ridley, J. Lu, N. Bui, F. Yan, and J. Avise. Changing Ozone Sensitivity in the South Coast Air Basin during the COVID-19 Period. *Atmospheric Chemistry and Physics*, Vol. 22, No. 19, 2022, pp. 12985–13000. https://doi.org/10.5194/ACP-22-12985-2022.
2. Pollack, I. B., T. B. Ryerson, M. Trainer, D. D. Parrish, A. E. Andrews, E. L. Atlas, D. R. Blake, S. S. Brown, R. Commane, B. C. Daube, J. A. De Gouw, W. P. Dubé, J. Flynn, G. J. Frost, J. B. Gilman, N. Grossberg, J. S. Holloway, J. Kofler, E. A. Kort, W. C. Kuster, P. M. Lang, B. Lefer, R. A. Lueb, J. A. Neuman, J. B. Nowak, P. C. Novelli, J. Peischl, A. E. Perring, J. M. Roberts, G. Santoni, J. P. Schwarz, J. R. Spackman, N. L. Wagner, C. Warneke, R. A. Washenfelder, S. C. Wofsy, and B. Xiang. Airborne and Ground-Based Observations of a Weekend Effect in Ozone, Precursors, and Oxidation Products in the California South Coast Air Basin. *Journal of Geophysical Research Atmospheres*, Vol. 117, No. 3, 2012, pp. 1–14. https://doi.org/10.1029/2011JD016772.
3. Warneke, C., J. A. De Gouw, J. S. Holloway, J. Peischl, T. B. Ryerson, E. Atlas, D. Blake, M. Trainer, D. D. Parrish, C. : Warneke, J. A. De Gouw, J. S. Holloway, J. Peischl, T. B. Ryerson, E. Atlas, D. Blake, M. Trainer, and D. D. Parrish. Multiyear Trends in Volatile Organic Compounds in Los Angeles, California: Five Decades of Decreasing Emissions. *Journal of Geophysical Research: Atmospheres*, Vol. 117, No. D21, 2012, pp. 0–17. https://doi.org/10.1029/2012JD017899.
4. Parrish, D. D., J. Xu, B. Croes, and M. Shao. Air Quality Improvement in Los Angeles—Perspectives for Developing Cities. *Frontiers of Environmental Science and Engineering*, Vol. 10, No. 5, 2016. https://doi.org/10.1007/s11783-016-0859-5.
5. Van Rooy, P., A. Tasnia, B. Barletta, R. Buenconsejo, J. D. Crounse, C. Kenseth, S. Meinardi, S. Murphy, H. Parker, B. Schulze, J. H. Seinfeld, P. O. Wennberg, D. R. Blake, and K. C. Barsanti. Observations of Volatile Organic Compounds in the Los Angeles Basin during COVID-19. *ACS Earth and Space Chemistry*, 2021. https://doi.org/10.1021/acsearthspacechem.1c00248.
6. McDonald, B. C., J. A. De Gouw, J. B. Gilman, S. H. Jathar, A. Akherati, C. D. Cappa, J. L. Jimenez, J. Lee-Taylor, P. L. Hayes, S. A. McKeen, Y. Y. Cui, S. W. Kim, D. R. Gentner, G. Isaacman-VanWertz, A. H. Goldstein, R. A. Harley, G. J. Frost, J. M. Roberts, T. B. Ryerson, and M. Trainer. Volatile Chemical Products Emerging as Largest Petrochemical Source of Urban Organic Emissions. *Science*, Vol. 359, No. 6377, 2018, pp. 760–764. https://doi.org/10.1126/science.aaq0524.
7. Lu, Q., B. N. Murphy, M. Qin, P. J. Adams, Y. Zhao, H. O. T. Pye, C. Efstathiou, C. Allen, and A. L. Robinson. Simulation of Organic Aerosol Formation during the CalNex Study: Updated Mobile Emissions and Secondary Organic Aerosol Parameterization for Intermediate-Volatility Organic Compounds. *Atmospheric Chemistry and Physics*, Vol. 20, No. 7, 2020, pp. 4313–4332. https://doi.org/10.5194/ACP-20-4313-2020.
8. Ryerson, T. B., A. E. Andrews, W. M. Angevine, T. S. Bates, C. A. Brock, B. Cairns, R. C. Cohen, O. R. Cooper, J. A. De Gouw, F. C. Fehsenfeld, R. A. Ferrare, M. L. Fischer, R. C. Flagan, A. H. Goldstein, J. W. Hair, R. M. Hardesty, C. A. Hostetler, J. L. Jimenez, A. O. Langford, E. McCauley, S. A. McKeen, L. T. Molina, A. Nenes, S. J. Oltmans, D. D. Parrish, J. R. Pederson, R. B. Pierce, K. Prather, P. K. Quinn, J. H. Seinfeld, C. J. Senff, A. Sorooshian, J. Stutz, J. D. Surratt, M. Trainer, R. Volkamer, E. J. Williams, and S. C. Wofsy. The 2010 California Research at the Nexus of Air Quality and Climate Change (CalNex) Field Study. *Journal of Geophysical Research Atmospheres*, Vol. 118, No. 11, 2013, pp. 5830–5866. https://doi.org/10.1002/jgrd.50331.

9. Pollack, I. B., T. B. Ryerson, M. Trainer, J. A. Neuman, J. M. Roberts, D. D. Parrish, C. : Pollack, T. B. Ryerson, M. Trainer, J. M. Roberts, and D. D. Parrish. Trends in Ozone, Its Precursors, and Related Secondary Oxidation Products in Los Angeles, California: A Synthesis of Measurements from 1960 to 2010. *Journal of Geophysical Research: Atmospheres*, Vol. 118, No. 11, 2013, pp. 5893–5911. https://doi.org/10.1002/JGRD.50472.
10. Gu, S., A. Guenther, and C. Faiola. Effects of Anthropogenic and Biogenic Volatile Organic Compounds on Los Angeles Air Quality. *Environmental Science and Technology*, Vol. 55, No. 18, 2021, pp. 12191–12201. https://doi.org/10.1021/acs.est.1c01481.
11. Seltzer, K., E. Pennington, V. Rao, B. Murphy, M. Strum, K. Isaacs, and H. Pye. Reactive Organic Carbon Emissions from Volatile Chemical Products. *Atmospheric Chemistry and Physics*, 2020, pp. 1–33. https://doi.org/10.5194/acp-2020-1111.
12. Coggon, M. M., G. I. Gkatzelis, B. C. McDonald, J. B. Gilman, R. H. Schwantes, N. Abuhassan, K. C. Aikin, M. F. Arendd, T. A. Berkoff, S. S. Brown, T. L. Campos, R. R. Dickerson, G. Gronoff, J. F. Hurley, G. Isaacman-Vanwertz, A. R. Koss, M. Li, S. A. McKeen, F. Moshary, J. Peischl, V. Pospisilova, X. Ren, A. Wilson, Y. Wu, M. Trainer, and C. Warneke. Volatile Chemical Product Emissions Enhance Ozone and Modulate Urban Chemistry. *Proceedings of the National Academy of Sciences of the United States of America*, Vol. 118, No. 32, 2021. https://doi.org/10.1073/pnas.2026653118.
13. Gkatzelis, G. I., M. M. Coggon, B. C. McDonald, J. Peischl, J. B. Gilman, K. C. Aikin, M. A. Robinson, F. Canonaco, A. S. H. Prevot, M. Trainer, and C. Warneke. Observations Confirm That Volatile Chemical Products Are a Major Source of Petrochemical Emissions in U.S. Cities. *Environmental Science and Technology*, Vol. 55, No. 8, 2021, pp. 4332–4343. https://doi.org/10.1021/ACS.EST.0C05471.
14. Wu, S., H. J. Lee, A. Anderson, S. Liu, T. Kuwayama, J. H. Seinfeld, and M. J. Kleeman. Direct Measurements of Ozone Response to Emissions Perturbations in California. *Atmospheric Chemistry and Physics*, Vol. 22, No. 7, 2022, pp. 4929–4949. https://doi.org/10.5194/acp-22-4929-2022.
15. Nussbaumer, C. M., and R. C. Cohen. The Role of Temperature and NO_x in Ozone Trends in the Los Angeles Basin. *Environmental Science and Technology*, Vol. 54, No. 24, 2020, pp. 15652–15659. https://doi.org/10.1021/acs.est.0c04910.
16. Jin, X., A. Fiore, A. Fiore, K. F. Boersma, I. De Smedt, and L. Valin. Inferring Changes in Summertime Surface Ozone-NO_x-VOC Chemistry over U.S. Urban Areas from Two Decades of Satellite and Ground-Based Observations. *Environmental Science and Technology*, Vol. 54, No. 11, 2020, pp. 6518–6529. https://doi.org/10.1021/acs.est.9b07785.
17. Zhao, Y., Y. Li, A. Kumar, Q. Ying, F. Vandenberghe, and M. J. Kleeman. Separately Resolving NO_x and VOC Contributions to Ozone Formation. *Atmospheric Environment*, Vol. 285, 2022, p. 119224. https://doi.org/10.1016/J.ATMOSENV.2022.119224.
18. Carter, W., D. Luo, I. Malkina, and J. Pierce. Environmental Chamber Studies of Atmospheric Reactivities of Volatile Organic Compounds: Effects of Varying Chamber and Light Source. 1995. https://doi.org/10.2172/57153.
19. Kleeman, M. J., T. M. Young, and P. G. Green. *Measurement of Volatile Chemical Products in Los Angeles and Biogenic vs. Anthropogenic VOC Analysis During Peak Ozone Events in the SoCAB*. Alpharetta, GA, 2022.
20. U.S. Environmental Protection Agency. *Method TO-11A: Compendium of Methods for the Determination of Toxic Organic Compounds in Ambient Air Second Edition Compendium Method TO-11A Determination of Formaldehyde in Ambient Air Using Adsorbent Cartridge Followed by High Performance Liquid Chromat*. 1999.
21. U.S. Environmental Protection Agency. *Compendium Method TO-17: Determination of Volatile Organic Compounds in Ambient Air Using Active Sampling Onto Sorbent Tubes*. 1999.

22. Lerner, B. M., J. B. Gilman, K. C. Aikin, E. L. Atlas, P. D. Goldan, M. Graus, R. Hendershot, G. A. Isaacman-Vanwertz, A. Koss, W. C. Kuster, R. A. Lueb, R. J. Mclaughlin, J. Peischl, D. Sueper, T. B. Ryerson, T. W. Tokarek, C. Warneke, B. Yuan, and J. A. De Gouw. An Improved, Automated Whole Air Sampler and Gas Chromatography Mass Spectrometry Analysis System for Volatile Organic Compounds in the Atmosphere. *Atmospheric Measurement Techniques*, Vol. 10, No. 1, 2017, pp. 291–313. https://doi.org/10.5194/AMT-10-291-2017.
23. Krechmer, J., F. Lopez-Hilfiker, A. Koss, M. Hutterli, C. Stoermer, B. Deming, J. Kimmel, C. Warneke, R. Holzinger, J. Jayne, D. Worsnop, K. Fuhrer, M. Gonin, and J. De Gouw. Evaluation of a New Reagent-Ion Source and Focusing Ion-Molecule Reactor for Use in Proton-Transfer-Reaction Mass Spectrometry. *Analytical Chemistry*, Vol. 90, No. 20, 2018, pp. 12011–12018. https://doi.org/10.1021/ACS.ANALCHEM.8B02641/ASSET/IMAGES/LARGE/AC-2018-02641V_0007.JPEG.
24. Xu, L., M. M. Coggon, C. E. Stockwell, J. B. Gilman, M. A. Robinson, M. Breitenlechner, A. Lamplugh, J. D. Crounse, P. O. Wennberg, J. A. Neuman, G. A. Novak, P. R. Veres, S. S. Brown, and C. Warneke. Chemical Ionization Mass Spectrometry Utilizing Ammonium Ions (NH4+ CIMS) for Measurements of Organic Compounds in the Atmosphere. *Atmospheric Measurement Techniques*, Vol. 15, No. 24, 2022, pp. 7353–7373. https://doi.org/10.5194/AMT-15-7353-2022.
25. Robinson, M. A., J. Andrew Neuman, L. G. Huey, J. M. Roberts, S. S. Brown, and P. R. Veres. Temperature-Dependent Sensitivity of Iodide Chemical Ionization Mass Spectrometers. *Atmospheric Measurement Techniques*, Vol. 15, No. 14, 2022, pp. 4295–4305. https://doi.org/10.5194/AMT-15-4295-2022.
26. Veres, P. R., J. Andrew Neuman, T. H. Bertram, E. Assaf, G. M. Wolfe, C. J. Williamson, B. Weinzierl, S. Tilmes, C. R. Thompson, A. B. Thames, J. C. Schroder, A. Saiz-Lopez, A. W. Rollins, J. M. Roberts, D. Price, J. Peischl, B. A. Nault, K. H. Møller, D. O. Miller, S. Meinardi, Q. Li, J. F. Lamarque, A. Kupc, H. G. Kjaergaard, D. Kinnison, J. L. Jimenez, C. M. Jernigan, R. S. Hornbrook, A. Hills, M. Dollner, D. A. Day, C. A. Cuevas, P. Campuzano-Jost, J. Burkholder, T. Paul Bui, W. H. Brune, S. S. Brown, C. A. Brock, I. Bourgeois, D. R. Blake, E. C. Apel, and T. B. Ryerson. Global Airborne Sampling Reveals a Previously Unobserved Dimethyl Sulfide Oxidation Mechanism in the Marine Atmosphere. *Proceedings of the National Academy of Sciences of the United States of America*, Vol. 117, No. 9, 2020, pp. 4505–4510. https://doi.org/10.1073/PNAS.1919344117/SUPPL_FILE/PNAS.1919344117.SAPP.PDF.
27. Veres, P. R., and J. M. Roberts. Development of a Photochemical Source for the Production and Calibration of Acyl Peroxynitrate Compounds. *Atmospheric Measurement Techniques*, Vol. 8, No. 5, 2015, pp. 2225–2231. https://doi.org/10.5194/AMT-8-2225-2015.
28. Wu, S., H. J. Lee, A. Anderson, S. Liu, T. Kuwayama, J. H. Seinfeld, and M. J. Kleeman. Direct Measurements of Ozone Response to Emissions Perturbations in California. *Atmospheric Chemistry and Physics*, Vol. 22, No. 7, 2022, pp. 4929–4949. https://doi.org/10.5194/acp-22-4929-2022.
29. Lerner, B. M., J. B. Gilman, K. C. Aikin, E. L. Atlas, P. D. Goldan, M. Graus, R. Hendershot, G. A. Isaacman-VanWertz, A. Koss, W. C. Kuster, R. A. Lueb, R. J. McLaughlin, J. Peischl, D. Sueper, T. B. Ryerson, T. W. Tokarek, C. Warneke, B. Yuan, and J. A. de Gouw. An Improved, Automated Whole Air Sampler and Gas Chromatography Mass Spectrometry Analysis System for Volatile Organic Compounds in the Atmosphere. *Atmospheric Measurement Techniques*, Vol. 10, No. 1, 2017, pp. 291–313. https://doi.org/10.5194/amt-10-291-2017.
30. Veres, P. R., J. Andrew Neuman, T. H. Bertram, E. Assaf, G. M. Wolfe, C. J. Williamson, B. Weinzierl, S. Tilmes, C. R. Thompson, A. B. Thames, J. C. Schroder, A. Saiz-Lopez, A. W. Rollins, J. M. Roberts, D. Price, J. Peischl, B. A. Nault, K. H. Møller, D. O. Miller, S. Meinardi, Q. Li, J. F. Lamarque, A. Kupc, H. G. Kjaergaard, D. Kinnison, J. L. Jimenez, C. M. Jernigan, R. S. Hornbrook, A. Hills, M. Dollner, D. A. Day, C. A. Cuevas, P.

Campuzano-Jost, J. Burkholder, T. Paul Bui, W. H. Brune, S. S. Brown, C. A. Brock, I. Bourgeois, D. R. Blake, E. C. Apel, and T. B. Ryerson. Global Airborne Sampling Reveals a Previously Unobserved Dimethyl Sulfide Oxidation Mechanism in the Marine Atmosphere. *Proceedings of the National Academy of Sciences of the United States of America*, Vol. 117, No. 9, 2020, pp. 4505–4510. https://doi.org/10.1073/PNAS.1919344117/SUPPL_FILE/PNAS.1919344117.SAPP.PDF.

31. Veres, P. R., and J. M. Roberts. Development of a Photochemical Source for the Production and Calibration of Acyl Peroxynitrate Compounds. *Atmospheric Measurement Techniques*, Vol. 8, No. 5, 2015, pp. 2225–2231. https://doi.org/10.5194/AMT-8-2225-2015.
32. Robinson, M. A., J. Andrew Neuman, L. G. Huey, J. M. Roberts, S. S. Brown, and P. R. Veres. Temperature-Dependent Sensitivity of Iodide Chemical Ionization Mass Spectrometers. *Atmospheric Measurement Techniques*, Vol. 15, No. 14, 2022, pp. 4295–4305. https://doi.org/10.5194/AMT-15-4295-2022.
33. Coggon, M. M., C. E. Stockwell, M. S. Claflin, E. Y. Pfannerstill, X. Lu, J. B. Gilman, J. Marcantonio, C. Cao, K. Bates, G. I. Gkatzelis, A. Lamplugh, E. F. Katz, C. Arata, E. C. Apel, R. S. Hornbrook, F. Piel, F. Majluf, D. R. Blake, A. Wisthaler, M. Canagaratna, B. M. Lerner, A. H. Goldstein, J. E. Mak, and C. Warneke. Identifying and Correcting Interferences to PTR-ToF-MS Measurements of Isoprene and Other Urban Volatile Organic Compounds. *EGUsphere*, 2023, pp. 1–41. https://doi.org/10.5194/egusphere-2023-1497.
34. Carter, W. P. L., and G. Heo. Development of Revised SAPRC Aromatics Mechanisms. *Atmospheric Environment*, Vol. 77, 2013, pp. 404–414. https://doi.org/10.1016/J.ATMOSENV.2013.05.021.
35. Liu, J., J. Lipsitt, M. Jerrett, and Y. Zhu. Decreases in Near-Road NO and NO2Concentrations during the COVID-19 Pandemic in California. *Environmental Science and Technology Letters*, No. 2, 2020. https://doi.org/10.1021/acs.estlett.0c00815.
36. Zhao, Y., Y. Li, A. Kumar, Q. Ying, F. Vandenberghe, and M. J. Kleeman. Separately Resolving NO_x and VOC Contributions to Ozone Formation. *Atmospheric Environment*, Vol. 285, 2022, pp. 119224–119224. https://doi.org/10.1016/J.ATMOSENV.2022.119224.
37. Russell, A. R., L. C. Valin, E. J. Bucsela, M. O. Wenig, and R. C. Cohen. Space-Based Constraints on Spatial and Temporal Patterns of NO_x Emissions in California, 2005–2008. *Environmental Science & Technology*, Vol. 44, No. 9, 2010, pp. 3608–3615. https://doi.org/10.1021/es903451j.
38. Gao, Y., M. Ma, F. Yan, H. Su, S. Wang, H. Liao, B. Zhao, X. Wang, Y. Sun, J. R. Hopkins, Q. Chen, P. Fu, A. C. Lewis, Q. Qiu, X. Yao, and H. Gao. Impacts of Biogenic Emissions from Urban Landscapes on Summer Ozone and Secondary Organic Aerosol Formation in Megacities. *Science of the Total Environment*, Vol. 814, 2022, p. 152654. https://doi.org/10.1016/j.scitotenv.2021.152654.
39. Karavalakis, G., D. Short, D. Vu, R. Russell, M. Hajbabaei, A. Asa-Awuku, and T. D. Durbin. Evaluating the Effects of Aromatics Content in Gasoline on Gaseous and Particulate Matter Emissions from SI-PFI and SIDI Vehicles. 2015. https://doi.org/10.1021/es5061726.
40. Gentner, D. R., R. A. Harley, A. M. Miller, and A. H. Goldstein. Diurnal and Seasonal Variability of Gasoline-Related Volatile Organic Compound Emissions in Riverside, California. *Environmental Science and Technology*, Vol. 43, No. 12, 2009, pp. 4247–4252. https://doi.org/10.1021/ES9006228/SUPPL_FILE/ES9006228_SI_001.PDF.
41. Coggon, M. M., B. C. McDonald, A. Vlasenko, P. R. Veres, F. Bernard, A. R. Koss, B. Yuan, J. B. Gilman, J. Peischl, K. C. Aikin, J. Durant, C. Warneke, S. M. Li, and J. A. De Gouw. Diurnal Variability and Emission Pattern of Decamethylcyclopentasiloxane (D5) from the Application of Personal Care Products in Two North American Cities. *Environmental Science and Technology*, Vol. 52, No. 10, 2018, pp. 5610–5618. https://doi.org/10.1021/ACS.EST.8B00506.
42. Pollack, I. B., T. B. Ryerson, M. Trainer, D. D. Parrish, A. E. Andrews, E. L. Atlas, D. R. Blake, S. S. Brown, R. Commane, B. C. Daube, J. A. De Gouw, W. P. Dubé, J. Flynn, G. J. Frost, J. B. Gilman, N. Grossberg, J. S.

Holloway, J. Kofler, E. A. Kort, W. C. Kuster, P. M. Lang, B. Lefer, R. A. Lueb, J. A. Neuman, J. B. Nowak, P. C. Novelli, J. Peischl, A. E. Perring, J. M. Roberts, G. Santoni, J. P. Schwarz, J. R. Spackman, N. L. Wagner, C. Warneke, R. A. Washenfelder, S. C. Wofsy, and B. Xiang. Airborne and Ground-Based Observations of a Weekend Effect in Ozone, Precursors, and Oxidation Products in the California South Coast Air Basin. *Journal of Geophysical Research Atmospheres*, Vol. 117, No. 3, 2012, pp. 1–14. https://doi.org/10.1029/2011JD016772.

43. Pusede, S. E., A. L. Steiner, and R. C. Cohen. Temperature and Recent Trends in the Chemistry of Continental Surface Ozone. *Chemical Reviews*, Vol. 115, No. 10, 2015, pp. 3898–3918. https://doi.org/10.1021/cr5006815.
44. Jin, X., A. Fiore, A. Fiore, K. F. Boersma, I. D. Smedt, and L. Valin. Inferring Changes in Summertime Surface Ozone-NO_x-VOC Chemistry over U.S. Urban Areas from Two Decades of Satellite and Ground-Based Observations. *Environmental Science and Technology*, Vol. 54, No. 11, 2020, pp. 6518–6529. https://doi.org/10.1021/acs.est.9b07785.
45. Schroeder, J. R., C. Cai, J. Xu, D. Ridley, J. Lu, N. Bui, F. Yan, and J. Avise. Changing Ozone Sensitivity in the South Coast Air Basin during the COVID-19 Period. *Atmospheric Chemistry and Physics*, Vol. 22, No. 19, 2022, pp. 12985–13000. https://doi.org/10.5194/ACP-22-12985-2022.
46. Perdigones, B. C., S. Lee, R. C. Cohen, J.-H. Park, and K.-E. Min. Two Decades of Changes in Summertime Ozone Production in California's South Coast Air Basin. *Environmental Science & Technology*, 2022. https://doi.org/10.1021/ACS.EST.2C01026.
47. Murphy, J. G., D. A. Day, P. A. Cleary, P. J. Wooldridge, D. B. Millet, A. H. Goldstein, and R. C. Cohen. The Weekend Effect within and Downwind of Sacramento – Part 1: Observations of Ozone, Nitrogen Oxides, and VOC Reactivity. *Atmospheric Chemistry and Physics*, Vol. 7, No. 20, 2007, pp. 5327–5339. https://doi.org/10.5194/acp-7-5327-2007.
48. Carter, W. P. L. Updated Maximum Incremental Reactivity Scale and Hydrocarbon Bin Reactivities for Regulatory Applications. *California Air Resources Board Contract*, 2009, pp. 339–339.
49. Venecek, M. A., C. Cai, A. Kaduwela, J. Avise, W. P. L. Carter, and M. J. Kleeman. Analysis of SAPRC16 Chemical Mechanism for Ambient Simulations. *Atmospheric Environment*, Vol. 192, 2018, pp. 136–150. https://doi.org/10.1016/J.ATMOSENV.2018.08.039.
50. Ott, W. R. A Physical Explanation of the Lognormality of Pollutant Concentrations. *Journal of the Air & Waste Management Association*, Vol. 40, No. 10, 1990, pp. 1378–1383. https://doi.org/10.1080/10473289.1990.10466789.
51. South Coast AQMD. South Coast Air Quality Management District 2022 Air Quality Management Plan. Dec 02, 2022.
52. Jiang, Z., H. Shi, B. Zhao, Y. Gu, Y. Zhu, K. Miyazaki, X. Lu, Y. Zhang, K. W. Bowman, T. Sekiya, and K.-N. Liou. Modeling the Impact of COVID-19 on Air Quality in Southern California: Implications for Future Control Policies. *Atmospheric Chemistry and Physics*, Vol. 21, No. 11, 2021, pp. 8693–8708. https://doi.org/10.5194/acp-21-8693-2021.
53. Parker, H. A., S. Hasheminassab, J. D. Crounse, C. M. Roehl, and P. O. Wennberg. Impacts of Traffic Reductions Associated With COVID-19 on Southern California Air Quality. *Geophysical Research Letters*, Vol. 47, No. 23, 2020, pp. 1–9. https://doi.org/10.1029/2020GL090164.
54. Zhang, H., J. Li, Q. Ying, B. B. Guven, and E. P. Olaguer. Source Apportionment of Formaldehyde during TexAQS 2006 Using a Source-Oriented Chemical Transport Model. *Journal of Geophysical Research Atmospheres*, Vol. 118, No. 3, 2013, pp. 1525–1535. https://doi.org/10.1002/JGRD.50197.
55. Bay Area AQMD. *Final 2017 Clean Air Plan*. Bay Area AQMD, 2017.

56. Lafranchi, B. W., A. H. Goldstein, and R. C. Cohen. Observations of the Temperature Dependent Response of Ozone to NO_x Reductions in the Sacramento, CA Urban Plume. *Atmospheric Chemistry and Physics*, Vol. 11, No. 14, 2011, pp. 6945–6960. https://doi.org/10.5194/acp-11-6945-2011.
57. Steiner, A. L., R. C. Cohen, R. A. Harley, S. Tonse, D. B. Millet, G. W. Schade, and A. H. Goldstein. VOC Reactivity in Central California: Comparing an Air Quality Model to Ground-Based Measurements. *Atmospheric Chemistry and Physics*, Vol. 8, No. 2, 2008, pp. 351–368. https://doi.org/10.5194/acp-8-351-2008.
58. Ying, Q., M. P. Fraser, R. J. Griffin, J. Chen, and M. J. Kleeman. Verification of a Source-Oriented Externally Mixed Air Quality Model during a Severe Photochemical Smog Episode. *Atmospheric Environment*, Vol. 41, No. 7, 2007, pp. 1521–1538. https://doi.org/10.1016/J.ATMOSENV.2006.10.004.
59. Chen, L. W. A., L. C. Chien, Y. Li, and G. Lin. Nonuniform Impacts of COVID-19 Lockdown on Air Quality over the United States. *Science of the Total Environment*, Vol. 745, 2020, pp. 13–16. https://doi.org/10.1016/j.scitotenv.2020.141105.
60. Naeger, A. R., and K. Murphy. Impact of COVID-19 Containment Measures on Air Pollution in California. *Aerosol and Air Quality Research*, Vol. 20, No. 10, 2020, pp. 2025–2034. https://doi.org/10.4209/aaqr.2020.05.0227.
61. Steiner, A. L., A. J. Davis, S. Sillman, R. C. Owen, A. M. Michalak, and A. M. Fiore. Observed Suppression of Ozone Formation at Extremely High Temperatures Due to Chemical and Biophysical Feedbacks. *Proceedings of the National Academy of Sciences*, Vol. 107, No. 46, 2010, pp. 19685–19690. https://doi.org/10.1073/pnas.1008336107.
62. de Foy, B., W. H. Brune, and J. J. Schauer. Changes in Ozone Photochemical Regime in Fresno, California from 1994 to 2018 Deduced from Changes in the Weekend Effect. *Environmental Pollution*, Vol. 263, 2020. https://doi.org/10.1016/j.envpol.2020.114380.
63. Jin, L., A. Loisy, and N. J. Brown. Role of Meteorological Processes in Ozone Responses to Emission Controls in California's San Joaquin Valley. *Journal of Geophysical Research: Atmospheres*, Vol. 118, No. 14, 2013, pp. 8010–8022. https://doi.org/10.1002/JGRD.50559.
64. San Joaquin Valley Air Pollution Control District. *San Joaquin Valley 2022 Plan for the 2015 8-Hour Ozone Standard*. San Joaquin Valley Air Pollution Control District, 2022.
65. Sillman, S. The Use of NO_y , H_2O_2 , and HNO_3 as Indicators for Ozone-NO_x -Hydrocarbon Sensitivity in Urban Locations. *Journal of Geophysical Research*, Vol. 100, No. D7, 1995, pp. 14175–14175. https://doi.org/10.1029/94JD02953.
66. Chossière, G. P., H. Xu, Y. Dixit, S. Isaacs, S. D. Eastham, F. Allroggen, R. L. Speth, and S. R. H. Barrett. Air Pollution Impacts of COVID-19–Related Containment Measures. *Science Advances*, Vol. 7, No. 21, 2021. https://doi.org/10.1126/SCIADV.ABE1178/ASSET/C9139A3B-89F3-4EC2-B4A0-1E6157B0E236/ASSETS/GRAPHIC/ABE1178-FX2.JPEG.
67. Duncan, B. N., Y. Yoshida, J. R. Olson, S. Sillman, R. V. Martin, L. Lamsal, Y. Hu, K. E. Pickering, C. Retscher, D. J. Allen, and J. H. Crawford. Application of OMI Observations to a Space-Based Indicator of NO_x and VOC Controls on Surface Ozone Formation. *Atmospheric Environment*, Vol. 44, No. 18, 2010, pp. 2213–2223. https://doi.org/10.1016/j.atmosenv.2010.03.010.
68. Martin, R. V., A. M. Fiore, and A. Van Donkelaar. Space-Based Diagnosis of Surface Ozone Sensitivity to Anthropogenic Emissions. *Geophysical Research Letters*, Vol. 31, No. 6, 2004, pp. 2–5. https://doi.org/10.1029/2004gl019416.
69. Schroeder, J. R., J. H. Crawford, A. Fried, J. Walega, A. Weinheimer, A. Wisthaler, M. Müller, T. Mikoviny, G. Chen, M. Shook, D. R. Blake, and G. S. Tonnesen. New Insights into the Column CH 2 O/NO 2 Ratio as an

Indicator of near-Surface Ozone Sensitivity. *Journal of Geophysical Research: Atmospheres*, Vol. 122, No. 16, 2017, pp. 8885–8907. https://doi.org/10.1002/2017JD026781.